A Switchable Single-Mode Fibre Coupler

A thesis submitted for the
degree of Doctor of Philosophy
in the University of London
and for the Diploma of membership
of Imperial College

by

Noorallah Nourshargh, BSc(Eng), ACGI

Department of Electrical Engineering
Imperial College
Exhibition Road
London, SW7 2BT

JULY 1983

Dedicated to my parents
and Hilary

A SWITCHABLE SINGLE-MODE FIBRE COUPLER

BY

N. NOURSHARGH

ABSTRACT

Existing integrated-optical switches and couplers have inherent problems associated with propagation loss and efficiency of coupling to circular fibres. This thesis describes an alternative structure which may overcome these problems.

The device considered uses low loss glass fibre cores as the guiding channels and operates on directional coupler principles. The structure consists of a pair of very fine parallel glass rods embedded into an electro-optic crystal which thus acts as an active cladding. Meta-nitroaniline was selected as the crystalline cladding because it has high electro-optic coefficients, low melting point and is relatively easy to grow in single crystal form.

The implications of having an active cladding were numerically investigated using the theory of a static fibre coupler. The extent to which fibre parameters affected the performance of the switch were determined; it was found, for example, that optimum performance would not be achieved if the cores were in contact.

In order to ensure that the device would be single-moded, it was essential to maintain a very small difference between the indices of the glass rods and of the crystal. This presented a serious problem as the glass rods underwent a significant index change, of perhaps 1% during the drawing process. The extent of this index variation and its possible causes were investigated.

The principle of operation of the switch was demonstrated by building a very much simpler version in which an index-matching oil was used as the cladding and its refractive index was varied by heating. With this structure nearly 100% switching was achieved between the two fibres. The experiment provided data which supported the earlier theoretical work.

ACKNOWLEDGEMENTS

I am grateful to Dr J R Cozens and Mr R B Dyott, without whose enthusiasm this project would never have started, and also to Dr J C Williams and Mr M F Stonefrost, without whose perpetual encouragement it might never have been completed.

On a more practical level, my thanks go to Mr D G Morris for his technical assistance and Mr L W Boroff for his essential help with the glass apparatus.

In the interest of strengthening long-standing friendships, I feel obliged to thank Vince Handerek, Bimal Nayar and Faramarz Hossein-Babai for many lively and fruitful (technical) discussions.

Well deserved thanks go to Sue Wood who dealt most efficiently with the unenviable task of transforming my scribbles into neat typescript.

I cannot repay the love, patience and understanding of my parents who have foregone much in order to support me throughout my lengthy education.

Finally, I would like to thank my wife who has given me unwavering support even when her own work has been equally demanding.

CONTENTS PAGE

CHAPTER 1 : OPTICAL FIBRE COMMUNICATIONS

1.1 Introduction

The demand for more extensive communication has been rapidly increasing since the advent of the telephone a century ago. This has resulted in a continual search for larger bandwidths, traditionally achieved by extending carrier frequencies ever upward. This trend, however, reaches something of an impasse in the vicinity of microwave frequencies. The problem is of a very fundamental nature. Classical electronic methods of signal detection tend to rely on assumptions about negligible electron transit times and also low capacitances of junctions etc. As frequencies rise above, say, GHz, these assumptions become progressively less valid, leading to rather acute practical problems. The paradox is that while these frequencies are 'high' by conventional standards, the quantum energy, $h\nu$, is still extremely small when compared with, say, chemical bond energies or even kT at room temperature. Thus we find that the higher microwave frequencies are becoming embarrassingly high for conventional techniques but are still too small to allow the use of quantum detectors.

In these circumstances a break from the conventional step by step progression through the frequency scale seems inevitable; a leap in carrier frequency across the sub-millimetre and far infra-red bands to the near infra-red and visible, where quantum energies are orders of magnitude higher, offers enormous advantages.

Research in lightwave communication began in earnest after the advent of the laser in 1960 (1). After some early wildly optimistic estimates of useful bandwidth, a more sober assessment of potential developed. The outstanding problem was clearly associated with the transmission medium. Free space propagation of optical signals was not a very practical solution since it would be limited to line of sight operation and severely handicapped by atmospheric changes. Following a proposal in 1966 by Kao and Hockham (2) that low loss glass fibres could be used as the transmission medium, research programs on glass fibres were launched by several organisations. These have now led to the development of optical fibres with losses reduced from the initial value of over 1000 dB/km to 0.2 dB/km (3). Low attenuation is not, however, the only significant property of a fibre lightguide.

The dispersive characteristics of the fibre, which influence pulse broadening and hence capacity, are also of great importance. In the next section we examine, in brief, the various types of optical fibre and outline their main characteristics.

1.2 Optical Fibre Waveguides

In its simplest form an optical fibre consists of a cylindrical glass core surrounded by a cladding of a somewhat lower refractive index, Fig (1.1). When the core radius is very much larger than a wavelength we can think of light waves in the fibre as rays that propagate by undergoing a series of total internal reflections at the core-cladding interface (4), Fig (1.2). The complete analysis of wave propagation in fibres is achieved by solving Maxwell's equations for propagation in the core and cladding regions with appropriate boundary conditions imposed on these solutions (5, 6). The results show that the fibre is generally capable of supporting many modes of propagation. Following the tradition of microwave engineering, the principal characteristics of a fibre can be schematically represented on an ω-β diagram (7), Fig (1.3). Each mode is represented by a line whose slope, $d\omega/d\beta$, at any point gives the group velocity of the mode. The two dotted lines represent the propagation of plane waves through bulk materials with indices n_1 and n_2. The diagram also shows that single-mode operation of the fibre is possible. In order to achieve this, however, we need very small values of the core radius - typically only a few microns.

It can be seen from the ω-β diagram that at any frequency different modes generally have different group velocities. When a pulse of light is launched into such a multimode fibre all the modes will be excited, each carrying some of the energy of the pulse. Since these modes do not have the same group velocity they arrive at the far end of the fibre at different times. This broadens the pulse thus reducing the maximum repetition rate of the pulses and hence the bandwidth. For a 10 km repeater spacing, for example, the maximum bandwidth of a step-index multimode fibre, with a GaAs laser source, is only about 20M bits/sec (8). For the same conditions a single-mode fibre has a bandwidth of about 5G bits/sec (8). Single mode fibres, however, have other problems associated with them. Launching light into single-mode

fibres and also butt-jointing two such fibres pose rather serious problems of alignment since the core radius is only a few microns. These difficulties have retarded the introduction of single-mode fibres into telecommunications.

In order to overcome the pulse spreading problem associated with step-index multimode fibres, the graded index fibre was developed (6). The index profile of this fibre is very nearly parabolic with a maximum at the core centre, Fig (1.4). This results in the approximate equalisation of the group velocities of all the modes. By sophisticated design of the index profile one can theoretically have bandwidths of up to 1.4G bits/sec for a 10 km repeater spacing. In practice bandwidths of about 100M bits/sec have already been achieved for the same repeater spacing. Graded index fibres, therefore, combine relatively large bandwidths with ease of launching and jointing. For these reasons the majority of the existing fibre links for communication purposes use graded index fibres.

1.3 Wave Propagation in Optical Fibres

The optical field equations within the fibre are required in later chapters for analysing the operation of the coupler. A derivation of these equations is given in this section. We begin with the wave equation, in cylindrical polar coordinates, for a homogeneous medium (6), Fig (1.5),

$$\nabla^2 A = \frac{1}{r}\frac{\partial}{\partial r}\left(r\frac{\partial A}{\partial r}\right) + \frac{1}{r^2}\frac{\partial^2 A}{\partial \phi^2} + \frac{\partial^2 A}{\partial^2 z} = \mu\mu_o\varepsilon\varepsilon_o\frac{\partial^2 A}{\partial t^2} \qquad (1.1)$$

where, A can be either the electric or the magnetic field. We now postulate a solution of the following general form

$$A = F_1(r)F_2(\phi)F_3(z)F_4(t) \qquad (1.2)$$

Since we expect the field to be a travelling wave in the positive z direction we try solutions for the z and t dependence of the form

$$F_3(z)F_4(t) = \exp i\,(\omega t - \beta z) \qquad (1.3)$$

where, β is the propagation constant in the z direction. Furthermore since we want the fields to be periodic in ϕ with the period 2π we try for

$$F_2(\phi) = \exp(i\nu\phi) \qquad (1.4)$$

where, ν can be a positive or a negative integer.
Substituting (1.2), (1.3) and (1.4) in (1.1) gives

$$\frac{d^2F_l}{dr^2} + \frac{1}{r}\frac{dF_l}{dr} + (\kappa^2 - \frac{\nu^2}{r^2})F_l = 0 \qquad (1.5)$$

where, $\kappa^2 = \omega^2\varepsilon\varepsilon_o\mu\mu_o - \beta^2 = n^2k_o^2 - \beta^2$

and $k_o = \frac{2\pi}{\lambda_o}$ is the free space wave vector.

Since κ^2 might be negative we introduce the symbol γ, which is related to κ as follows:

$$\kappa = i\gamma$$

Equation (1.5) can, therefore, take one of the following forms

$$\frac{d^2F_l}{dr^2} + \frac{1}{r}\frac{dF_l}{dr} + (\kappa^2 - \frac{\nu^2}{r^2})F_l = 0 \qquad (1.6)$$

or

$$\frac{d^2F_l}{dr^2} + \frac{1}{r}\frac{dF_l}{dr} - (\gamma^2 + \frac{\nu^2}{r^2})F_l = 0 \qquad (1.7)$$

Equations (1.6) and (1.7) are both Bessel equations and the general solutions to them consist of pairs of cylinder functions. For guided modes the solutions inside the core must remain finite at $r = 0$, while the solutions in the cladding must decay for $r \to \infty$. With these points in mind we choose the Bessel function $J_\nu(\kappa r)$ for the core solution and the Hankel function $H_\nu^{(1)}(i\gamma r)$ to represent the field in the cladding (5). We have, therefore, inside the core, ie for $r < a$

$$E_z = AJ_\nu(\kappa r)\exp(i\nu\phi)\exp i(\omega t - \beta z) \qquad (1.8)$$

and

$$H_z = BJ_\nu(\kappa r)\exp(i\nu\phi)\exp i(\omega t - \beta z) \qquad (1.9)$$

where, $\kappa^2 = n_1^2k_o^2 - \beta^2$ (1.10)

And for the cladding, ie $r > a$

$$E_z = CH_\nu^{(1)}(i\gamma r)\exp(i\nu\phi)\exp i(\omega t - \beta z) \qquad (1.11)$$

and

$$H_z = DH_\nu^{(1)}(i\gamma r)\exp(i\nu\phi)\exp i(\omega t - \beta z) \qquad (1.12)$$

where, $\gamma^2 = \beta^2 - n_2^2k_o^2$ (1.13)

The remaining field components are readily derived from the z components (5). For $r < a$ and omitting the two exponential terms (1.3) and (1.4) which are common to all the field equations we obtain

$$E_r = -\frac{i}{\kappa^2}[\beta\kappa A J'_\nu(\kappa r) + i\omega\mu_o \frac{\nu}{r} B J_\nu(\kappa r)] \tag{1.14}$$

$$E_\phi = -\frac{i}{\kappa^2}[i\beta\frac{\nu}{r} A J_\nu(\kappa r) - \kappa\omega\mu_o B J'_\nu(\kappa r)] \tag{1.15}$$

$$H_r = -\frac{i}{\kappa^2}[-i\omega\varepsilon_1\frac{\nu}{r} A J_\nu(\kappa r) + \kappa\beta B J'_\nu(\kappa r)] \tag{1.16}$$

$$H_\phi = -\frac{i}{\kappa^2}[\kappa\omega\varepsilon_1 A J'_\nu(\kappa r) + i\beta\frac{\nu}{r} B J_\nu(\kappa r)] \tag{1.17}$$

And for $r > a$

$$E_r = -\frac{1}{\gamma^2}[\beta\gamma C H^{(i)\prime}_\nu(i\gamma r) + \omega\mu_o\frac{\nu}{r} D H^{(i)}_\nu(i\gamma r)] \tag{1.18}$$

$$E_\phi = -\frac{1}{\gamma^2}[\beta\frac{\nu}{r} C H^{(i)}_\nu(i\gamma r) - \gamma\omega\mu_o D H^{(i)\prime}_\nu(i\gamma r)] \tag{1.19}$$

$$H_r = -\frac{1}{\gamma^2}[-\omega\varepsilon_2\frac{\nu}{r} C H^{(i)}_\nu(i\gamma r) + \gamma\beta D H^{(i)\prime}_\nu(i\gamma r)] \tag{1.20}$$

$$H_\phi = -\frac{1}{\gamma^2}[\gamma\omega\varepsilon_2 C H^{(i)\prime}_\nu(i\gamma r) + \beta\frac{\nu}{r} D H^{(i)}_\nu(i\gamma r)] \tag{1.21}$$

In equations (1.14) to (1.21) the prime indicates differentiation with respect to the argument, ie κr for the Bessel functions and $i\gamma r$ for the Hankel functions. The constants A, B, C, D and the value of β are determined by taking into account the boundary conditions. These require that the tangential field components are continuous at $r = a$, ie E_ϕ, E_z, H_ϕ and H_z must have the same value on the inside and outside the fibre core at $r = a$. Implementing these requirements with the help of equations (1.8), (1.9), (1.11), (1.12), (1.15), (1.17), (1.19) and (1.21) results in the following system of equations

$$A J_\nu(\kappa a) \qquad\qquad -C H^{(i)}_\nu(i\gamma a) \qquad\qquad = 0 \tag{1.22}$$

$$\frac{\beta}{\kappa^2}\frac{\nu}{a} A J_\nu(\kappa a) + \frac{i\omega\mu_o}{\kappa} B J'_\nu(\kappa a) + \frac{\beta}{\gamma^2}\frac{\nu}{a} C H^{(i)}_\nu(i\gamma a) - \frac{\omega\mu_o}{\gamma} D H^{(i)\prime}_\nu(i\gamma a) = 0 \tag{1.23}$$

$$B J_\nu(\kappa a) \qquad\qquad -D H^{(i)}_\nu(i\gamma a) = 0 \tag{1.24}$$

$$-\frac{i\omega\varepsilon_1}{\kappa} A J'_\nu(\kappa a) + \frac{\beta}{\kappa^2}\frac{\nu}{a} B J_\nu(\kappa a) + \frac{\omega\varepsilon_2}{\gamma} C H^{(i)\prime}_\nu(i\gamma a) + \frac{\beta}{\gamma^2}\frac{\nu}{a} D H^{(i)}_\nu(i\gamma a) = 0 \tag{1.25}$$

Equations (1.22) and (1.24) can be used to connect the coefficients A, C and B, D

$$C = \frac{J_\nu(\kappa a)}{H_\nu^{(1)}(i\gamma a)} A \tag{1.26}$$

and

$$D = \frac{J_\nu(\gamma a)}{H_\nu^{(1)}(i\gamma a)} B \tag{1.27}$$

Similarly A and B can be connected using (1.25), (1.26) and (1.27)

$$B = \frac{i}{\nu} \frac{a\kappa\gamma[\varepsilon_1\gamma J'_\nu(\kappa a)H_\nu^{(1)}(i\gamma a) + i\varepsilon_2\kappa J_\nu(\kappa a)H_\nu^{(1)'}(i\gamma a)]}{\omega(\varepsilon_1-\varepsilon_2)\mu_o\beta J_\nu(\kappa a)H_\nu^{(1)}(i\gamma a)} \tag{1.28}$$

The relation

$$\kappa^2 + \gamma^2 = k_1^2 - k_2^2 = \omega^2(\varepsilon_1 - \varepsilon_2)\mu_o$$

was used to simplify this expression.

In order to obtain a non-trivial solution to the system of equations (1.22) to (1.25) we must set the determinant of the coefficients equal to zero.

$$\begin{vmatrix} J_\nu(\kappa a) & 0 & -H_\nu^{(1)}(i\gamma a) & 0 \\ \frac{\nu}{a}\frac{\beta}{\kappa^2}J_\nu(\kappa a) & i\frac{\omega\mu_o}{\kappa}J'_\nu(\kappa a) & \frac{\nu}{a}\frac{\beta}{\gamma^2}H_\nu^{(1)}(i\gamma a) & -\frac{\omega\mu_o}{\gamma}H_\nu^{(1)'}(i\gamma a) \\ 0 & J_\nu(\kappa a) & 0 & -H_\nu^{(1)}(i\gamma a) \\ -i\frac{\omega\varepsilon_1}{\kappa}J'_\nu(\kappa a) & \frac{\nu}{a}\frac{\beta}{\kappa^2}J_\nu(\kappa a) & \frac{\omega\varepsilon_2}{\gamma}H_\nu^{(1)'}(i\gamma a) & \frac{\nu}{a}\frac{\beta}{\gamma^2}H_\nu^{(1)}(i\gamma a) \end{vmatrix} = 0 \tag{1.29}$$

Evaluation of the determinant results in the eigenvalue equation

$$\left(\frac{\varepsilon_1}{\varepsilon_2}\frac{a\gamma^2}{\kappa}\frac{J'_\nu(\kappa a)}{J_\nu(\kappa a)} + i\gamma a\frac{H_\nu^{(1)'}(i\gamma a)}{H_\nu^{(1)}(i\gamma a)}\right)\left(\frac{a\gamma^2}{\kappa}\frac{J'_\nu(\kappa a)}{J_\nu(\kappa a)} + i\gamma a\frac{H_\nu^{(1)'}(i\gamma a)}{H_\nu^{(1)}(i\gamma a)}\right) = \left[\nu\left(\frac{\varepsilon_1}{\varepsilon_2} - 1\right)\frac{\beta k_2}{\kappa^2}\right]^2 \tag{1.30}$$

The propagation constant, β, is determined by a numerical solution of this equation which requires the core radius, a, and the dielectric constants, ε_1 and ε_2, of the core and the cladding as inputs. The dielectric constants are related to be refractive indices, n_1 and n_2, of the core and the cladding by the following equations

$$\varepsilon_1 = \varepsilon_o n_1^2$$

and

$$\varepsilon_2 = \varepsilon_o n_2^2$$

In general a fibre can support many modes of propagation, corresponding to different values of ν in (1.30). An important parameter for each mode is its cut-off frequency. A mode is called cut-off when its field no longer decays on the outside of the core. The rate of decay of the field with increasing r is determined by the value of the constant γ. The function $H_\nu^{(1)}(i\gamma r)$ decays like an exponential function for large values of its argument. The asymptotic approximation for large argument is (9)

$$H_\nu^{(1)}(i\gamma r) = \sqrt{2/\pi i\gamma r}\ \exp -i(\pi\nu/2 + \pi/4)\ \exp(-\gamma r) \qquad (1.31)$$

$$\text{for } \gamma r >> 1$$

For large values of γ the field is tightly concentrated inside and close to the core. With decreasing values of γ, the field reaches further out into the space outside the core. Finally for $\gamma = 0$, the field detaches itself from the guide. The frequency at which this happens is called the cut-off frequency. The cut-off condition is thus

$$\gamma = \sqrt{\beta^2 - n_2^2 k_o^2} = 0 \qquad \text{ie: } \beta = n_2 k_o \qquad (1.32)$$

This is the propagation constant of a plane wave travelling in a material of refractive index n_2. It confirms that the fields are no longer bound to the core.

From equations (1.10) and (1.13)

$$\kappa^2 + \gamma^2 = k_o^2(n_1^2 - n_2^2) \qquad (1.33)$$

At cut-off $\gamma = 0$ and $\kappa = \kappa_c$, ie

$$\kappa_c = k_o\sqrt{n_1^2 - n_2^2}$$

or

$$a\kappa_c = V = \frac{2\pi a}{\lambda}\sqrt{n_1^2 - n_2^2} \qquad (1.34)$$

where, a is the core radius.

V is called the normalised frequency of the fibre and is clearly related to the cut-off condition. For $V < 2.405$ the fibre can support only the HE_{11} mode, ie we have a single-mode fibre (5, 6). As V increases beyond 2.405 the fibre becomes progressively more multimode. For large values of V the number, N, of the propagating modes in the fibre is given by (6)

$$N \simeq \frac{V^2}{2} \qquad (1.35)$$

for $V >> 1$

1.4 Operating Wavelength And Modulation

The majority of the first generation of optical fibre links use GaAs based sources and operate at a wavelength near 0.83 μm. There is, however, a growing interest in sources and detectors for operation in the wavelength range 1.3 - 1.6 μm. Near 1.3 μm material dispersion can be made vanishingly small (10), thus reducing pulse broadening and increasing the bandwidth-repeater spacing product of the fibre. On the other hand, the lowest fibre losses occur at $\lambda \simeq 1.55$ μm (3). Operating at $\lambda \simeq 1.3$ or 1.55 μm will, therefore, allow larger bandwidths and/or longer distances between repeaters to be used. In order to benefit from these advantages, the second generation of optical fibre links are already being developed for operation at $\lambda \simeq 1.3$ - 1.6 μm.

The majority of optical communication systems developed for use in telecommunications carry their information in a two-level binary form (6). This digital modulation is achieved in most cases by modulating the source directly. There is, however, a strong case to be made for using external modulators in some systems. The most important of these are perhaps coherent optical communication systems which are currently receiving considerable attention (11). The main attraction of using a heterodyne type receiving technique is the significant improvement that can be obtained in the equivalent receiver sensitivity. This can be over 20 dB for $\lambda \simeq 1.55$ μm and is particularly important since for this wavelength silica fibre losses are at their lowest (~0.2 dB/km) and good detectors for direct detection are not available (3, 11). A 20 dB improvement in detector sensitivity will allow the repeater spacing to be increased by 100 km when the fibre loss is 0.2 dB/km.

In a heterodyne system one beats a local oscillator (eg a second laser) with the incoming signal to obtain an intermediate frequency, IF, typically 0.2 - 2 GHz, which contains the information. Since the IF frequency is about 10^5 - 10^6 times smaller than the carrier frequency (typically 200 THz) a very high degree of frequency stability is required. Extensive research aimed at developing highly wavelength selective semiconductor lasers has been in progress for many years. This has led to significant advances in the development of distributed feedback lasers (31) and injection locking techniques for semiconductor lasers (32). Nevertheless the realisation of a practical device with a sufficiently high degree of frequency stability is still many years away. Currently available semiconductor lasers can, however, be made to operate with a highly stable wavelength and narrow linewidth. This requires the drive current and/or the temperature of the laser to be accurately controlled using feedback loops (11). The laser must, therefore, be run cw and external modulation will have to be used.

External modulators are also needed for applications where very fast modulation speeds, eg >10 GHz, are required. The maximum practical analogue modulation frequency of currently available laser diodes is about 5 GHz (12). This frequency is limited by a combination of laser-relaxation resonance, laser parasitics and drive current necessary for long-life operation (12). On the other hand, external modulators have already been demonstrated with modulation speeds extending to 18 GHz (29), and are theoretically capable of frequencies in excess of 60 GHz (30). Such extremely high frequencies, while unlikely to be necessary in telecommunications, would be of great value in microwave and radar applications.

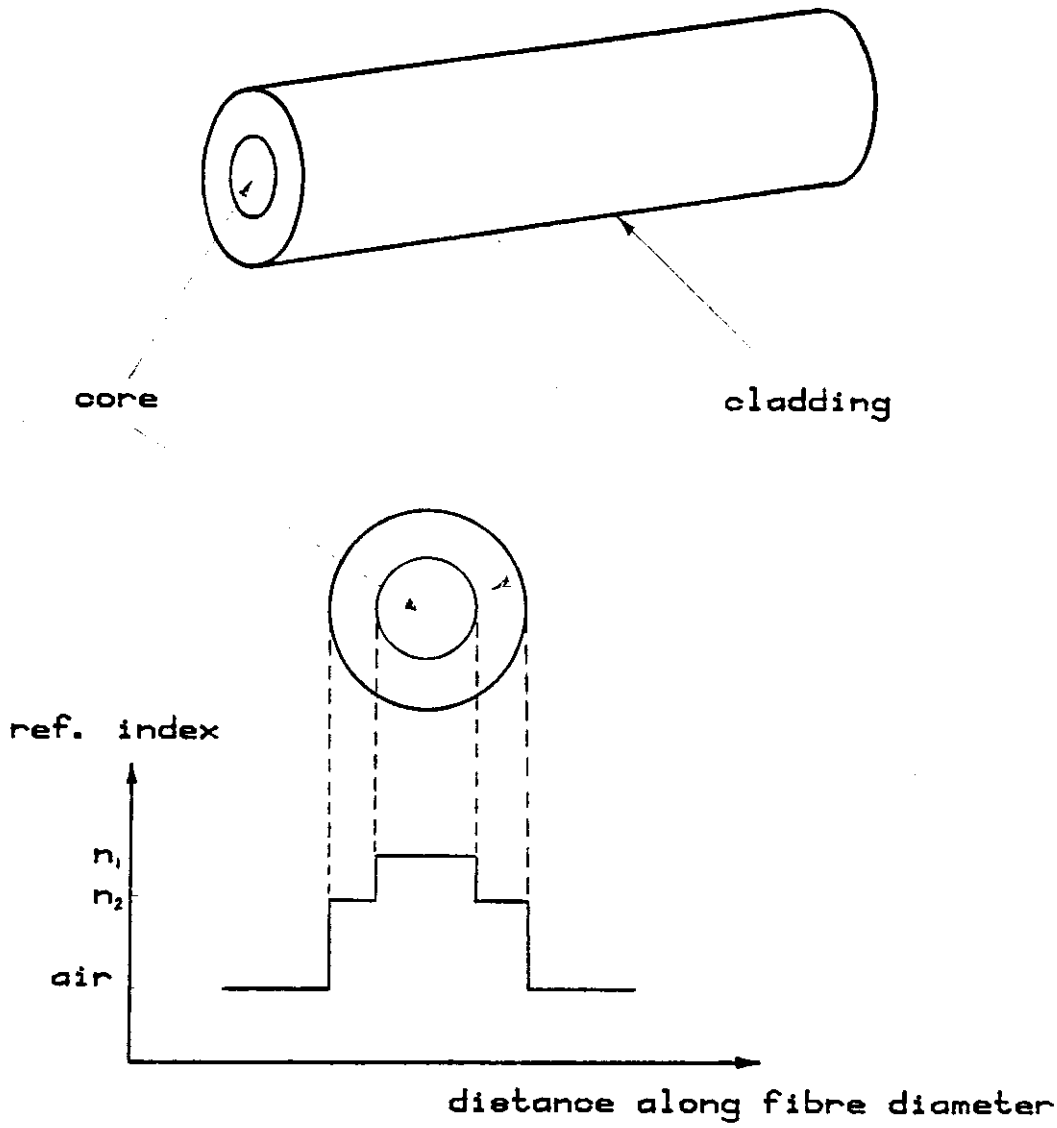

FIG[1.1] Step index multimode fibre.

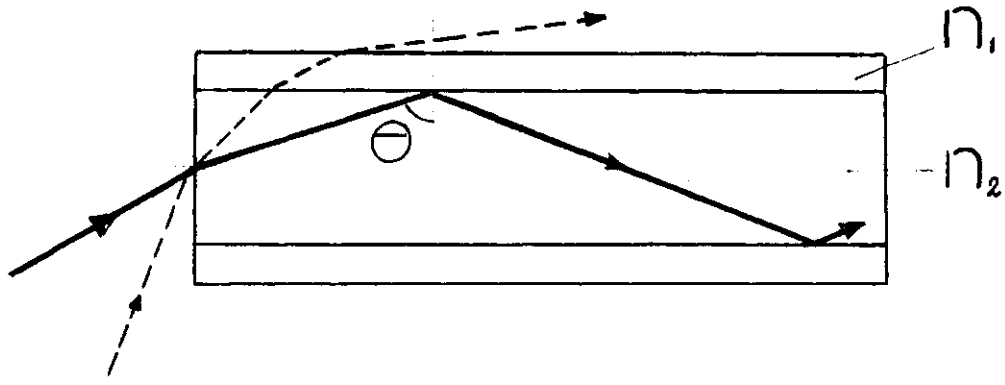

$$\theta > \sin^{-1}(n_1/n_2)$$

FIG[1.2] Ray diagram for a step index multimode fibre.

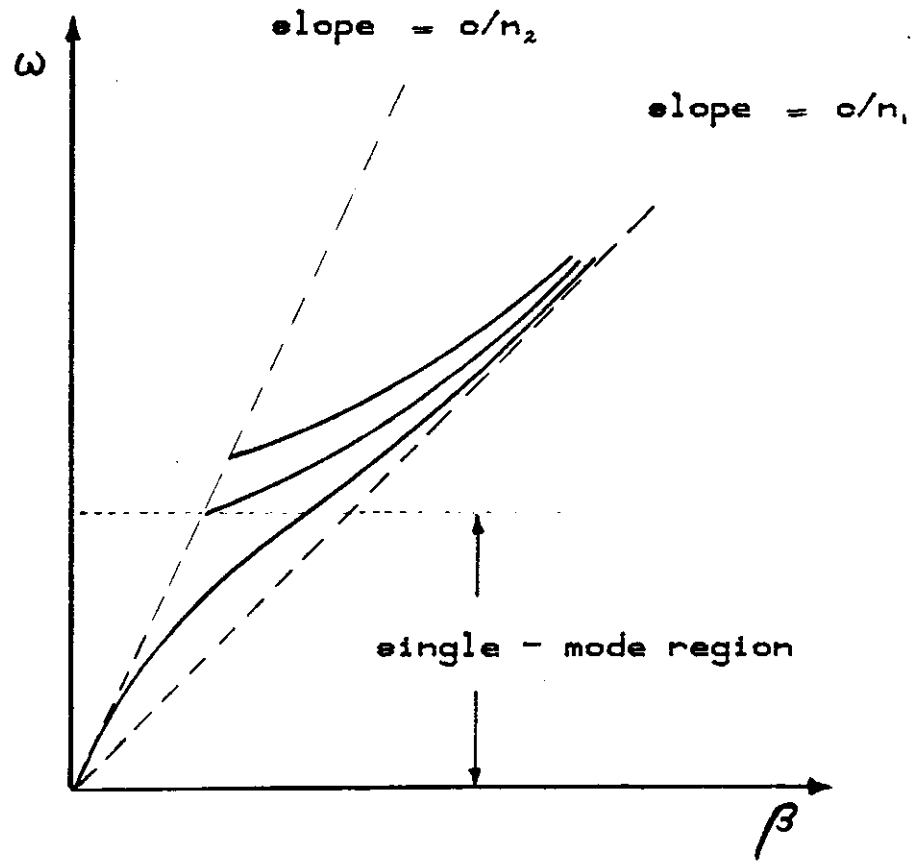

FIG[1.3] Schematic ω-β diagram for a multimode fibre.

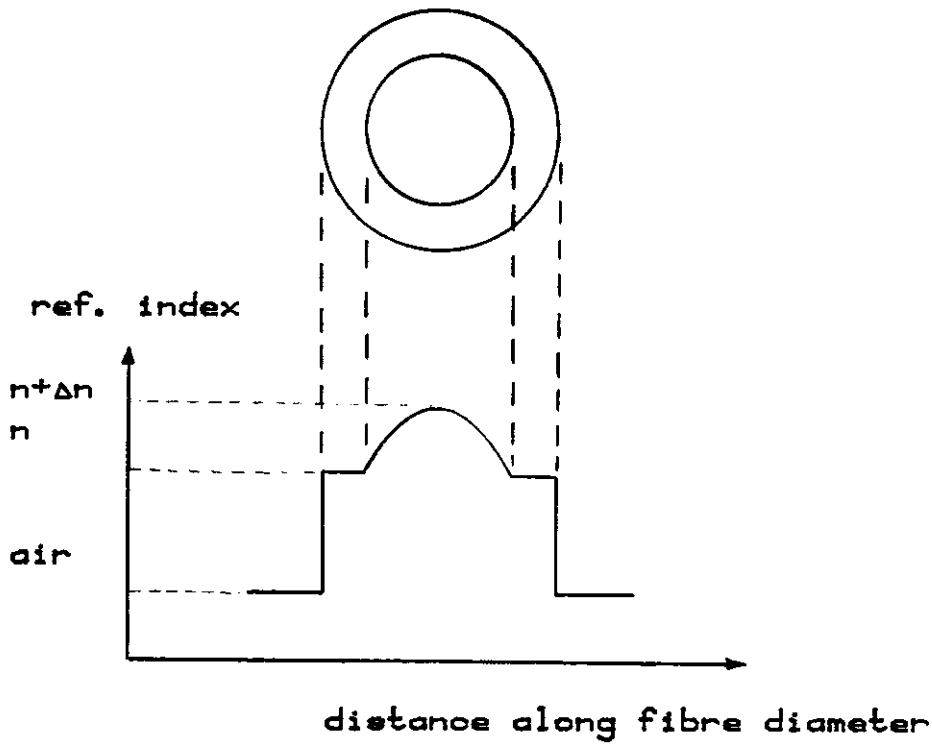

FIG[1.4] Refractive index profile in a graded index fibre.

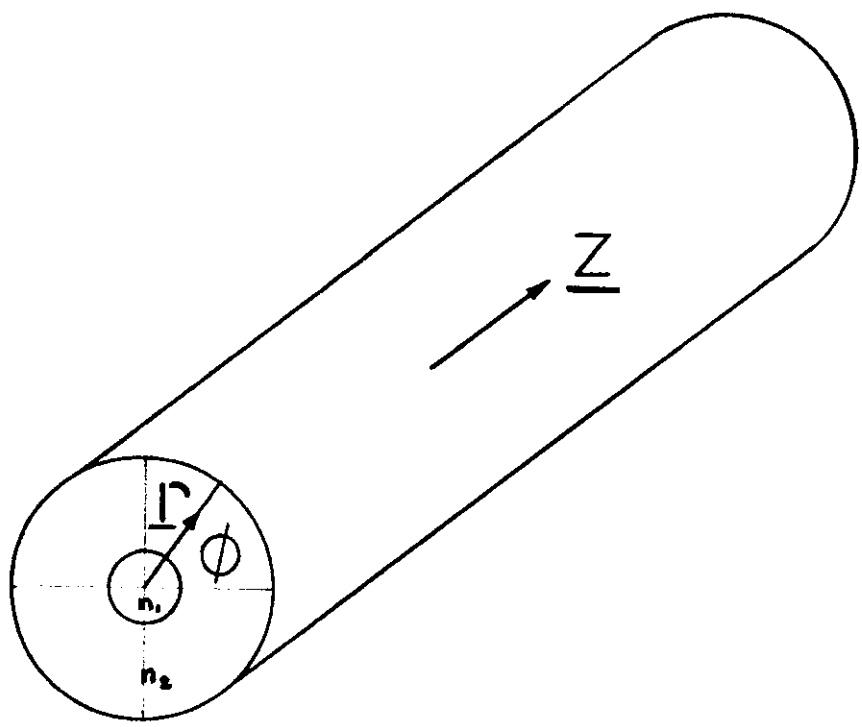

FIG[1.5] Cylindrical polar coordinates for an optical fibre.

CHAPTER 2 : EXTERNAL MODULATORS

2.1 Introduction

In order to convey information on an optical wave it is necessary to modulate some property of the wave in accordance with the information signal (8). Analogue or digital techniques could be used to modulate the wave intensity, phase, frequency, polarisation or direction. The choices are dictated by the characteristics of the transmission medium, the availability of sources and detectors, and by systems considerations. Probably the main attraction of analogue modulation is its simplicity. But the large signal to noise ratios required limit its use to relatively narrow bandwidth, short distance applications (15). Digital modulation provides noise immunity at the expense of large bandwidth. It is, therefore, ideally suited to fibre transmission where the available bandwidths are large.

The majority of the existing fibre links developed for telecommunications use digital intensity modulation and direct detection. Since the present systems have been geared to this mode of operation any external modulator intended for use in a fibre telecommunication link must be capable of producing digital intensity modulation of the light wave.

The optical wave property that lends itself most readily to external modulation by a number of physical effects is the phase. Once phase modulation is realised, intensity, polarisation or direction variations can be achieved with passive components. The most commonly used physical effects in external modulators are the electro-optic, magneto-optic and acousto-optic effects whereby the refractive index n of a transparent medium is changed by Δn in proportion to an applied electric field, magnetisation or strain respectively. Each of these effects serves to change the phase of the optical carrier passing through a length L of the material by $2\pi\Delta nL/\lambda$ where λ is the optical wavelength. Intensity modulation is obtained by interfering a phase modulated wave with an unmodulated wave or by combining two waves modulated in phase opposition.

External modulators can be divided into two broad categories; bulk and waveguide modulators. Bulk modulators have simple structures but since their dimensions are limited by diffraction effects, their

modulating power efficiencies can be poor. Furthermore, very little attention has been paid, so far, to the problem of efficient coupling of modulators to sources and fibres. On the other hand, waveguide devices have the potential advantages of ease of fabrication using photolithographic techniques and compatibility with single-mode fibres. In addition, because diffraction effects do not limit the modulator dimensions, their modulating power efficiencies can be orders of magnitude better than bulk devices. This ability to operate with a low drive power becomes particularly important at high modulation speeds (eg > a few GHz) where large amounts of rf power are not readily available.

One type of waveguide modulator that has received considerable attention in recent years is the optical directional coupler. Before we discuss the operation of this device a brief review of the underlying theory of two coupled waveguides is given.

2.2 Coupling Between Two Parallel Waveguides

The fields of a dielectric waveguide are not fully contained inside the core, but they reach out into the outside region where they decay exponentially. If two such waveguides are placed close enough to one another to ensure some overlap of these evanescent fields, coupling will take place between them. The wave amplitudes a_1 and a_2, in guides 1 and 2 respectively, are related to one another through the following simultaneous equations (5):

$$\frac{\partial a_1}{\partial z} = -i\beta_1 a_1 + ic_1 a_2 \qquad (2.1)$$

$$\frac{\partial a_2}{\partial z} = -i\beta_2 a_2 + ic_2 a_1 \qquad (2.2)$$

where, β_1 = propagation constant in guide 1
β_2 = propagation constant in guide 2
c_1 = coupling coefficient of guide 2 to guide 1
c_2 = coupling coefficient of guide 1 to guide 2

The derivation of (2.1) and (2.2) will be given in the next chapter, but the equations have such a clear intuitive meaning that it is possible to write them down without derivation. Note, for example, that in the absence of coupling, ie $c_1 = c_2 = 0$, the equations are reduced to:

$$\frac{\partial a_1}{\partial z} = -i\beta_1 a_1 \tag{2.3}$$

$$\frac{\partial a_2}{\partial z} = -i\beta_2 a_2 \tag{2.4}$$

Giving,

$$a_1 = A_1 e^{-i\beta_1 z} \tag{2.5}$$

and

$$a_2 = A_2 e^{-i\beta_2 z} \tag{2.6}$$

where A_1 and A_2 are the constant field amplitudes in the two guides. Equations (2.5) and (2.6) represent the spatial variation of the fields in the two guides along the fibre lengths. The terms $c_1 a_2$ and $c_2 a_1$ in equations (2.1) and (2.2) represent the effect of each guide on the other. If the waveguide materials are not lossy c_1 and c_2 will both be real and furthermore they must be equal for conservation of power between the two guides (5).

When there is coupling between the guides we must allow A_1 and A_2 to become functions of z. With this in mind we can use equations (2.5) and (2.6) to write equations (2.1) and (2.2) in a different form:

$$\frac{\partial A_1}{\partial z} = ic_1 A_2 \exp i(\beta_1 - \beta_2)z \tag{2.7}$$

$$\frac{\partial A_2}{\partial z} = ic_2 A_1 \exp -i(\beta_1 - \beta_2)z \tag{2.8}$$

where, A_1 and A_2 are now functions of z.

It is easy to see that substantial amounts of power can be transferred only if $\beta_1 = \beta_2$. Let us assume that $A_2 = 0$ at $z = 0$. We then obtain from (2.8) and after an interaction length L

$$A_2(L) = ic_2 \int_0^L A_1(z) \exp -i(\beta_1 - \beta_2)\, dz \tag{2.9}$$

If $\beta_1 - \beta_2 \neq 0$, the function $A_1(z)$ is multiplied by $\exp -i(\beta_1 - \beta_2)z$ which is a rapidly oscillating function and prevents any appreciable build up of the integral (2.9). However, if $\beta_1 - \beta_2 = 0$, the integral grows proportional to L (at least initially when $A_1(z)$ has not yet changed very much). This consideration shows that $A_2(z)$ can obtain appreciable values only if the propagation constants of the two guides are the same.

If the two guides are identical and loss-less, ie $\beta_1 = \beta_2$ and $c_1 = c_2 = c$ and if initially only guide 1 is excited - ie $A_2(0) = 0$ - equations (2.7) and (2.8) have the following solutions:

$$A_1(z) = A_1(0) \cos (cz) \tag{2.10}$$

$$A_2(z) = iA_1(0) \sin (cz) \tag{2.11}$$

Since the power, P, in each guide is proportional to $|A|^2$ we get from (2.10) and (2.11)

$$P_1(z) = P_1(0) \cos^2 (cz) \tag{2.12}$$

$$P_2(z) = P_1(0) \sin^2 (cz) \tag{2.13}$$

where, $P_1(z)$ = power in guide 1
$P_2(z)$ = power in guide 2

Equations (2.12) and (2.13) show clearly that energy is continuously exchanged between the two waveguides.

Any light launched into guide 1 at $z = 0$ will be completely transferred to guide 2 over a length z given by $z = \pi/2c$. The length over which a complete cycle of energy transfer takes place is called the beatlength, λ_B, and is clearly given by

$$\lambda_B = \frac{\pi}{c} \tag{2.14}$$

We have, therefore, shown that if two coupled waveguides have significantly different propagation constants, no appreciable exchange of energy can take place between them. If the two waveguides are synchronous, there will be a periodic exchange of power between them with a periodicity λ_B given by equation (2.14).

2.3 Electro-Optical Directional Couplers

These will probably be the fundamental building blocks of the future electro-optical signal processing devices. They can be used either for modulating the light or switching it from one channel to another. Fig (2.1a) schematically shows the construction of a simple version of an electro-optical directional coupler.

The device consists of a z-cut lithium niobate substrate into which titanium channels are diffused to form the waveguides (16). An electric field can be applied to the device via the electrodes which are deposited on top of the waveguides.

In the absence of an applied electric field, the propagation constants of the two waveguides are equal and the power coupled from the input waveguide to the adjacent channel varies sinusoidally with the length of the coupler. The device is constructed such that the coupler length is an odd multiple of half beatlengths. This means that any power launched into one guide emerges from the adjacent guide.

In order to switch the power back to the first guide, an electric potential difference is applied to the electrodes. This will have opposite effects on the two guides, Fig (2.1b); increasing the index of one and reducing that of the other. As a result the two guides will no longer be synchronous, ie $\beta_1 \neq \beta_2$. We showed in section 2.2 that no appreciable coupling can take place if the propagation constants of the two guides are not the same. The energy that was initially coupled to the second guide, therefore, couples back to the first guide. Removing the electric field allows the energy to couple to the second guide yet again.

The chief difficulty with the directional-coupler switch is that its dimensions must be carefully controlled in order that complete coupling from guide 1 to guide 2 takes place with no applied electric field; otherwise 100% switching cannot be realised. This difficulty has been overcome in the so-called $\Delta\beta$-switch by splitting the electrode pattern in two as in Fig (2.2) in order to introduce an additional degree of freedom. Analysis of this structure shows that complete switching is possible without the critical dimentional requirements (16).

These planar electro-optic couplers have several weak points; they are, for example, polarisation sensitive because of the anisotropy of $LiNbO_3$ and the fact that TE and TM modes have different coupling coefficients. This could cause problems if the modulator was used with a single-mode optical fibre, because light coupled from the fibre is likely to have an unknown elliptical polarisation (14) or

indeed no polarisation, and both TE and TM modes will be excited in the directional-coupler. Device performance, therefore, depends on identical processing of both polarisation states. In general the planar electro-optic directional-couplers do not possess polarisation-insensitive characteristics.

The other problems associated with these couplers include high propagation loss - compared to optical fibres - through the crystalline material of the waveguide and inefficient jointing to circular optical fibres due to mismatch of field patterns in the two structures.

We propose an alternative structure for an electro-optic coupler that will reduce, to a large extent, all the above-mentioned problems. Our device consists of two thin parallel glass rods embedded in an electro-optic crystal with electrodes deposited on the two sides of the crystal, Fig (2.3).

Before analysing the operation of the device let us consider the advantages it has over the couplers with planar geometry.

Since the guiding channels are glass, the propagation loss through this coupler can be made negligibly small. Simple and efficient jointing to optical fibres can be achieved since the structures and therefore the field patterns can be made very similar. Furthermore, it will be shown in the next chapter that the polarisation sensitivity of this coupler is very small indeed. This device does, however, have several problems mainly associated with fabrication. These will be discussed in later chapters.

The principle of operation of the new coupler is somewhat different from the previously mentioned couplers. Here, since the applied field affects the two guides in exactly the same way, they always stay in synchronism, ie $\beta_1 = \beta_2$. Applying the field, however, changes the coupling coefficient, c, and hence the beatlength, equation (2.14). One can, therefore, have the situation where a device that is N beatlengths long initially will become, in effect, $N + \frac{1}{2}$ beatlengths long when the correct voltage is applied to it, Fig (2.4). A half beatlength change in the effective length of the device would result

in a complete switch over of light from one fibre to the other. Removing the electric field switches the light back to the first guide.

Clearly the performance of the device depends very strongly on the magnitude of the change in the beatlength that can be achieved by applying a given voltage to the crystal.

A detailed analysis of the performance of the device as a function of the various parameters of the fibre and the crystal is given in Chapter 3.

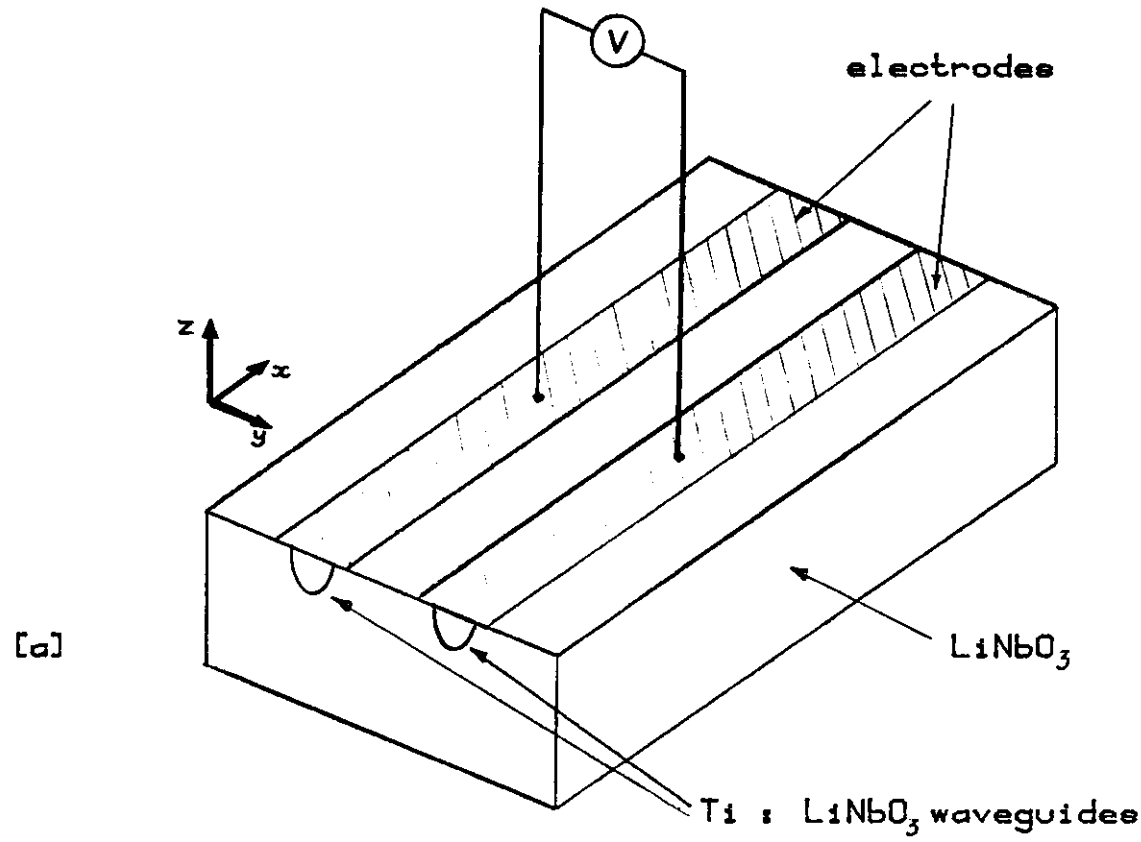

[a]

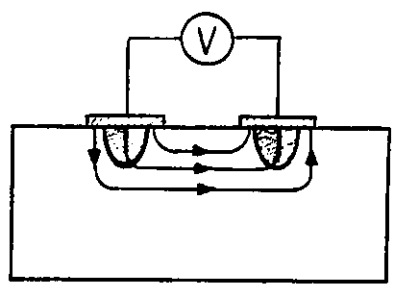

[b]

FIG[2.1] Integrated optic directional coupler switch modulator.

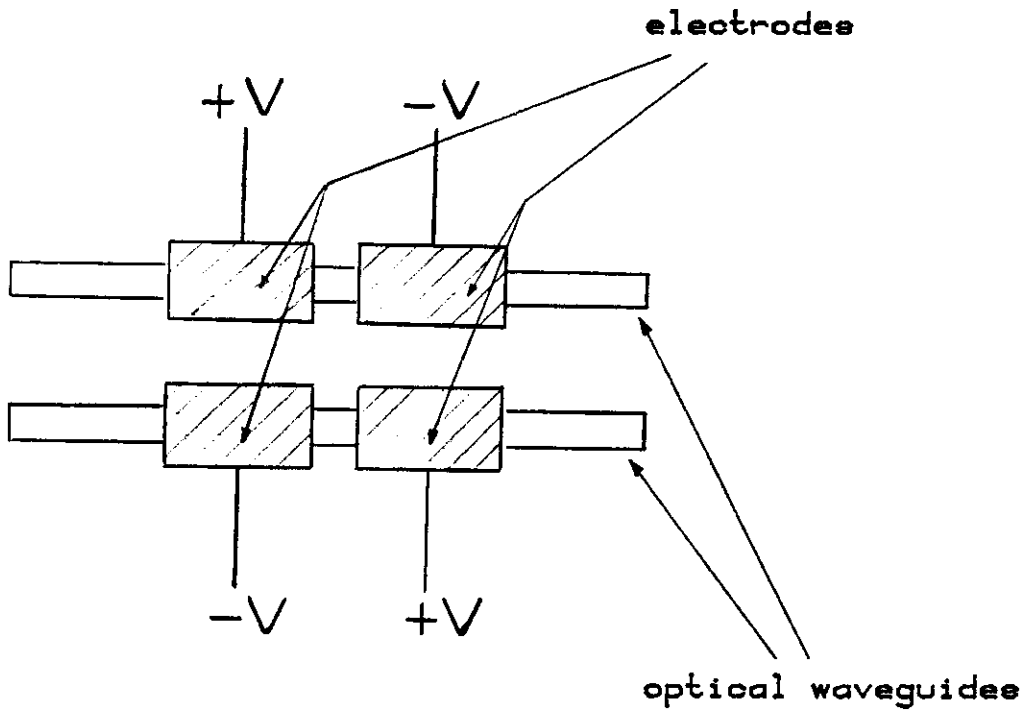

FIG[2.2] Electrode arrangement in the stepped $\Delta\beta$ reversal configuration.

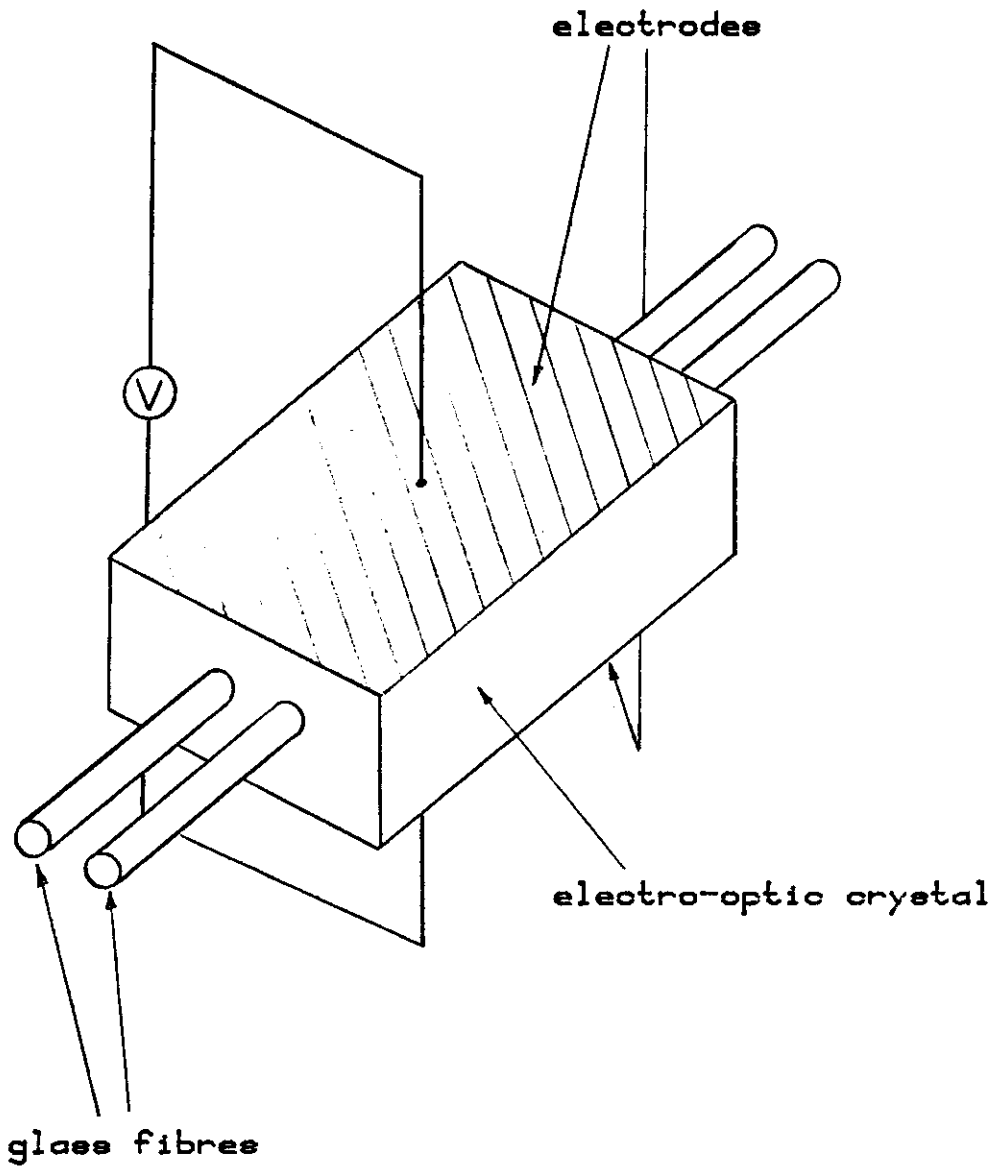

FIG[2.3] Schematic structure of the proposed coupler switch .

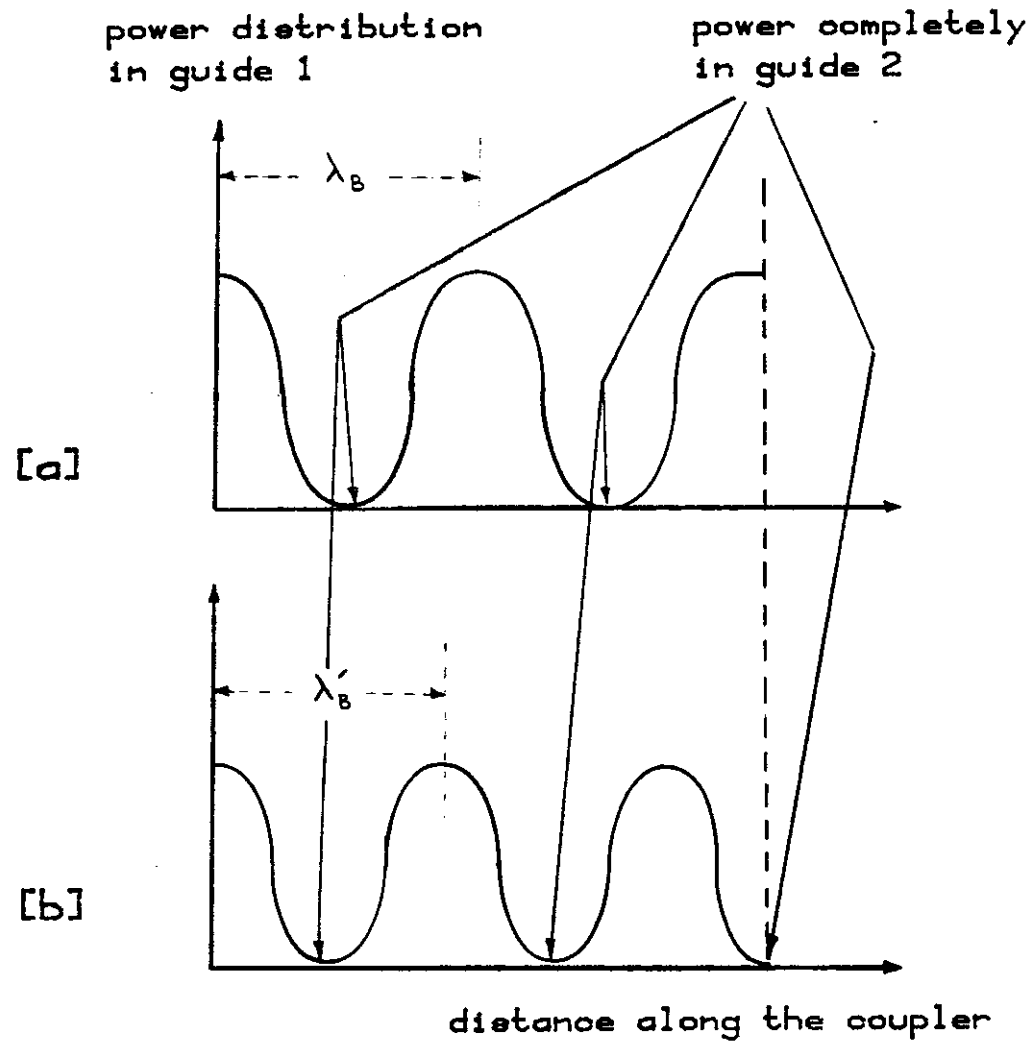

FIG[2.4] Schematic representation of the power distribution in the coupler [a] without and [b] with an applied electric field.

CHAPTER 3 : PERFORMANCE OF THE COUPLER SWITCH: A THEORETICAL INVESTIGATION

3.1 Introduction

In order to investigate the performance of the coupler, it is necessary to determine the coupling coefficients as a function of the normalised frequency of the fibres. Furthermore, it is necessary to establish the dependence of the coupling coefficients on the centre to centre separation of the fibres. We shall start by deriving the coupled wave equations (2.1) and (2.2). These will be used to determine the coupling between the HE_{11} modes of two round fibres. The results will then be used to predict the change in the refractive index of the cladding that is necessary for 100% switching. It will be shown that for the fibre-crystal combination that we have selected, the required index change is in the range 10^{-3} - 10^{-4}. For a more realistic value of, say 10^{-5}, only a few percent of the total power can be switched between the guides. It will also be shown that the coupler is virtually polarisation insensitive.

3.2 Coupled Wave Equations

The coupled wave equations (2.1) and (2.2) are quite general and apply to any two coupled waveguides. In this section we shall give an approximate derivation of these equations for the case of two arbitrary dielectric waveguides (5). Each waveguide consists of a dielectric medium with a maximum of the refractive index in the region of the waveguide and a constant value outside this region. The distributions of the square of the refractive indices of the two guides are shown in Fig (3.1) under the assumption that each exists by itself. If the waveguides are placed side by side, the square of the refractive index of the medium in which both guides are present can be expressed as

$$n^2 = (n_1^2 - n_3^2) + (n_2^2 - n_3^2) + n_3^2 \qquad (3.1)$$

where n_1^2 and n_2^2 are the index distributions shown in Fig (3.1a) and Fig (3.1b) respectively. Equation (3.1) gives the correct index distribution everywhere provided that the two waveguides do not overlap. We shall represent the fields of each guide in the absence of the other by subscripts 1 and 2 attached to the field quantities. We, therefore, have for each guide

$$\underset{\sim}{E}_\nu = \hat{\underset{\sim}{E}}_\nu \exp i\,(\omega t - \beta_\nu z) \qquad (3.2)$$

and

$$\underset{\sim}{H}_\nu = \hat{H}_\nu \exp i\ (\omega t - \beta_\nu z) \tag{3.3}$$

where, $\nu = 1, 2$. These fields satisfy Maxwell's equations in the following form

$$\underset{\sim}{\nabla}_t \times \underset{\sim}{H}_\nu - i\beta_\nu(\hat{z} \times \underset{\sim}{H}_\nu) - i\omega\varepsilon_o n_\nu^2 \underset{\sim}{E}_\nu = 0 \tag{3.4}$$

$$\underset{\sim}{\nabla}_t \times \underset{\sim}{E}_\nu - i\beta_\nu(\hat{z} \times \underset{\sim}{E}_\nu) + i\omega\mu_o \underset{\sim}{H}_\nu = 0 \tag{3.5}$$

where, $\nu = 1, 2$

$\hat{z}$ = unit vector in z direction

$\underset{\sim}{\nabla}_t$ = transverse part of the $\underset{\sim}{\nabla}$ operator

When the waveguides are placed near each other we can approximately express the total field as a superposition of the unperturbed fields of the two guides. However, since we anticipate the two guides will influence each other we must allow for the possibility that the field amplitudes might vary with distance. The total field can, therefore, be expressed as

$$\underset{\sim}{E} = A_1(z)\underset{\sim}{E}_1 + A_2(z)\underset{\sim}{E}_2 \tag{3.6}$$

$$\underset{\sim}{H} = A_1(z)\underset{\sim}{H}_1 + A_2(z)\underset{\sim}{H}_2 \tag{3.7}$$

These field expressions are, of course, not exact since we have assumed that the fields of each guide are not affected by the presence of the other. Additional small terms are required to express the fields exactly (5). The total electric field E and magnetic field H satisfy Maxwell's equations

$$\underset{\sim}{\nabla} \times \underset{\sim}{H} = i\omega\varepsilon_o n^2 \underset{\sim}{E} \tag{3.8}$$

$$\underset{\sim}{\nabla} \times \underset{\sim}{E} = -i\omega\mu_o \underset{\sim}{H} \tag{3.9}$$

where n^2 is given by equation (3.1). Substituting (3.6) and (3.7) into (3.8) and (3.9) leads to

$$\begin{aligned} &A_1[\underset{\sim}{\nabla}_t \times \underset{\sim}{H}_1 - i\beta_1(\hat{z} \times \underset{\sim}{H}_1)] + \frac{\partial A_1}{\partial z}(\hat{z} \times \underset{\sim}{H}_1) - i\omega\varepsilon_o n^2 A_1 \underset{\sim}{E}_1 \\ &+A_2[\underset{\sim}{\nabla}_t \times \underset{\sim}{H}_2 - i\beta_2(\hat{z} \times \underset{\sim}{H}_2)] + \frac{\partial A_2}{\partial z}(\hat{z} \times \underset{\sim}{H}_2) - i\omega\varepsilon_o n^2 A_2 \underset{\sim}{E}_2 = 0 \end{aligned} \tag{3.10}$$

and

$$\begin{aligned} &A_1[\underset{\sim}{\nabla}_t \times \underset{\sim}{E}_1 - i\beta_1(\hat{z} \times \underset{\sim}{E}_1)] + \frac{\partial A_1}{\partial z}(\hat{z} \times \underset{\sim}{E}_1) + i\omega\mu_o A_1 \underset{\sim}{H}_1 \\ &+A_2[\underset{\sim}{\nabla}_t \times \underset{\sim}{E}_2 - i\beta_2(\hat{z} \times \underset{\sim}{E}_2)] + \frac{\partial A_2}{\partial z}(\hat{z} \times \underset{\sim}{E}_2) + i\omega\mu_o A_2 \underset{\sim}{H}_2 = 0 \end{aligned} \tag{3.11}$$

With the help of equations (3.1), (3.4) and (3.5) we can simplify these equations so that they assume the form

$$\frac{\partial A_1}{\partial z}(\hat{z} \times \underset{\sim}{H}_1) - i\omega\varepsilon_0(n_2^2 - n_3^2)A_1\underset{\sim}{E}_1 + \frac{\partial A_2}{\partial z}(\hat{z} \times \underset{\sim}{H}_2) - i\omega\varepsilon_0(n_1^2 - n_3^2)A_2\underset{\sim}{E}_2 = 0 \tag{3.12}$$

and

$$\frac{\partial A_1}{\partial z}(\hat{z} \times \underset{\sim}{E}_1) + \frac{\partial A_2}{\partial z}(\hat{z} \times \underset{\sim}{E}_2) = 0 \tag{3.13}$$

The next step in the derivation of the coupled wave equations is to take the scalar product of (3.12) with $\underset{\sim}{E}_1^*$ and a similar product of (3.13) with $\underset{\sim}{H}_1^*$ and subtract the two equations. The resulting equation is then integrated over the infinite cross-section.

$$\int_{-\infty}^{+\infty}\int\{\frac{\partial A_1}{\partial z}[\underset{\sim}{E}_1^*.(\hat{z} \times \underset{\sim}{H}_1) - \underset{\sim}{H}_1^*.(\hat{z} \times \underset{\sim}{E}_1)] + \frac{\partial A_2}{\partial z}[\underset{\sim}{E}_1^*.(\hat{z} \times \underset{\sim}{H}_2) - \underset{\sim}{H}_1^*.(\hat{z} \times \underset{\sim}{E}_2)] - i\omega\varepsilon_0(n_2^2 - n_3^2)A_1\underset{\sim}{E}_1^*\underset{\sim}{E}_1 - i\omega\varepsilon_0(n_1^2 - n_3^2)A_2\underset{\sim}{E}_1^*\underset{\sim}{E}_2\}dx\,dy = 0 \tag{3.14}$$

This equation can be simplified by neglecting small terms. The expression $n_2^2 - n_3^2$ vanishes outside the region of the second guide. In the region where this term makes its contribution, the field of the first guide is already quite weak. Since it is the square of $\underset{\sim}{E}_1$ - ie $\underset{\sim}{E}_1.\underset{\sim}{E}_1^*$ - that is multiplied with $n_2^2 - n_3^2$, the entire term is small of second order and can be neglected. The product $\underset{\sim}{E}_1^*.(\hat{z} \times \underset{\sim}{H}_1)$ is a zero order term as far as its magnitude is concerned. The term $(n_1^2 - n_3^2)\underset{\sim}{E}_1^*.\underset{\sim}{E}_2$ is small of first order, since $n_1^2 - n_3^2$ is non-vanishing only in the region of the first guide where the field of the second guide, $\underset{\sim}{E}_2$, is small. This comparison of orders of magnitude suggests that the derivatives $\partial A/\partial z$ are quantities that are themselves of first order. Since the product $\underset{\sim}{E}_1^*.(\hat{z} \times \underset{\sim}{H}_2)$ is a first order term, because the fields of different guides overlap only slightly, we see that the term with $\partial A_2/\partial z$ is also small of second order and thus be neglected. Keeping only first order terms we get

$$\int_{-\infty}^{+\infty}\int\{\frac{\partial A_1}{\partial z}[\underset{\sim}{E}_1^*.(\hat{z} \times \underset{\sim}{H}_1) - \underset{\sim}{H}_1^*.(\hat{z} \times \underset{\sim}{E}_1)] - i\omega\varepsilon_0(n_1^2 - n_3^2)A_2\underset{\sim}{E}_1^*.\underset{\sim}{E}_2\}\,dx\,dy = 0 \tag{3.15}$$

Since A_1 and A_2 are independent of the transverse co-ordinates x and y, equation (3.15) can be written as

$$\frac{\partial A_1}{\partial z} = -i\omega\varepsilon_o A_2 \frac{\int_{-\infty}^{+\infty}\int (n_1^2 - n_3^2)\hat{E}_1^*.\hat{E}_2 \, dx \, dy}{\int_{-\infty}^{+\infty}\int \hat{z}.(\hat{E}_1^* \times \hat{H}_1 + \hat{E}_1 \times \hat{H}_1^*)dx \, dy}$$

This can be written as

$$\frac{\partial A_1}{\partial z} = i \, c_1 \, A_2 \exp i(\beta_1 - \beta_2)z \tag{3.16}$$

with

$$c_1 = -\omega\varepsilon_o \frac{\int_{-\infty}^{+\infty}\int (n_1^2 - n_3^2)\hat{E}_1^*.\hat{E}_2 \, dx \, dy}{\int_{-\infty}^{+\infty}\int \hat{z}.(\hat{E}_1^* \times \hat{H}_1 + \hat{E}_1 \times \hat{H}_1^*) \, dx \, dy} \tag{3.17}$$

To indicate that the term $\exp(\pm i\beta_\nu z)$ has been removed, we use the notation $\hat{E}_1$, $\hat{E}_1^*$ etc, introduced in (3.2) and (3.3). Similarly, by multiplying (3.12) and (3.13) by $\underline{E}_2^*$ and $\underline{H}_2^*$ we obtain the equation

$$\frac{\partial A_2}{\partial z} = i \, c_2 \, A_1 \exp -i \, (\beta_1 - \beta_2)z \tag{3.18}$$

with

$$c_2 = -i\omega\varepsilon_o \frac{\int_{-\infty}^{+\infty}\int (n_2^2 - n_3^2)\hat{E}_2^*.\hat{E}_1 \, dx \, dy}{\int_{-\infty}^{+\infty}\int \hat{z}.(\hat{E}_2^* \times \hat{H}_2 + \hat{E}_2 \times \hat{H}_2^*) \, dx \, dy} \tag{3.19}$$

In deriving equations (3.16) and (3.18) we neglected certain second order terms and in addition we limited the analysis to only two modes. The coupled wave equations (3.16) and (3.18) are, therefore, not exact. However, we showed in section (2.2) that only modes with identical propagation constants can exchange appreciable amounts of energy. Limiting the analysis to only two modes,is, therefore, a good approximation and allows us to study the exchange of energy between two modes to a high accuracy.

The expression in the denominator of equation (3.17) can be interpreted as 4P, with P being the power of the mode in guide 1 (for $A_1 = 1$), (5). Furthermore, if the two guides are identical we obtain, instead of (3.17) and (3.19)

$$c_1 = c_2 = -\frac{\omega\varepsilon_o}{4P}\int_{-\infty}^{+\infty}\int (n_2^2 - n_3^2)\hat{E}_2^*.\hat{E}_1 \, dx \, dy \tag{3.20}$$

We now introduce the wave amplitudes

$$a_\nu = A_\nu \exp -i\beta_\nu z, \; \nu = 1. \; 2 \tag{3.21}$$

Using (3.21) we can write equations (3.16) and (3.18) in the familiar form (see section 2.2)

$$\frac{\partial a_1}{\partial z} = - i\beta_1 a_1 + ic_1 a_2 \tag{3.22}$$

and

$$\frac{\partial a_2}{\partial z} = - i\beta_2 a_2 + ic_2 a_1 \tag{3.23}$$

For two identical fibres, ie $\beta_1 = \beta_2 = \beta$ and $c_1 = c_2 = c$, the coupled mode equations (3.22) and (3.23) have the following solutions, (5)

$$\begin{aligned} a_1(z) &= \tfrac{1}{2}[a_1(0) + a_2(0)]\exp -i(\beta - \Delta\beta)z \\ &\quad + \tfrac{1}{2}[a_1(0) - a_2(0)]\exp -i(\beta + \Delta\beta)z \end{aligned} \tag{3.24}$$

and

$$\begin{aligned} a_2(z) &= \tfrac{1}{2}[a_2(0) + a_1(0)]\exp -i(\beta - \Delta\beta)z \\ &\quad - \tfrac{1}{2}[a_1(0) - a_2(0)]\exp -i(\beta + \Delta\beta)z \end{aligned} \tag{3.25}$$

where, $\Delta\beta = c$ and $a_1(0)$ and $a_2(0)$ are the values of a_1 and a_2 at $z = 0$. It is clear from equations (3.24) and (3.25) that the solutions of the coupled wave equations consist of the superposition of two new modes with propagation constants

$$\beta_+ = \beta + \Delta\beta \tag{3.26}$$

and

$$\beta_- = \beta - \Delta\beta \tag{3.27}$$

The coupled waveguides have, therefore, two normal modes with altered propagation constants (3.26) and (3.27). If at $z = 0$ only guide 1 is excited, ie $a_2 = 0$, we get from (3.24) and (3.25)

$$a_1(z) = a_1(0) \cos (cz) \exp -i\beta z \tag{3.28}$$

and

$$a_2(z) = i\, a_1(0) \sin (cz) \exp -i\beta z \tag{3.29}$$

These clearly show that for real values of c and β energy is continuously exchanged between the two guides. This continual exchange of power can, of course, be interpreted as beating between the two normal modes of the composite structure.

It follows from equations (3.28) and (3.29) that for unit power launched into guide 1 the power variation in the two guides is given by - see section 2.2 -

$$P_1(z) = \cos^2(cz) \tag{3.30}$$

$$P_2(z) = \sin^2(cz) \tag{3.31}$$

where

$P_1(z)$ = normalised power in guide 1

$P_2(z)$ = normalised power in guide 2

After a distance $z = \pi/2c$ all the power in guide 1 will be transferred to guide 2; the beatlength, λ_B, is clearly given by $\lambda_B = \pi/c$, (2.14). In order to analyse the performance of the coupler we must determine the coupling coefficient, c, and its dependence on the various parameters of the fibres in particular the cladding index. As a first step, therefore, equation (3.20) must be solved for the case of two identical single-mode fibres.

3.3 Coupling Of HE_{11} Modes Of Round Fibres

The detailed analysis of the coupling of HE_{11} modes of two round fibres is given in reference (5), where, the coupling coefficients are determined for two fibres with thin cladding surrounded by a medium of lower refractive index, Fig (3.2). We shall give the main results of this analysis and then simplify them for a structure in which the fibres do not have an intermediate cladding, Fig (3.3).

The field components for the HE_{11} mode of a fibre with a thin cladding are as follows, (5),

inside the core

$$\hat{E}_z = AJ_1(\kappa r)\cos\phi \tag{3.32}$$

$$\hat{H}_z = BJ_1(\kappa r)\sin\phi \qquad 0 \leq r \leq a \tag{3.33}$$

in the cladding

$$\hat{E}_z = [CH_1^{(1)}(i\gamma r) + DH_1^{(2)}(i\gamma r)]\cos\phi \tag{3.34}$$

$$\hat{H}_z = [FH_1^{(1)}(i\gamma r) + GH_1^{(2)}(i\gamma r)]\sin\phi \qquad a \leq r \leq b \tag{3.35}$$

and finally the field in the surrounding medium is given by

$$\hat{E}_z = MH_1^{(1)}(i\rho r)\cos\phi \tag{3.36}$$

$$\hat{H}_z = NH_1^{(1)}(i\rho r)\sin\phi \qquad b \leq r < \infty \tag{3.37}$$

The parameters κ, γ and ρ are given by

$$\kappa = \sqrt{n_c^2 k_o^2 - \beta^2} \tag{3.38}$$

$$\gamma = \sqrt{\beta^2 - n_m^2 k_o^2} \tag{3.39}$$

$$\rho = \sqrt{\beta^2 - n_3^2 k_o^2} \tag{3.40}$$

where, $k_o = \omega \sqrt{\varepsilon_o \mu_o}$

The coefficients A, B, C and F are related through the following expressions

$$B = \sqrt{\frac{\varepsilon_o}{\mu}} \frac{a^2 k_o \kappa^2 \gamma^2}{\beta(\kappa^2+\gamma^2)} \left\{ \frac{n_c^2}{\kappa a} \left[\frac{1}{\kappa a} - \frac{J_o(\kappa a)}{J_1(\kappa a)} \right] + \frac{n_m^2}{\gamma a} \left[\frac{1}{\gamma a} - \frac{i H_o^{(1)}(i\gamma a)}{H_1^{(1)}(i\gamma a)} \right] \right\} \tag{3.41}$$

and

$$\frac{C}{A} = \frac{F}{B} = \frac{J_1(\kappa a)}{H_1^{(1)}(i\gamma a)} \tag{3.42}$$

To the approximation that the field intensity is weak at the interface between the cladding and the surrounding medium, we have

$$D = G = 0 \tag{3.43}$$

The coefficients M and N can be related to C and F by replacing the Hankel Functions by their approximations for large arguments,

$$M = \left(\frac{\rho}{\gamma}\right)^{3/2} \exp(\rho-\gamma)b \left\{ C\left[\left(\frac{\beta}{b}\right)^2 \left(1 - \frac{\gamma^2}{\rho^2}\right)^2 \left(\frac{\gamma}{\rho} - 1\right) - k_o^2 \gamma^2 \left(1 + \frac{\gamma}{\rho}\right) \left\{ n_m^2 + n_3^2 \frac{\gamma^2}{\rho^2} + \frac{\gamma}{\rho}(n_m^2 - n_3^2) \right\} \right] + 2\omega\mu_o F \gamma \frac{\beta}{b} \left(1 - \frac{\gamma^2}{\rho^2}\right) \right\}$$

$$\frac{}{\left[\frac{\beta}{b}\left(1 - \frac{\gamma^2}{\rho^2}\right)\right]^2 - k_o^2 \gamma^2 \left(1 + \frac{\gamma}{\rho}\right)\left(n_m^2 + n_3^2 \frac{\gamma}{\rho}\right)} \tag{3.44}$$

and

$$N = -\sqrt{\rho/\gamma} \exp(\rho-\gamma)b \; \frac{2Fk_o^2\gamma^2\left(n_m^2 + n_3^2\frac{\gamma}{\rho}\right) + 2\omega n_m^2 \varepsilon_o \gamma \frac{\beta}{b}\left(\frac{\gamma^2}{\rho^2} - 1\right)C}{\left[\frac{\beta}{b}\left(1 - \frac{\gamma^2}{\rho^2}\right)\right]^2 - k_o^2\gamma^2\left(1 + \frac{\gamma}{\rho}\right)\left(n_m^2 + n_3^2 \frac{\gamma}{\rho}\right)} \tag{3.45}$$

The coefficient A, finally, is related to the power carried by the mode,

$$P = (\pi/4)\sqrt{\epsilon_o/\mu_o}\, A^2\{\frac{k_o\beta}{\kappa^4}[(a\kappa)^2(J_o^2(\kappa a)+J_1^2(\kappa a))-2J_1^2(\kappa a)](n_c^2+\frac{\mu_o}{\epsilon_o}\frac{B^2}{A^2})$$

$$+ \frac{k_o\beta}{\gamma^4}[(a\gamma)^2(1-(\frac{iH_o^{(1)}(i\gamma a)}{H_1^{(1)}(i\gamma a)})^2) + 2]J_1^2(\kappa a)(n_m^2+\frac{\mu_o}{\epsilon_o}\frac{B^2}{A^2})$$

$$+ 2\sqrt{\mu_o/\epsilon_o}\,\frac{B}{A}[\frac{\beta_o^2+n_c^2k_o^2}{\kappa^4} - \frac{\beta_o^2+n_m^2k_o^2}{\gamma^4}]J_1^2(\kappa a)\} \qquad (3.46)$$

The coupling coefficients then follow (5), for horizontal polarisation

$$c_h = \sqrt{\epsilon_o/\mu_o}\,\frac{A^2}{2P}\cdot\frac{M}{A}\cdot\frac{1}{k_o}\sqrt{2\pi/\rho R}\,\exp(-\rho R)$$

$$\cdot\{\frac{\exp(\rho-\gamma)b.J_1(\kappa a)}{\pi\sqrt{\rho\gamma}\,H_1^{(1)}(i\gamma a)}[(1+\frac{\beta^2}{\gamma\rho})(\gamma+\rho)+\frac{\beta^2}{b\gamma^2\rho^2}(\rho^2-\gamma^2)(1-\frac{k_o}{\beta}\sqrt{\mu_o/\epsilon_o}\frac{B}{A})]$$

$$+ iJ_1(i\rho a)[a(\frac{\beta^2}{\kappa}-\kappa)J_o(\kappa a) + a(\frac{\beta^2}{\gamma}+\gamma)\frac{iH_o^{(1)}(i\gamma a)}{H_1^{(1)}(i\gamma a)}J_1(\kappa a)$$

$$- \frac{\beta^2}{\kappa^2\gamma^2}(\kappa^2+\gamma^2)(1-\frac{k_o}{\beta}\sqrt{\mu_o/\epsilon_o}\frac{B}{A})J_1(\kappa a)]\} \qquad (3.47)$$

and for vertical polarisation

$$c_v = \frac{A^2}{2P}\cdot\frac{N}{A}\cdot\frac{1}{\rho}\sqrt{2\pi/\rho R}\,\exp(-\rho R)$$

$$\cdot\{\frac{\exp(\rho-\gamma)b\cdot J_1(\kappa a)}{\pi\gamma b\sqrt{\rho\gamma}\,H_1^{(1)}(i\gamma a)}[k_o\sqrt{\mu_o/\epsilon_o}\,\frac{B}{A}((\gamma+\rho)b+\frac{\rho^2-\gamma^2}{\gamma\rho}) - \frac{\beta}{\gamma\rho}(\rho^2-\gamma^2)]$$

$$+i\rho J_1(i\rho a)[k_o a\sqrt{\mu_o/\epsilon_o}\,\frac{B}{A}(\frac{1}{\kappa}J_o(\kappa a) + \frac{1}{\gamma}\frac{iH_o^{(1)}(i\gamma a)}{H_1^{(1)}(i\gamma a)}J_1(\kappa a))$$

$$+ \frac{\beta}{\kappa^2\gamma^2}(\kappa^2+\gamma^2)(1-\frac{k_o}{\beta}\sqrt{\mu_o/\epsilon_o}\,\frac{B}{A})J_1(\kappa a)\} \qquad (3.48)$$

If the fibre claddings are removed completely (eg by etching) the structure shown in Fig (3.3) is obtained. As a result, the following changes have to be made in the equations for the field coefficients

$$\begin{aligned} b &\rightarrow a \\ n_m &\rightarrow n_3 \\ \rho &\rightarrow \gamma \end{aligned} \qquad (3.49)$$

This as expected leads to - from (3.44) and (3.45) -

$$\begin{aligned} M &= C \\ N &= F \end{aligned} \qquad (3.50)$$

Equation (3.41) remains unaltered and the power equation (3.46) is only slightly modified

$$P = (\pi/4)\sqrt{\varepsilon_o/\mu_o}A^2\{\frac{k_o\beta}{\kappa^4}[(a\kappa)^2(J_o^2(\kappa a) + J_1^2(\kappa a)) - 2J_1^2(\kappa a)](n_c^2 + \frac{\mu_o}{\varepsilon_o}\frac{B^2}{A^2})$$

$$+ \frac{k_o\beta}{\gamma^4}[(a\gamma)^2(1 - (\frac{iH_o^{(1)}(i\gamma a)}{H_1^{(1)}(i\gamma a)})^2) + 2]J_1^2(\kappa a)(n_3^2 + \frac{\mu_o}{\varepsilon_o}\frac{B^2}{A^2})$$

$$+ 2\sqrt{\mu_o/\varepsilon_o}\frac{B}{A}[\frac{\beta_o^2+n_c^2k_o^2}{\kappa^4} - \frac{\beta_o^2+n_3^2k_o^2}{\gamma^4}]J_1^2(\kappa a)\} \qquad (3.51)$$

The coupling coefficients become

$$c_h = \sqrt{\varepsilon_o/\mu_o}\cdot\frac{A^2}{2P}\cdot\frac{C}{A}\cdot\frac{1}{k_o}\sqrt{2\pi/\gamma R}\exp(-\gamma R)\{\frac{2J_1(\kappa a)}{\pi H_1^{(1)}(i\gamma a)}(1 + \frac{\beta^2}{\gamma^2})$$

$$+ iJ_1(i\gamma a)[a(\frac{\beta^2}{\kappa} - \kappa)J_o(\kappa a) + a(\frac{\beta^2}{\gamma} + \gamma)\frac{iH_o^{(1)}(i\gamma a)}{H_1^{(1)}(i\gamma a)}J_1(\kappa a)$$

$$- \frac{\beta^2}{\kappa^2\gamma^2}(\kappa^2+\gamma^2)(1 - \frac{k_o}{\beta}\sqrt{\mu_o/\varepsilon_o}\frac{B}{A})J_1(\kappa a)]\} \qquad (3.52)$$

and

$$c_v = \frac{A^2}{2P}\cdot\frac{C}{A}\cdot\frac{B}{A}\cdot\frac{1}{\gamma}\sqrt{2\pi/\gamma R}\exp(-\gamma R)\{\frac{2k_oJ_1(\kappa a)}{\pi\gamma H_1^{(1)}(i\gamma a)}\sqrt{\mu_o/\varepsilon_o}\frac{B}{A}$$

$$+ i\gamma J_1(i\gamma a)[k_oa\sqrt{\mu_o/\varepsilon_o}\frac{B}{A}(\frac{1}{\kappa}J_o(\kappa a) + \frac{1}{\gamma}\frac{iH_o^{(1)}(i\gamma a)}{H_1^{(1)}(i\gamma a)}J_1(\kappa a)$$

$$+ \frac{\beta}{\kappa^2\gamma^2}(\kappa^2 + \gamma^2)(1 - \frac{k_o}{\beta}\sqrt{\mu_o/\varepsilon_o}\frac{B}{A})J_1(\kappa a)]\} \qquad (3.53)$$

3.4 Calculation Of Coupling Coefficients

It was shown in section 2.2 that the operation of the switch is based on changing the coupling coefficient via a change in the cladding index. It is, therefore, necessary to calculate not only the magnitudes of the coupling coefficients, but also their rate of change with the cladding index. An analytic determination of $\partial c/\partial n_3$ - from equations (3.52) and (3.53) - cannot be carried out and instead a numerical approach must be adopted. For this purpose, the coupling coefficients c_h and c_v were calculated for five values of V in the range $1.75 \leqslant V \leqslant 3.0$. For each value of V the coupling coefficients were calculated as a function of the centre to centre separation, R, of the fibres. This procedure was carried out for four values of the core radius, a, in the range $1\ \mu m \leqslant a \leqslant 5\ \mu m$. In all the calculations the

refractive index of the cladding was taken to be 1.675. This is the smallest of the three indices of meta-nitroaniline, the electro-optic crystal that was selected for the experiments. Details about this crystal and the reasons for choosing it for the active cladding are given in the next chapter.

The parameters β, γ and κ which are necessary for determining the coupling coefficients were calculated by numerically solving the eigenvalue equation (1.30), (17). For each value of the core radius c_h was plotted against V for several values of fibre separation, R, Fig (3.4), (3.5), (3.6) and (3.7). In addition, in order to determine the sensitivity of the coupler to polarisation, a graph of $\frac{c_h - c_v}{c_h}$ x 100% was plotted against V for different values of the core radius, Fig (3.8). These graphs contain several important features. In general the coupling coefficient decreases (ie the beatlength increases) for increasing values of V and R. The situation is slightly different when the cores are in contact, ie R = 2a. In this case the coupling coefficient peaks at V $\simeq$ 2.2 and decreases on either side. This can be explained qualitatively by considering how the fields in the core and the cladding vary when V is changed. The coupling coefficient is determined by the extent of the overlap of the cladding field of one fibre with the core field of the second fibre, equation (3.20). A clear insight into the dependence of c on V can be obtained by considering two extreme values of V. For a low value of V (eg V $\simeq$ 1.0) the rate of decay of the field in the cladding is very slow. As a result a significant amount of the cladding field of one fibre reaches the core of the second fibre, Fig (3.9a). However, since the magnitude of the normalised field in the core of the second fibre is not appreciable at low values of V, the resultant field overlap will be small. This gives rise to a small coupling coefficient. At the other extreme, for large values of V, the field decays very fast in the cladding and hence very little field reaches the core of the second fibre. Therefore, despite the fact that the normalised field in the core of the second fibre is quite strong, there will be little overlap, Fig (3.9c), and the resultant coupling coefficient will again be small. Clearly as V increases from a very small to a very large value, the field in the core increases while that in the cladding diminishes. The overlap of the fields, therefore, is small at the two extremes and reaches a maximum for some intermediate value of V, Fig (3.9b). When the two cores are in

contact this maximum occurs at V ≃ 2.2. For increasing values of R, the peak in the c versus V graph moves progressively towards lower values of V - outside the range covered by the graphs. Similar results can be found in reference (18).

Increasing the separation, R, between the two fibres leads to less of the cladding field of one fibre reaching the core of the second fibre. Consequently, an increase in R always results in a decrease in the coupling coefficient. Maximum coupling is achieved for the two cores in contact, ie R = 2a. The coupling coefficient is very strongly dependant on the separation between the fibres; doubling R reduces c by more than one order of magnitude for low (≃ 1.75) values of V, whereas for a high V (eg ≃ 3.0) the reduction in c is more than two orders of magnitude.

It can be seen from Fig (3.4) - (3.7) that as the core radius is made smaller the coupling coefficient increases. In order to demonstrate this variation more clearly a graph of c_h v. r was plotted at V = 2.3 and for several values of R, Fig (3.10). For each value of R the points lie on a straight line with a slope of -2, thus demonstrating that c_h varies inversely with r^2, ie, $c_h \alpha 1/r^2$. This inverse square law dependence can be deduced from the coupling integral (3.20). The term $(n_2^2 - n_3^2)$ is non-zero only within the core of the second fibre. In this region it can be expressed in terms of the core radius and the V of the fibres, using equation (1.34),

$$n_2^2 - n_3^2 = \frac{V^2\lambda^2}{4\pi^2 a^2} \tag{3.54}$$

The coupling integral, therefore, becomes

$$c = -\left(\frac{\omega\varepsilon_o}{4P}.\frac{V^2\lambda^2}{4\pi^2}\right) \frac{1}{a^2} \iint \hat{E}_2^*.\ \hat{E}_1\ dx\ dy \tag{3.55}$$

with the integration carried out over the cross-sectional area of the second fibre. If V and the fibre separation, R, remain constant, E_1 and E_2 will be independant of the core radius - at least to a good approximation. It, therefore, follows from equation (3.55) that $c \alpha 1/a^2$. The same inverse square law dependence is obtained if the weakly guiding approximations are used to derive the coupling coefficients (19).

The polarisation dependence of the coupling coefficient is shown in Fig (3.8) and Fig (3.11). The coupling coefficients for the vertically and horizontally polarised fields differ only very slightly - less than 1% for a = 1 μm at V = 2.3, Fig (3.8). The difference between the coupling coefficients for the two polarisations decreases as the core radius is increased, Fig (3.11). For a = 5 μm and V = 2.2 this is less than 0.04%. The fact that a small difference remains between the two coupling coefficients is simply because the fields inside the fibre are not strictly linearly polarised. Figure (3.12) schematically shows the transverse electric field lines for one polarisation of the HE_{11} mode in the core of a fibre. The field magnitude at A differs slightly from that at B. Consequently the strength of the coupling achieved with a second fibre with centre O' will depend on whether O' is on the OA or the OB axis. If V is reduced, the fibre fields become more plane-wave like and as a result the two coupling coefficients become closer in magnitude. Increasing the core radius while keeping V constant will have the same effect, since this makes $n_1 - n_2$ smaller. Both these effects are clearly illustrated in Figures (3.8) and (3.11). It must be emphasised that the most important feature of Figures (3.8) and (3.11) is that for all practical values of V and a there is virtually no polarisation dependence in the coupling coefficients. This insensitivity to polarisation is one of the advantages that this structure for an electro-optic switch has over the existing integrated optic directional couplers.

3.5 Power Switching Between Two Fibres

It was shown earlier in this chapter that any power launched into guide 1 switches back and forth between the two guides with periodicity λ_B given by equation (2.14). We shall now calculate the amount of power switching, δP, caused by a given change, δc, in the coupling coefficient. From equation (3.30), for a coupler of length L, we have at the output of the first guide

$$P_1(L) = \cos^2(Lc) \tag{3.56}$$

If the coupling coefficient is changed by δc, there will be a corresponding change δP_1 in the power coming out of guide 1. We, therefore, have

$$P(L) + \delta P_1 = \cos^2 [L(c+\delta c)] \tag{3.57}$$

Subtracting (3.56) from (3.57)

$$\delta P_1 = \cos^2[L(c+\delta c)] - \cos^2(Lc) \tag{3.58}$$

Equation (3.58) can be written as

$$\delta P_1 = -[\sin(2Lc).\cos(L\delta c)+\cos(2Lc).\sin(L\delta c)]\sin(L\delta c) \tag{3.59}$$

Clearly, the value of L plays an important role in determining δP_1. We shall, therefore, consider two special cases

$$L = N\frac{\pi}{2c} \tag{3.60}$$

and

$$L = (2N+1)\frac{\pi}{4c} \tag{3.61}$$

where, N is a positive integer. When $L = N\pi/2c$, we get from (3.59)

$$|\delta P_1| = \sin^2(L\delta c) \tag{3.62}$$

And for $L = (2N+1)\pi/4c$, equation (3.59) yields

$$|\delta P_1| = \tfrac{1}{2}\sin(2L\delta c) \tag{3.63}$$

In both cases, it is the product $L\delta c$ that determines the amount of power switching. Note that when $L = (2N+1)\pi/4c$ the power at the output of the coupler is equally divided between the two guides, ie from (3.30), (3.31) and (3.61)

$$P_1(L) = P_2(L) = 0.5$$

On the other hand, for $L = N\pi/2c$, all the power emerges out of one fibre. This explains why $|\delta P_1|$ has a maximum value of 1 according to (3.62) but is limited to 0.5 by (3.63). It is important too to note that for small values of $L\delta c$, equation (3.63) gives larger values of $|\delta P_1|$ than does (3.62). In both cases, however, the same value of $L\delta c = \pi/4$ is required to produce a $|\delta P_1|$ of 0.5. These points are illustrated in Fig (3.13). It must be pointed out that the two special cases that were considered are both limiting cases. This means that for an arbitrary value of L and a given δc, the associated switched power, $|\delta P_1|$, will have a value between those given by (3.62) and (3.63).

It was explained earlier that the switching action of the device is obtained by changing the coupling coefficient via a change in the refractive index, n_2, of the cladding. Of course, it would be desirable to achieve a large δP for a relatively small δn_2 (and hence a small δc). Since it is the product $L\delta c$ that determines δP,

one must use the largest possible value of L in the construction of the device. This is limited by the length of a single-crystal of the electro-optic material that can be grown for the cladding. It is unlikely that L can be larger than a few centimetres in practice. We shall, therefore, limit our calculations to values of L in the range 1 cm $\leqslant$ L $\leqslant$ 5 cm.

From equation (3.62) we find that in order to achieve a δP of 1.0, we require

$$\delta c = \frac{1}{L} \cdot \frac{\pi}{2} \qquad (3.64)$$

For a coupler of length 1 cm, we find, from (3.64), δc = 157.1 rad/m. We assume that the fibres in the coupler have a V of 2.3 in the absence of an electric field applied to the cladding. With the help of the graphs in Figures (3.4) - (3.7), one can read off the change, δV, in V that is required to give δc = 157.1 rad/m. Equation (1.34) can then be used to calculate the corresponding δn_2. Note that in the majority of cases there are two values of δV - one positive and the other negative - that give the same δc. Virtually in every case the negative value of δV is smaller than the positive value. In order to maintain the single moded nature of the fibres it is important to ensure that V does not rise above 2.405 - see section 1.3. The easiest way of achieving this is to choose the polarity of the field such that it causes a reduction in V. Bearing this point in mind, and also taking into account the fact that for the same δc the negative value of δV is, in general, smaller than the positive value, it was decided to base all our calculations on the negative values of δV.

Three values of L were chosen, L = 1, 3, 5 cm. For each value of L we determined the required δn_2 for achieving 100% switching* between two fibres with touching cores, ie R = 2a. This procedure was carried out for three values of the core radius (a = 1.5, 2.5, 5.0 μm) and the graph in Fig (3.14) was plotted. As expected, larger values of L lead to a smaller δn_2 for complete coupling. It is also interesting to note that δn_2 is smaller for larger values of the core radius - keeping everything else the same.

---

* A prerequisite for achieving 100% switching, ie $|\delta P_1| = 1$, is that the length, L, of the coupler satisfies (3.60). For each case, therefore, L was adjusted - typically by a few percent of the quoted value - so that it satisfied this requirement. It was this new corrected value that was subsequently used in the analysis.

We also investigated the effect of the separation of the fibres on the required δn_2 for complete switching. In Fig (3.15) the required δn_2 for 100% switching is plotted against the centre to centre separation, R, of the fibres. It is interesting to note that the 'best' case is <u>not</u> when the two cores are in contact. The optimum separation of the core centres is about 2.5 times the core radius. Figure (3.15) refers to the specific case of a = 2.5 μm and L = 3.0 cm, its shape is nevertheless quite general. For all the core radii, a, and device lengths, L, that we considered, it was found that the optimum centre to centre separation was given by $R \simeq 2.5a$. This is a very important point since it could substantially reduce the voltage required for switching. It can be seen from Fig (3.15) that when $R = 2.5a$ we need only half the δn_2 that would be required for $R = 2.0a$. For a linear electro-optic crystal, such as meta-nitroaniline, this reduces the drive voltage by a factor of 2. It must, however, be pointed out that keeping two fibres parallel, but not in contact, over a length of one or two centimetres will be a formidable task. Nevertheless, the potential is there if the practical difficulties can be overcome.

So far the performance of the switch has been considered theoretically and without taking into account the practical difficulties which will inevitably hamper its operation. The two main limiting factors to the performance are the length, L, and the δn_2 that can be obtained in practice. A realistic value for L is about 1 cm and a typical δn_2 for mNA is approximately 10^{-5} - see section 4.3. It is unlikely that the length of the coupler can be increased to a value significantly larger than 1 cm. On the other hand, it is conceivable that δn_2, for mNA, can be increased to 10^{-4} by using a high enough voltage and/or reducing the gap between the electrodes. It is, therefore, important to know how much power can be switched between the guides if L = 1 cm and $10^{-5} \leqslant \delta n_2 \leqslant 10^{-4}$. Figure (3.16) shows the percentage switched power (ie, $\delta P \times 100\%$) as a function of the core radius and assuming $\delta n_2 = 10^{-5}$ and R = 2a (ie touching cores). The two lines correspond to the special cases (3.60) and (3.61)*

*L was very nearly 1 cm for both cases and only minor adjustments of less than a few percent had to be made to its value to satisfy (3.60) and (3.61).

As explained earlier, these are limiting cases and if L is about 1 cm but does not quite satisfy either (3.60) or (3.61), the switched power will lie somewhere between the two lines on the graph.

Figure (3.16) shows that the coupler is only capable of switching very small amounts of power. The exact length of the coupler plays a very important role in determining the amount of switched power; a few percent change in L alters δP by several orders of magnitude. The other interesting point about these results is that the switched power is very nearly independent of the core radius, c.f. Fig (3.10). δn_2 was increased to 10^{-4} and the calculations were repeated, Fig (3.17). The switched power has clearly been increased significantly. The results are still nearly independent of the core radius. The exact value of L is still important but much less than the previous case.

In order to show the improvement that one can achieve by spacing the fibres apart, we plotted $\delta P \times 100\%$ against R assuming that $\delta n_2 = 10^{-4}$ and $r = 1.5\ \mu m$, Fig (3.18). For $R \simeq 2.5a$ the switched power is about 22%, c.f. Fig (3.16) and Fig (3.17).

The analysis so far has been largely based on a V value of 2.3. This choice was made somewhat arbitrarily and was only guided by two criteria. Firstly it was necessary, for single mode operation, to have $V < 2.405$. On the other hand, a large value of V was desirable in order to relax the fabrication tolerances - see Chapter 5. $V = 2.3$ was, therefore, arrived at as a compromise. However, similar calculations were also carried out for $V = 1.8$, 2.2 and 3.0. The results are illustrated in Figures (3.19) - (3.21). The shapes of these curves are very much the same as those for $V = 2.3$. Some of the results, however, have quite different magnitudes. $V = 1.8$ for example, gives considerably better results than the other values of V. The main reason for this is that the slope of c-V graph becomes quite large for small values of V - see Figures (3.4) - (3.7) and (5.17) and also reference (18). As a result only a small δV (and hence δn_2) is required for producing a large δc (and hence δP). However, it will be shown in Chapter 5 that constructing a device for operation at $V = 1.8$ would be extremely difficult due to the very strict tolerances that would be imposed on the core-cladding index difference.

It can also be seen from Figs (3.20) and (3.21) that, in general, $V = 2.2$ produces worse results than the other values of V. This is due to the fact that for $R = 2a$ the c-V graphs, Figs (3.4)-(3.7), have a turning point in the vicinity of $V = 2.2$. Consequently a given change in V will result in a small change in c and thus cause very little power switching. For maximum efficiency, therefore, the coupler switch should be designed with a V value as far away from 2.2 as possible.

The results presented in this chapter demonstrate the potentials and the limitations of the proposed structure for a single-mode fibre switch. Even assuming that an index change of 10^{-4} can be achieved in practice, this will result in no more than a few percent of the power to be switched between the guides. This will only be good enough as a demonstration of the principle of operation of the switch. Whether or not the device will ever have a practical application depends largely on how much improvement can be made on the index change of 10^{-4}. Nevertheless, it was decided to proceed and construct the device in order to substantiate the theoretical predictions that we have presented in this chapter.

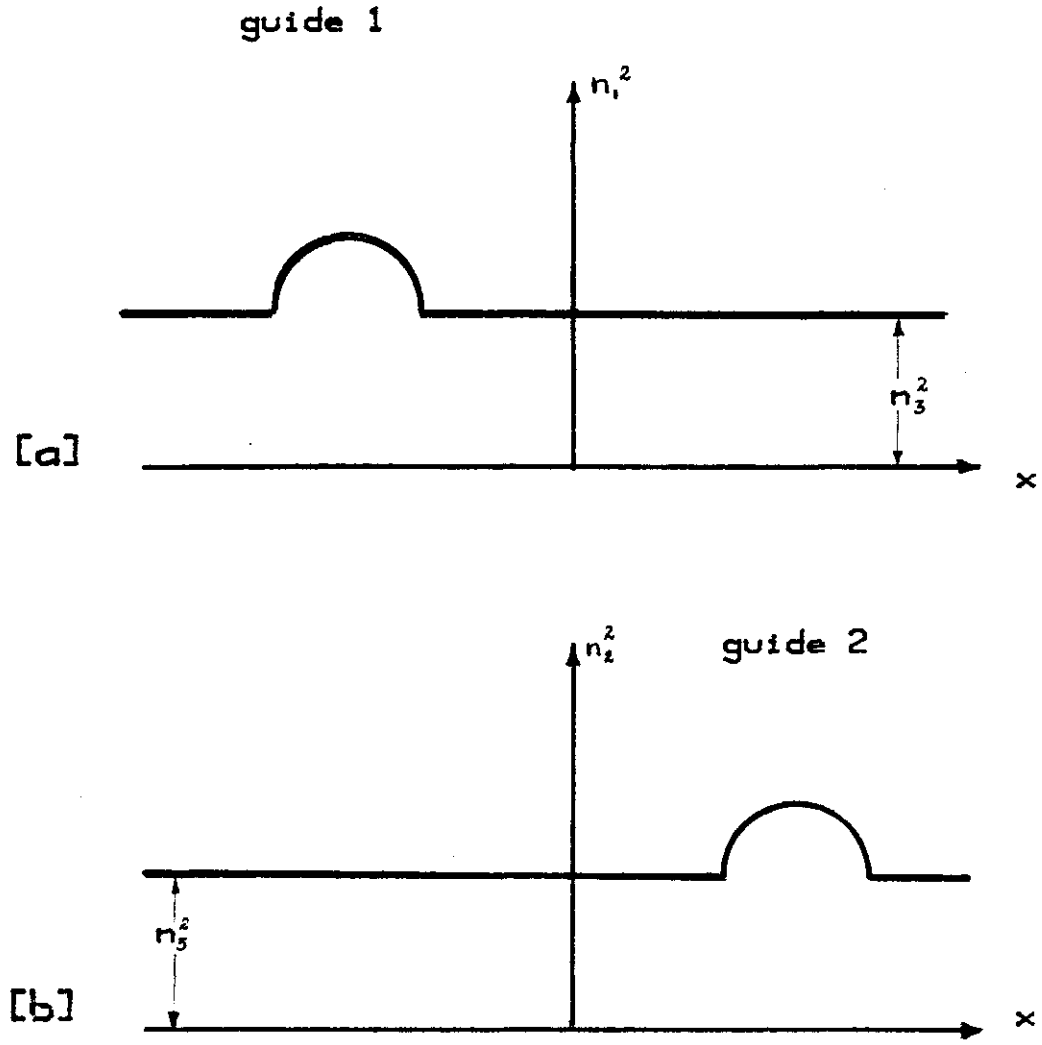

FIG[3.1] Transverse distributions of the refractive index defining the two wave guides, each in the absence of the other.

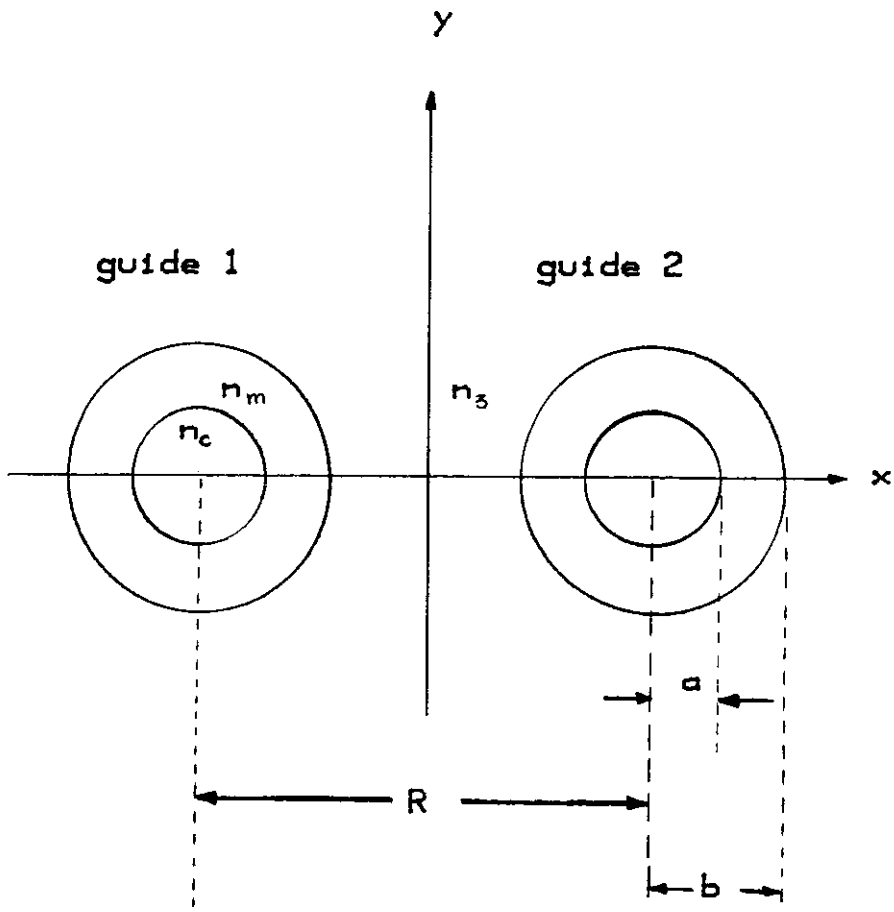

FIG[3.2] Coupled cladded optical fibres.

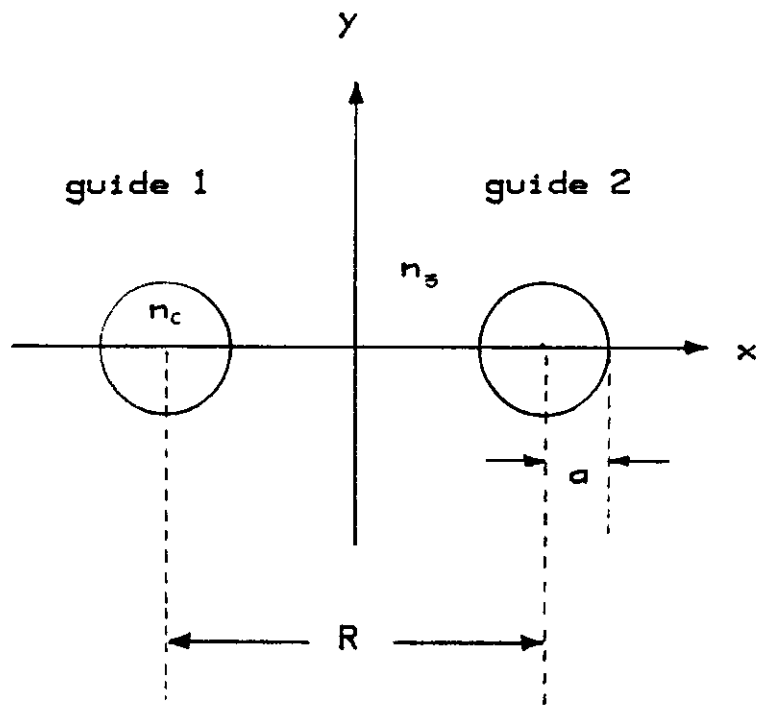

FIG[3.3] Coupled optical fibres with a common cladding.

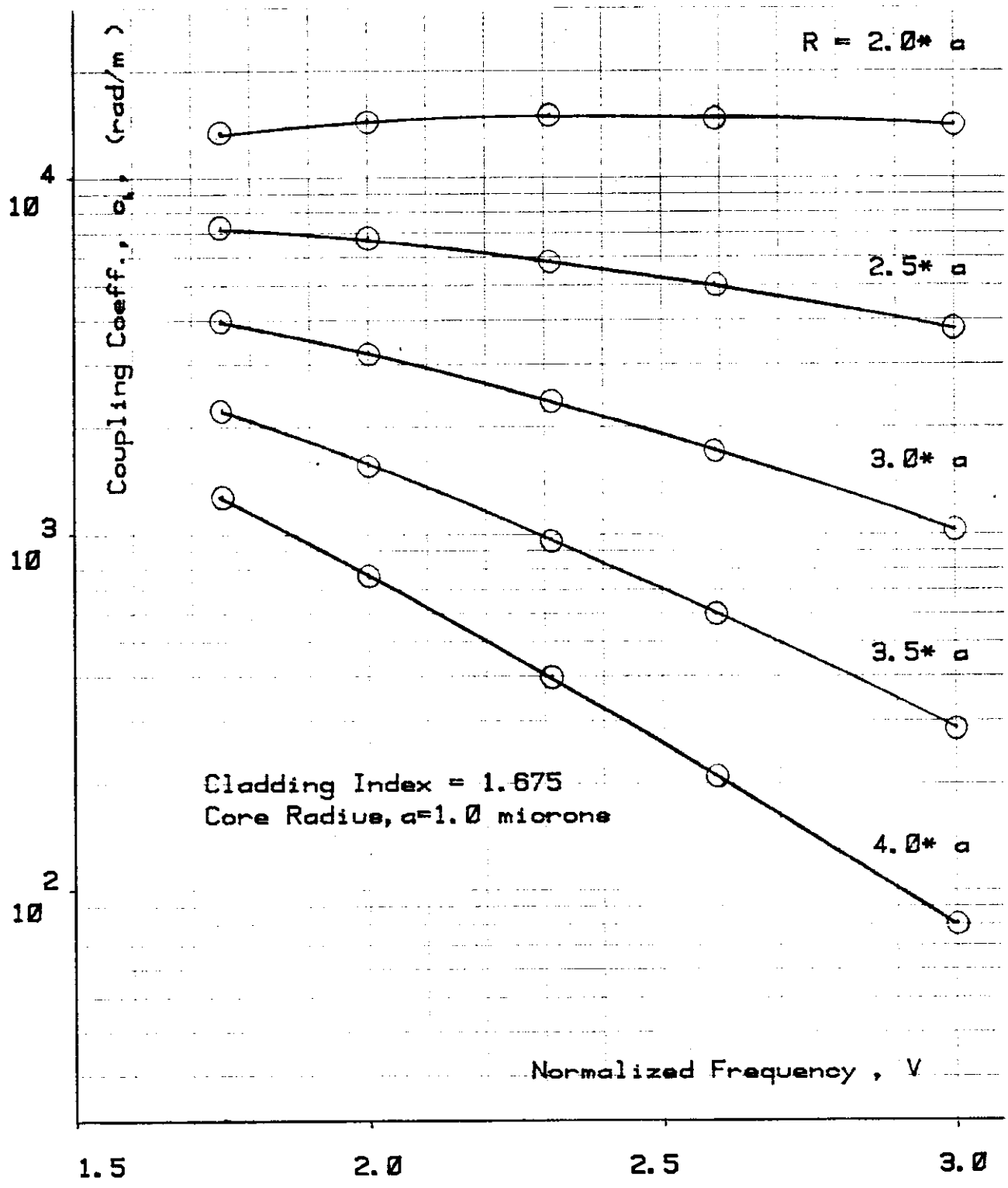

FIG[3.4] Variation of coupling coefficient with normalized frequency .

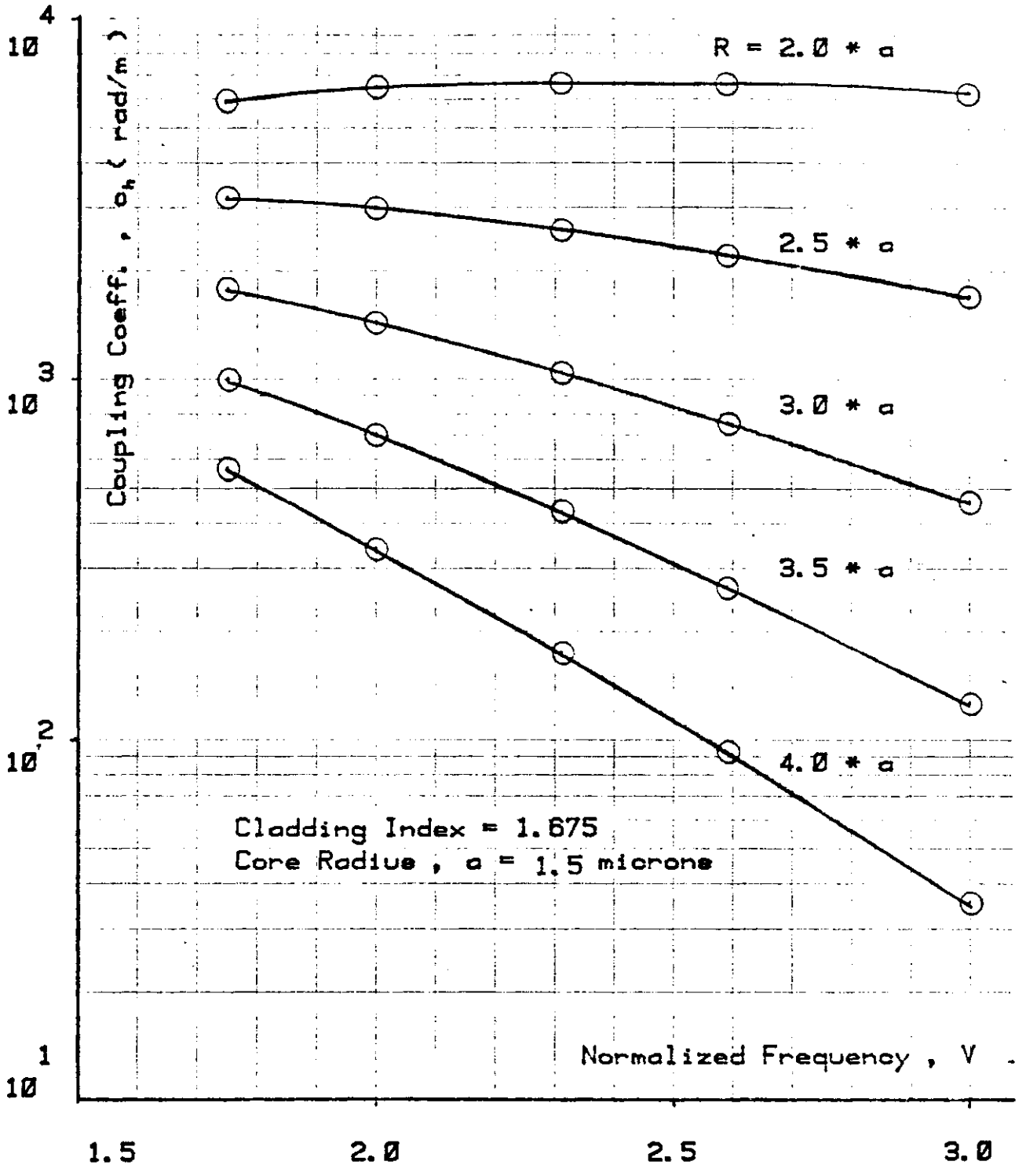

FIG[3.5] Variation of coupling coefficient with normalized frequency .

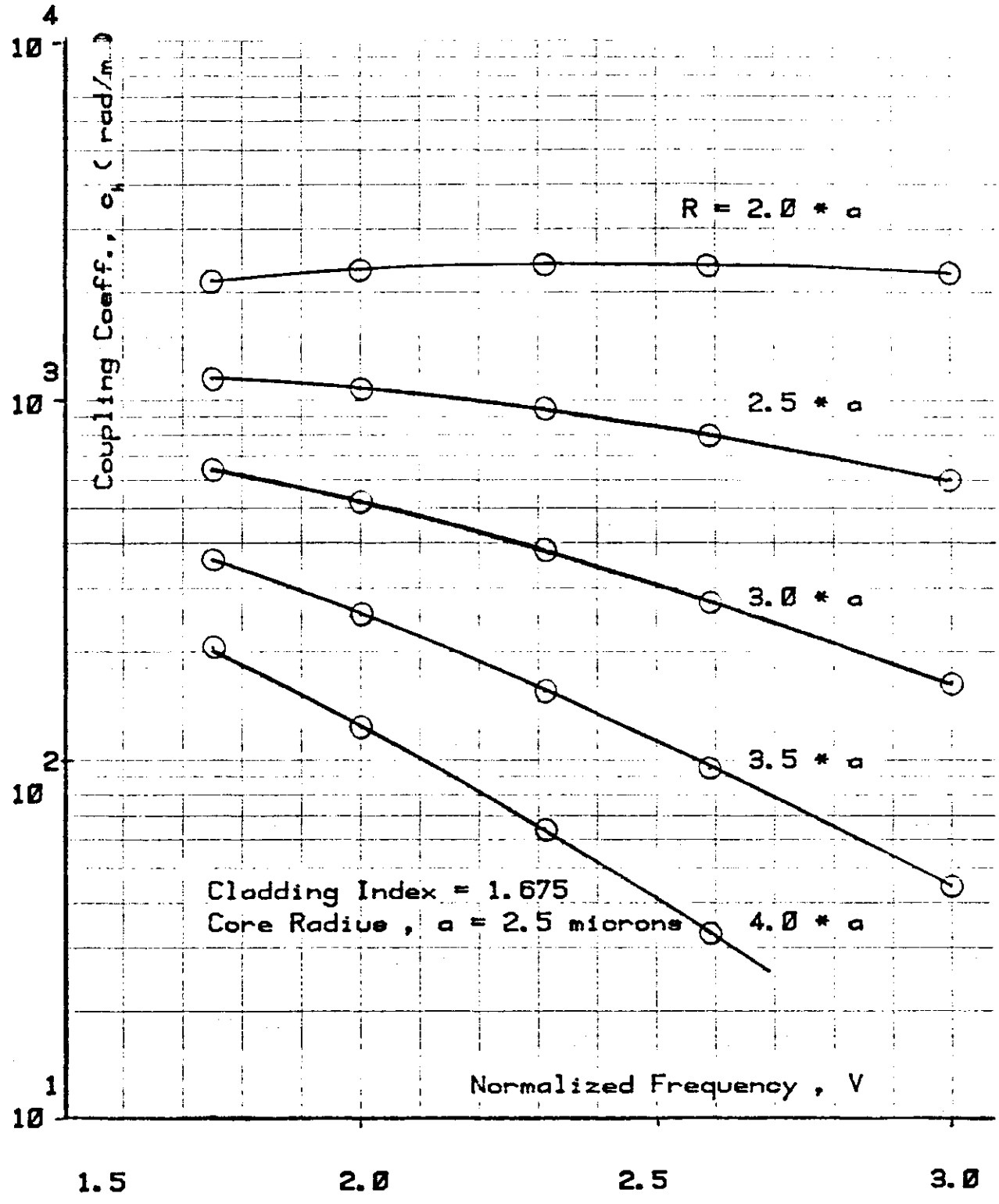

FIG[3.6] Variation of coupling coefficient with normalized frequency .

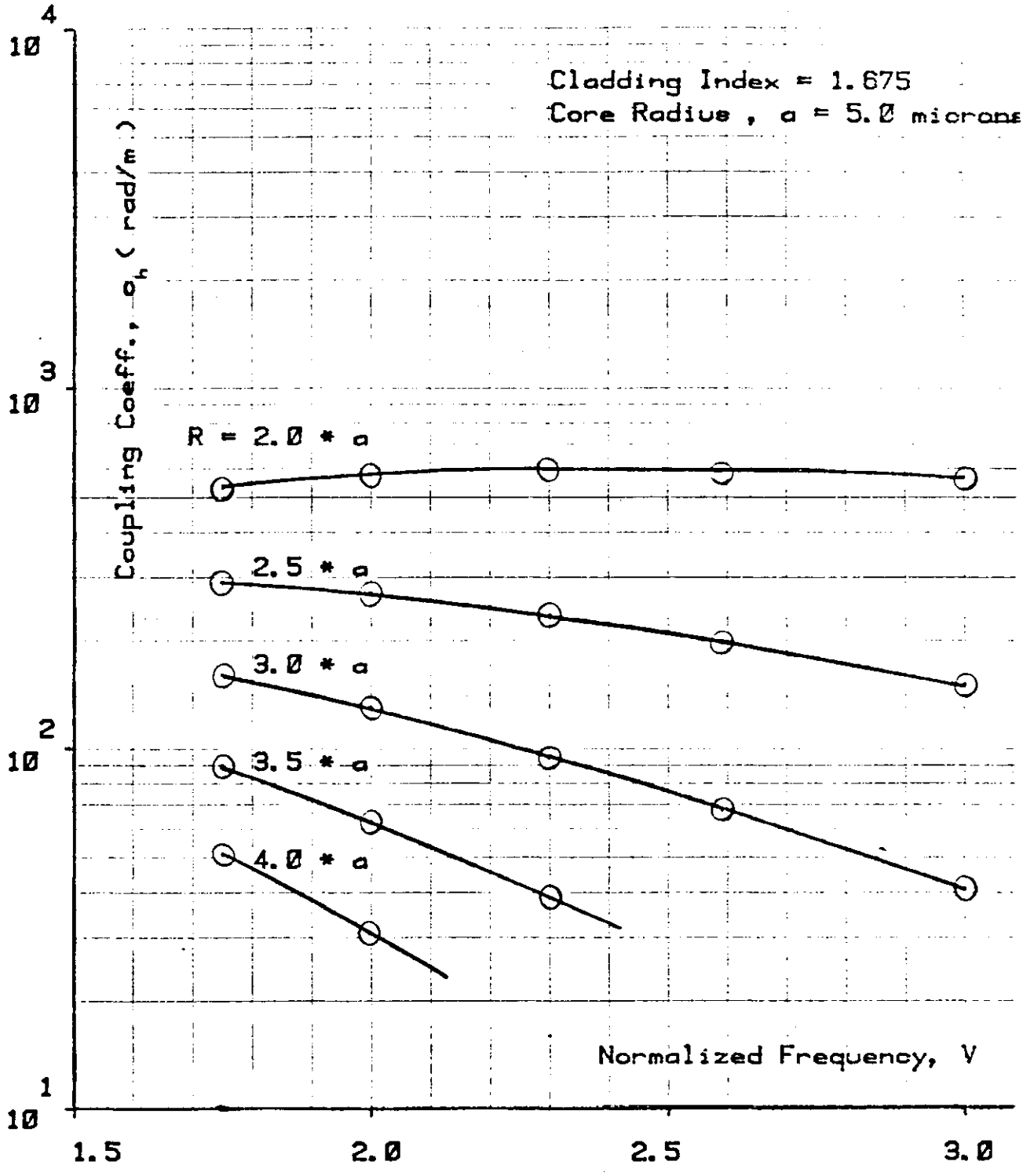

FIG[3.7] Variation of coupling coefficient with normalized frequency .

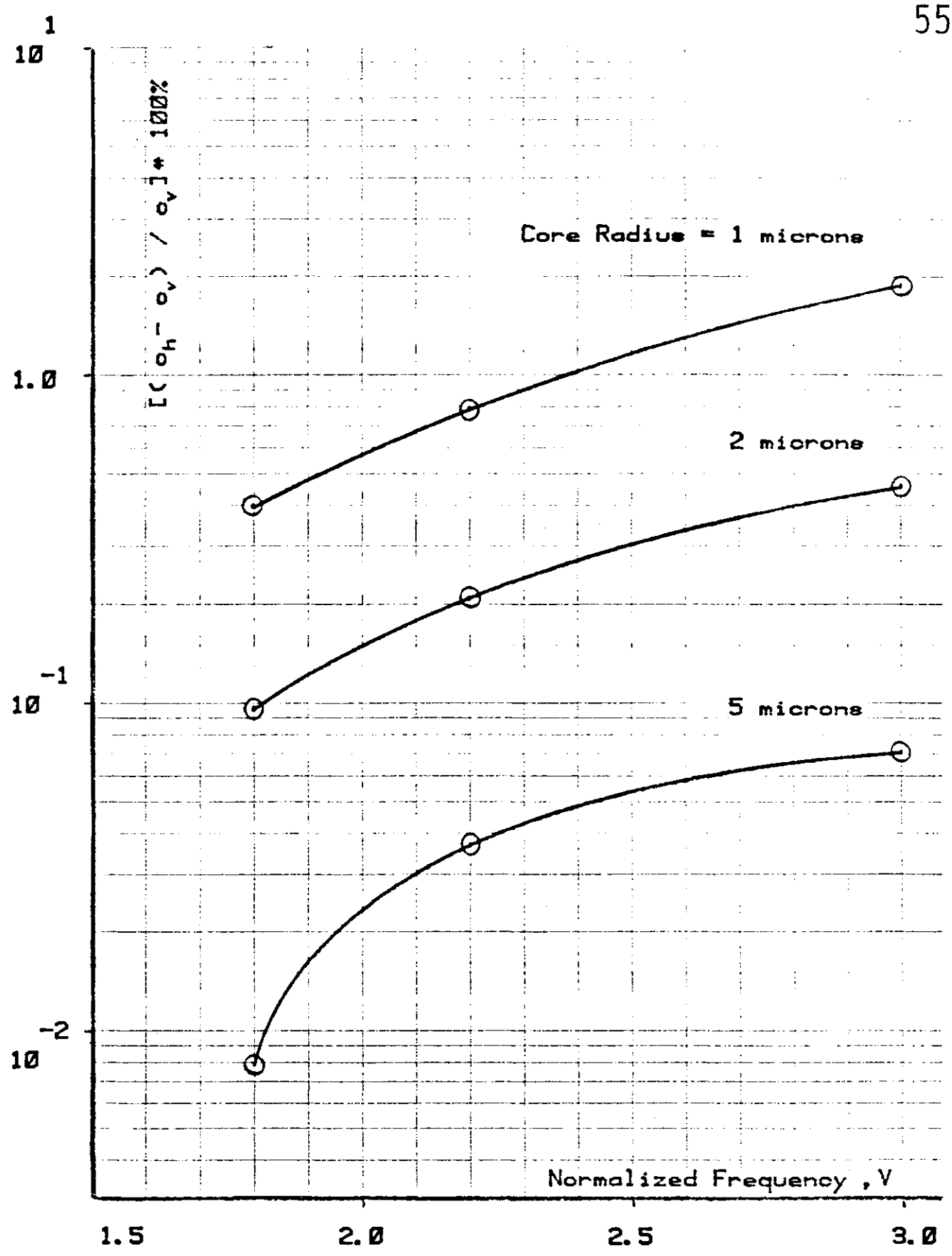

FIG[3.8] Polarization dependence of the coupling strength .

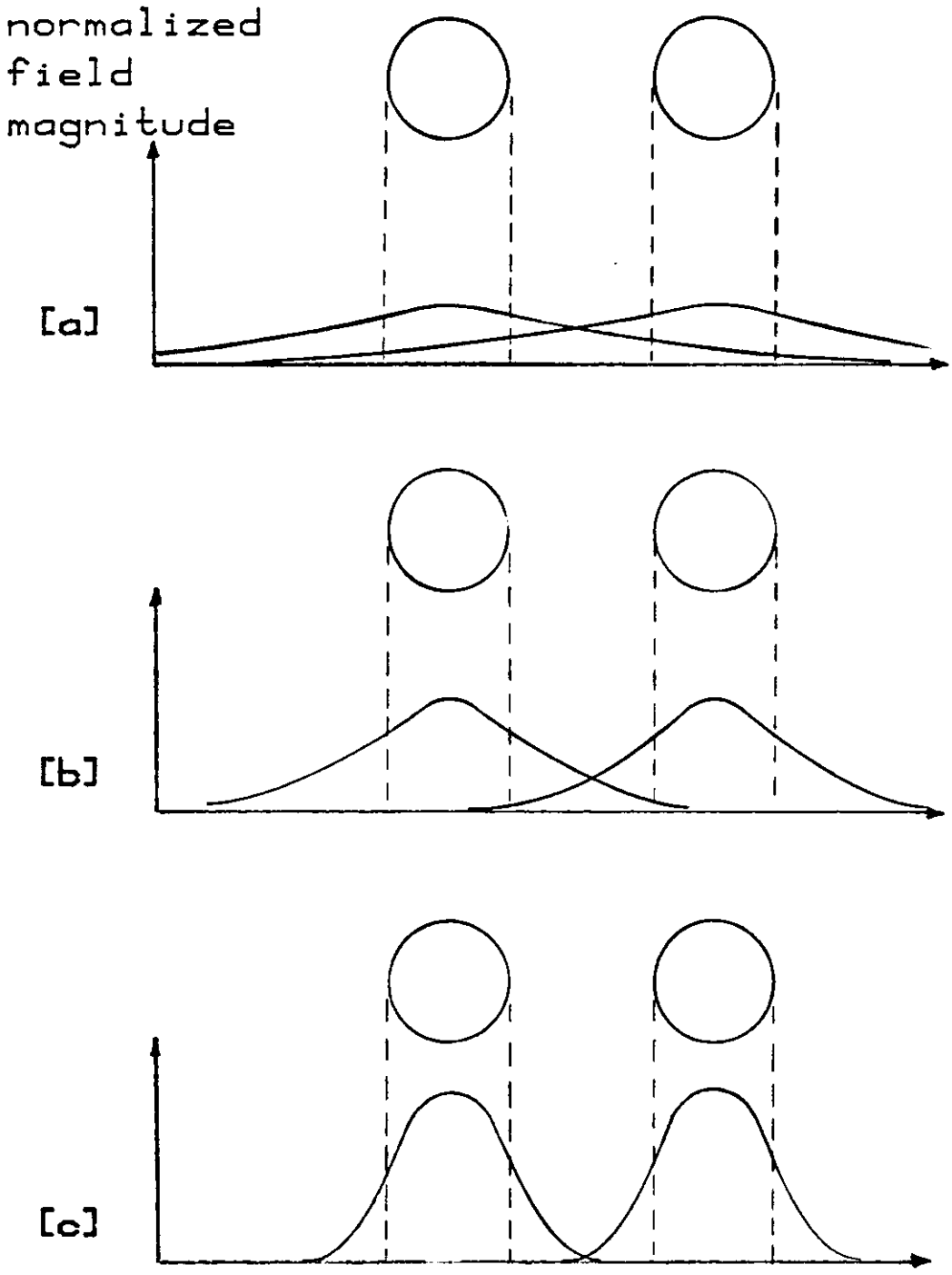

FIG[3.9] Field overlap between two adjacent fibres for [a] small, [b] intermediate and [c] large values of normalized frequenoy.

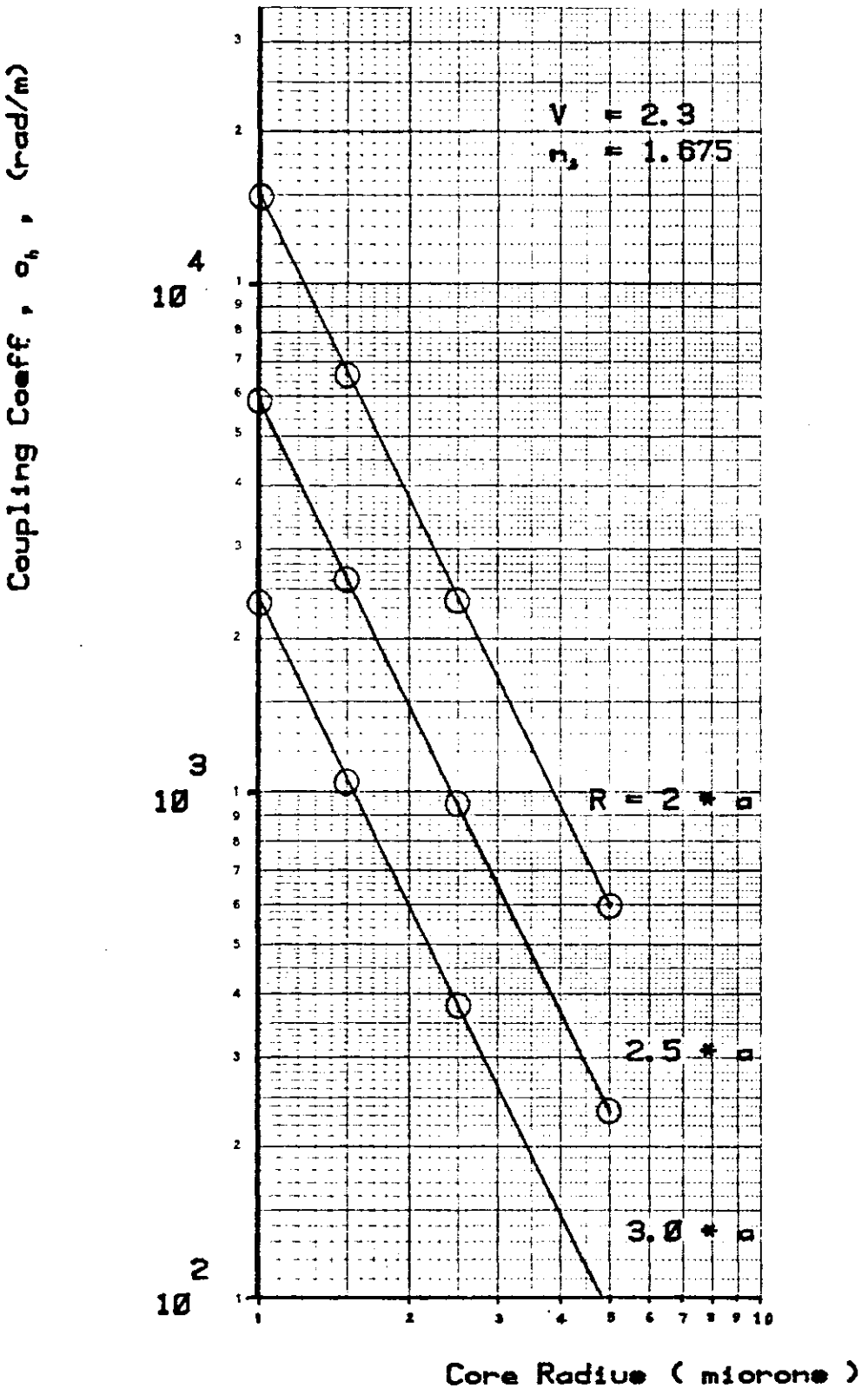

FIG[3.10] Variation of coupling coefficient with core radius .

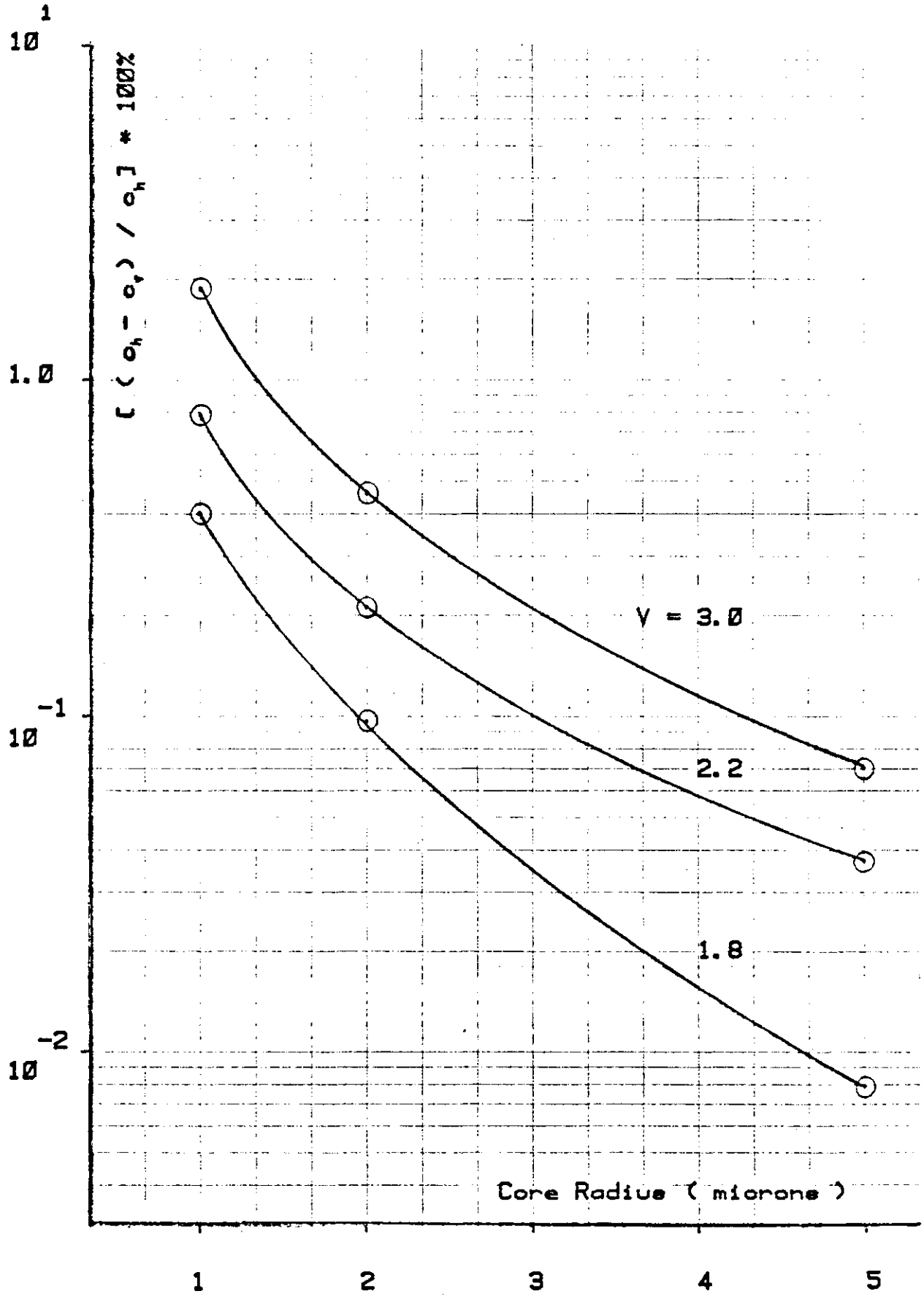

FIG[3.11] Polarization dependence of the coupling strength.

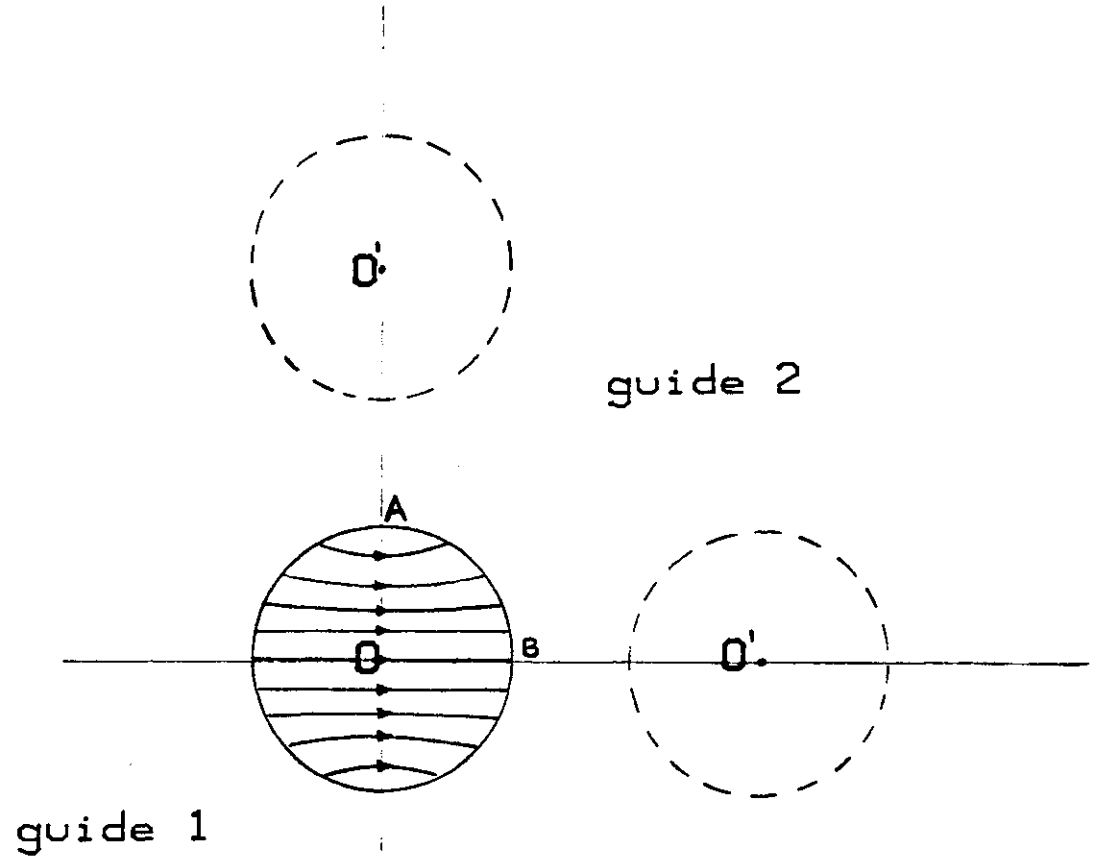

FIG[3.12] Schematic representation of the transverse electric field lines for the HE_{11} mode.

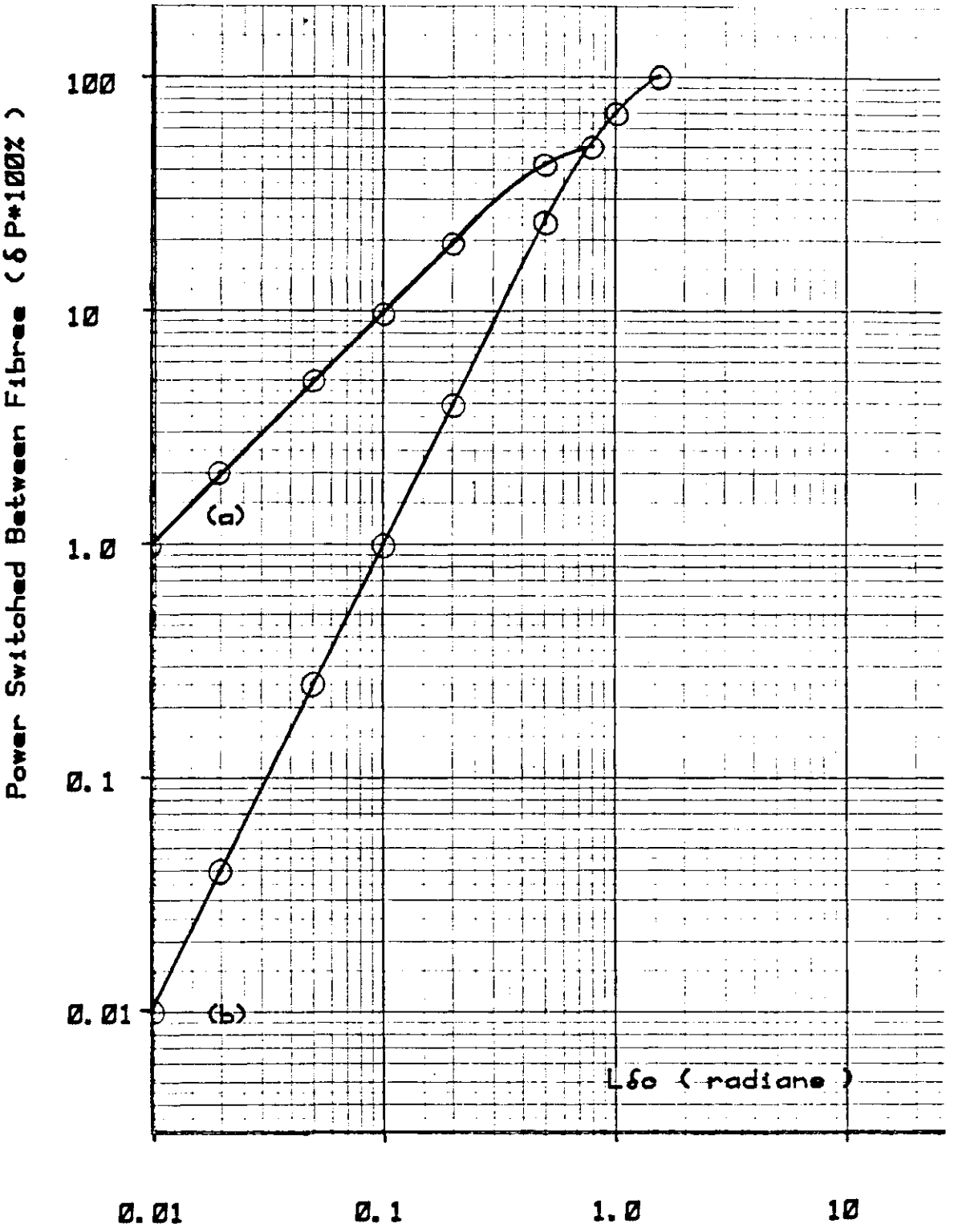

FIG[3.13] Percentage switched power as a function of Lδc for [a] L=[2N+1]π/4c and [b] L=Nπ/2c .

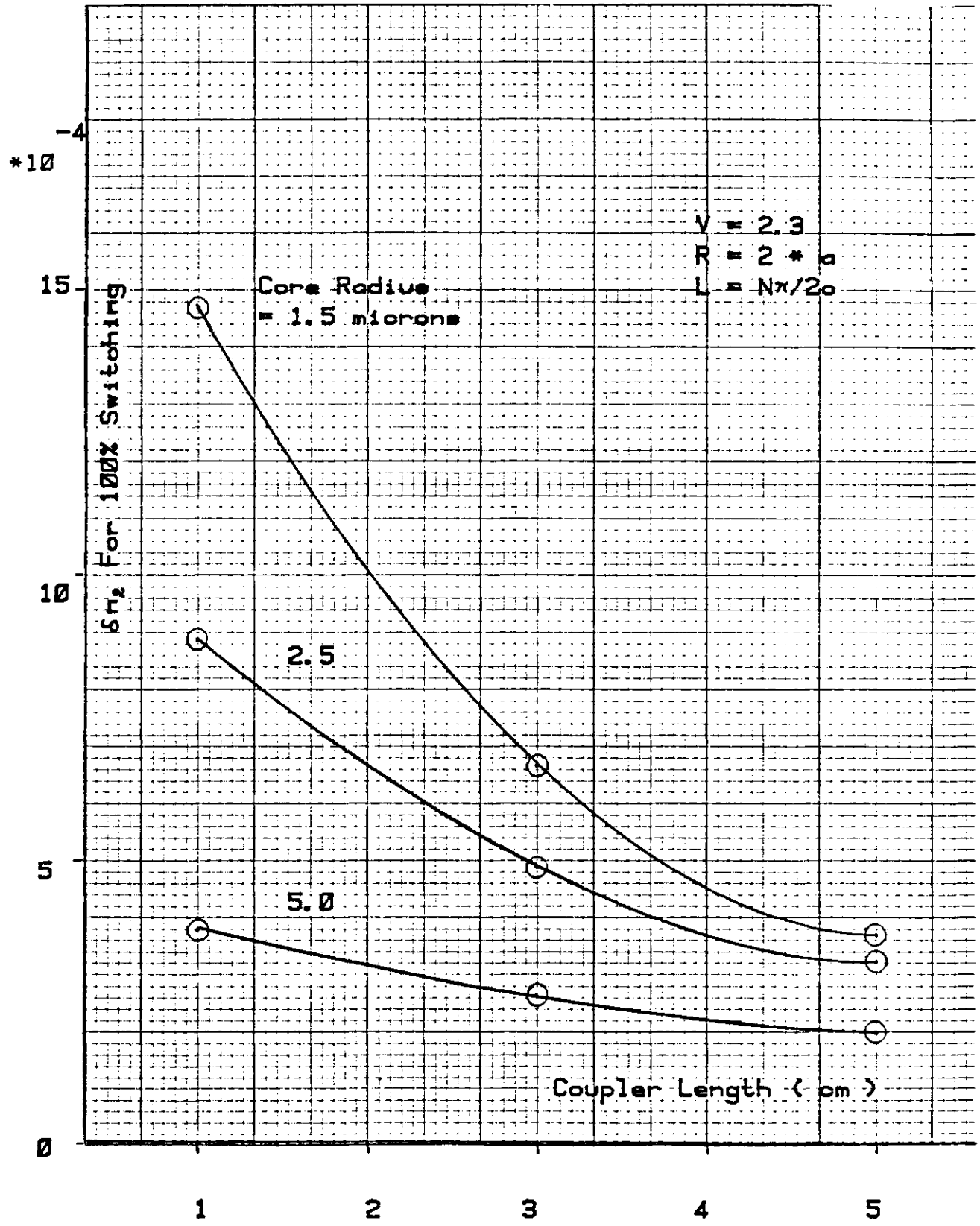

Fig[3.14] δn_2 required for 100% switching as a function of the length of the coupler.

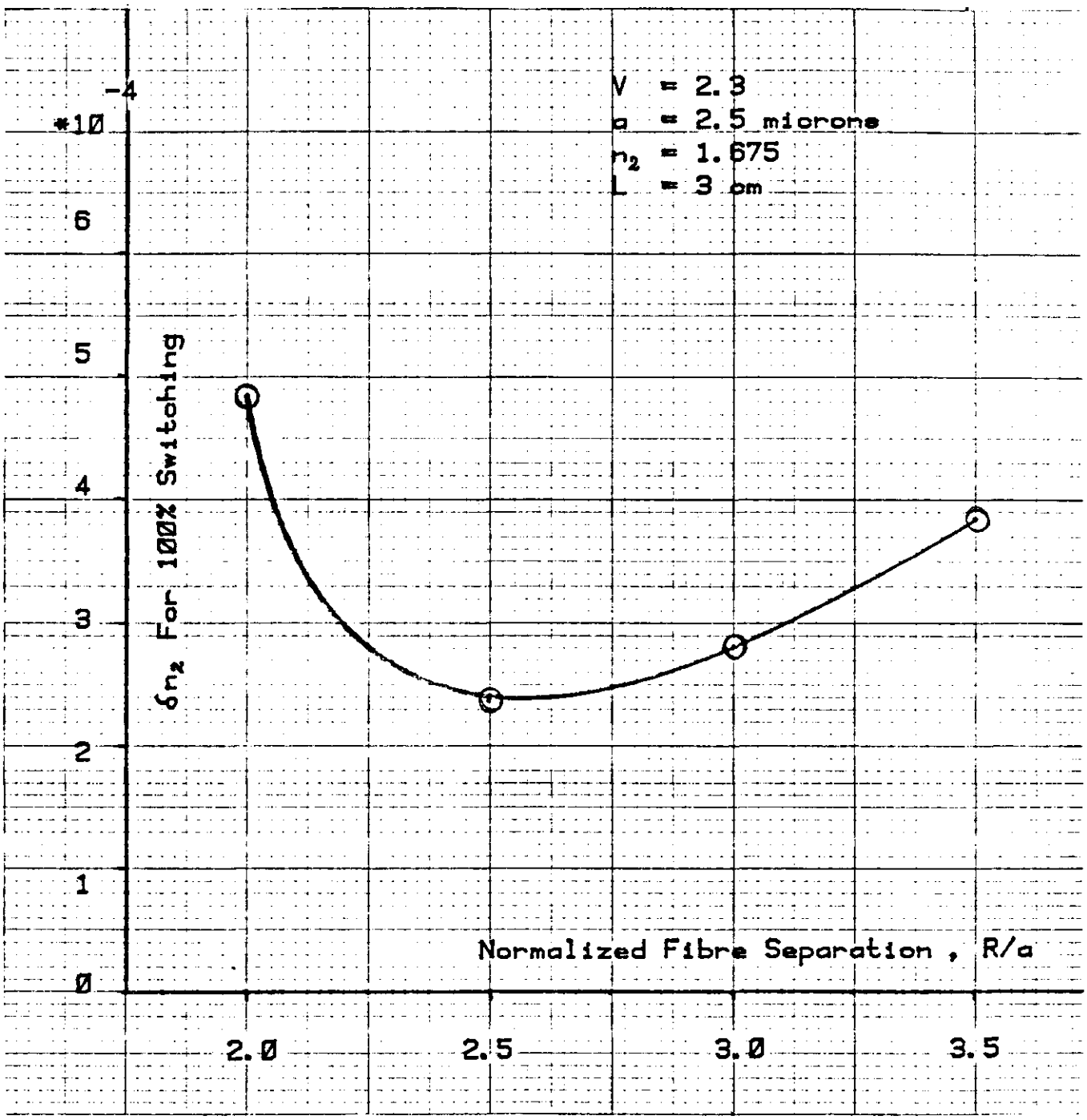

FIG[3.15] δn_2 for 100% switching as a function of the centre to centre separatio of the fibres.

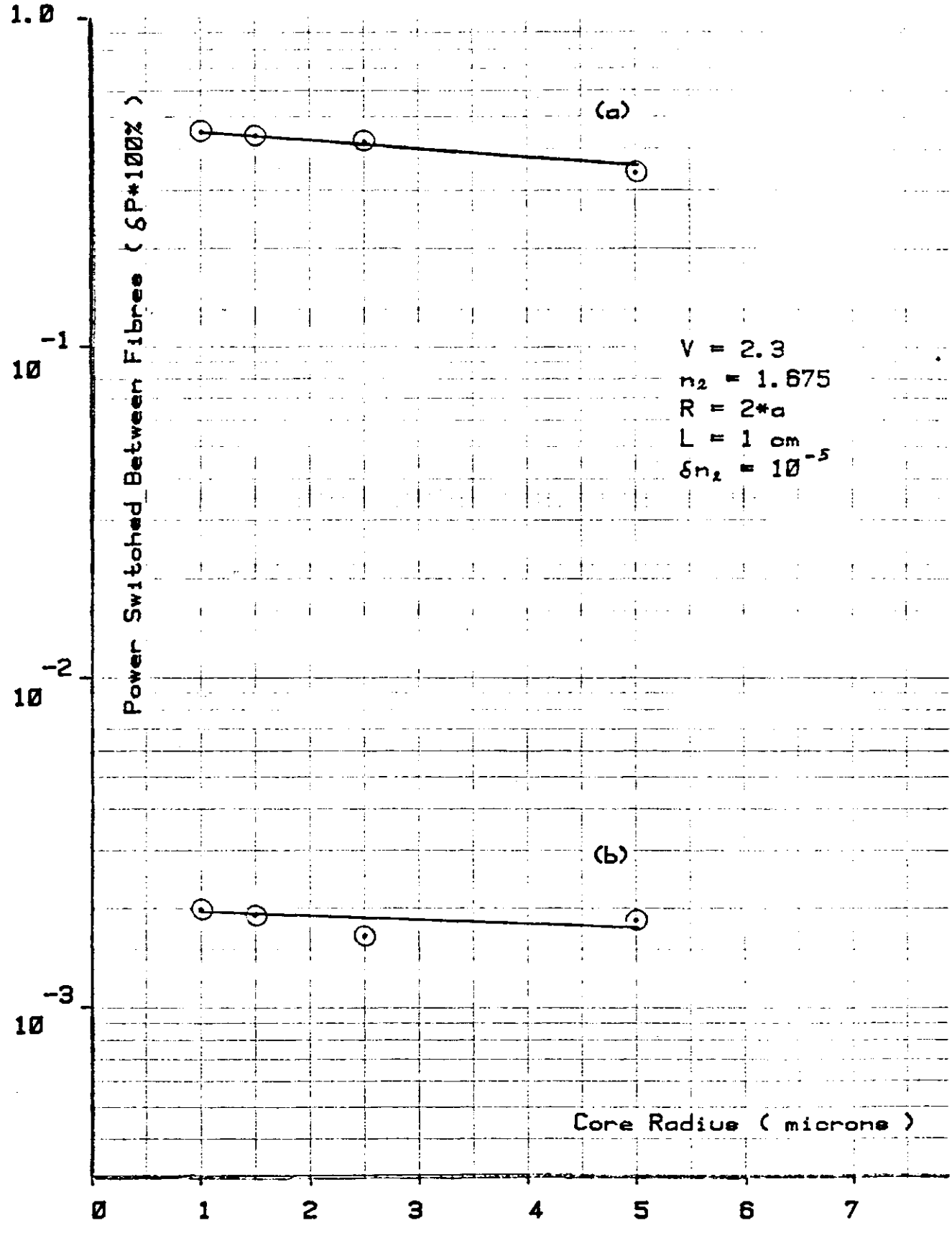

FIG[3.16] Percentage switched power as a function of core radius , for (a) $L=(2N+1)\pi/4c$ and (b) $L=N\pi/2c$.

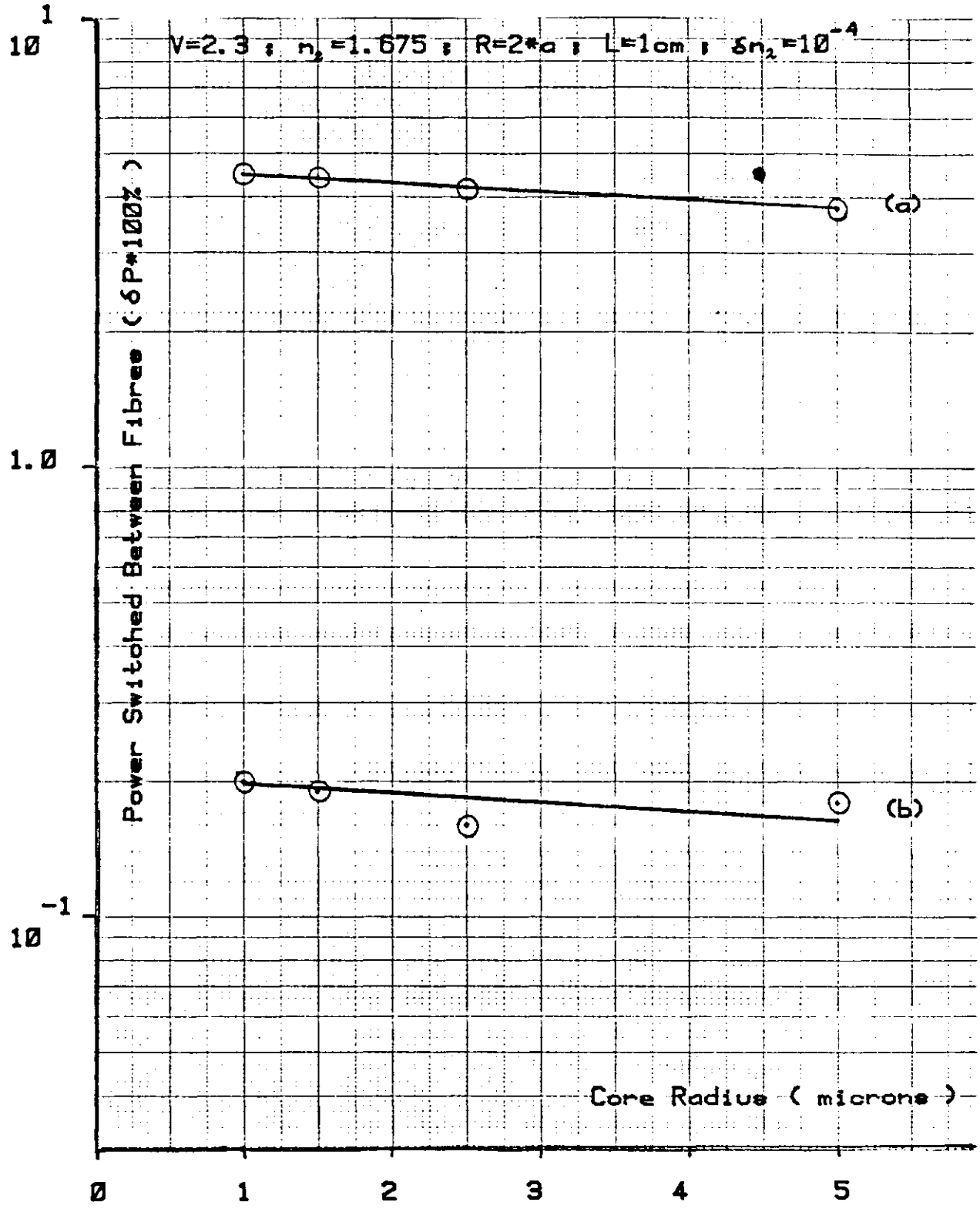

FIG[3.17] Percentage switched power as a function of core radius , for (a) $L=(2N+1)\pi/4c$ and (b) $L=N\pi/2c$.

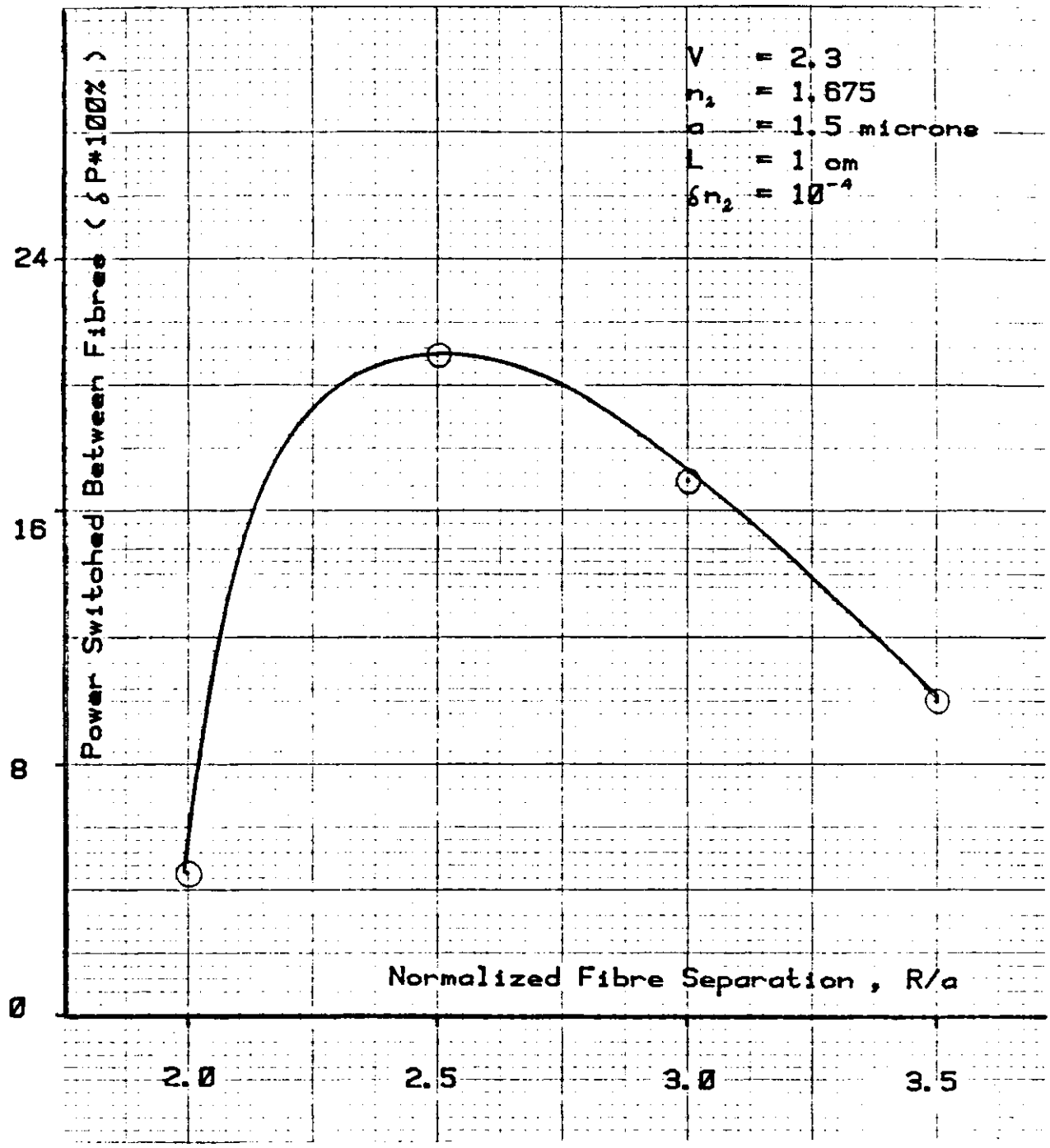

FIG[3.18] Percentage switched power as a function of fibre separation.

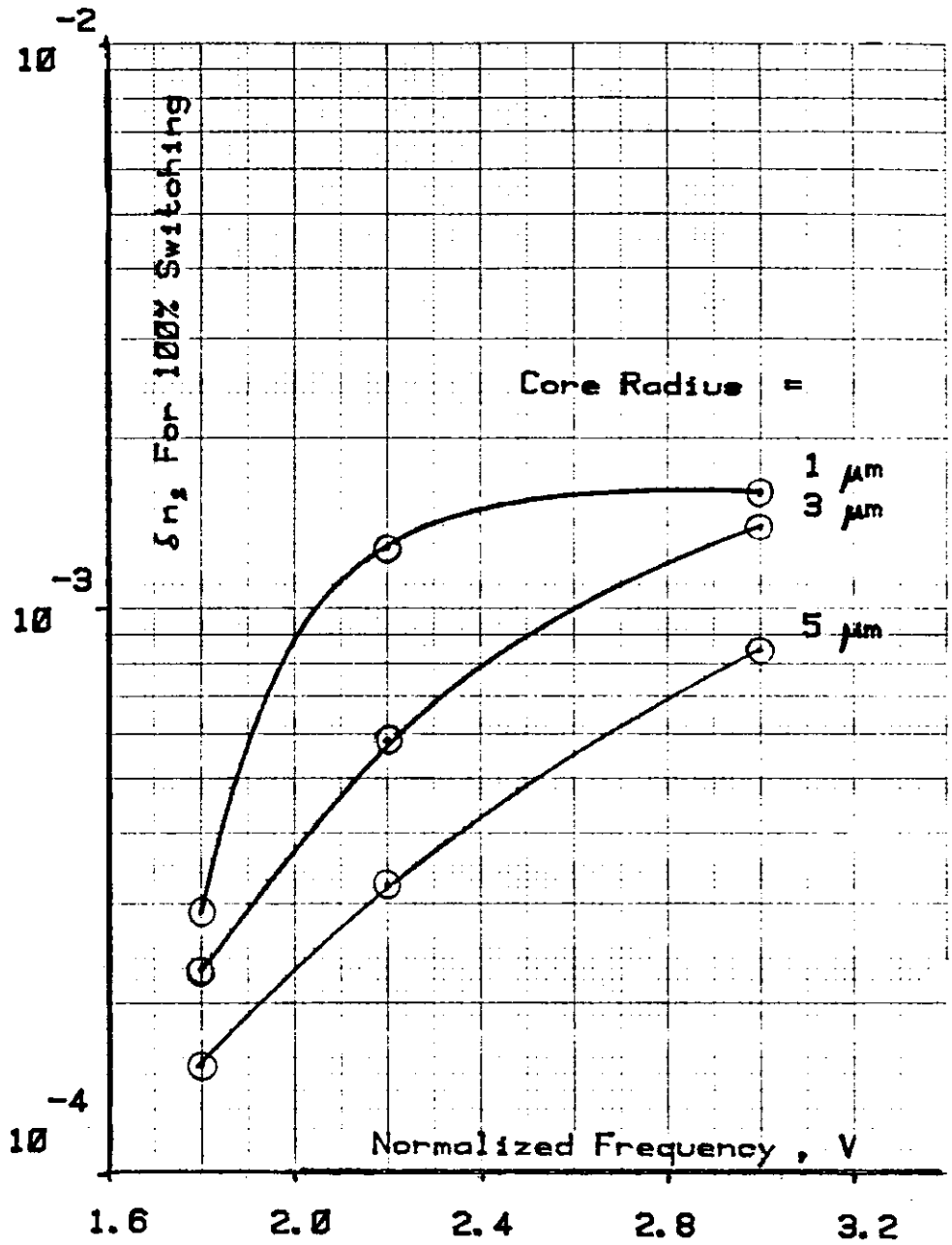

FIG[3.19] δn_2 for 100% switching as a function of normalized frequency .

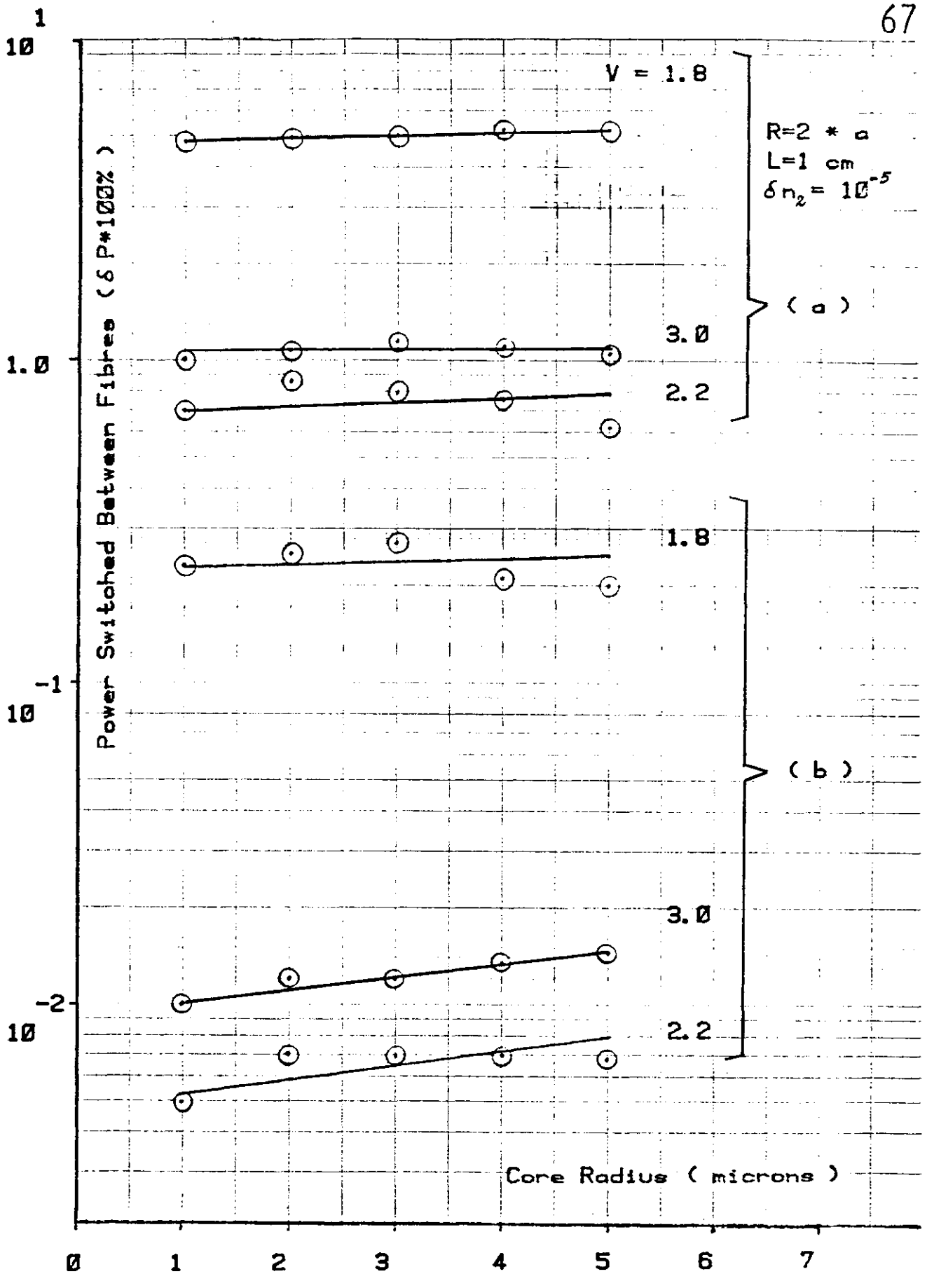

FIG[3.20] Percentage switched power as a function of core radius and normalized frequency for (a) $L=(2N+1)\pi/4c$ and (b) $L=N\pi/2c$.

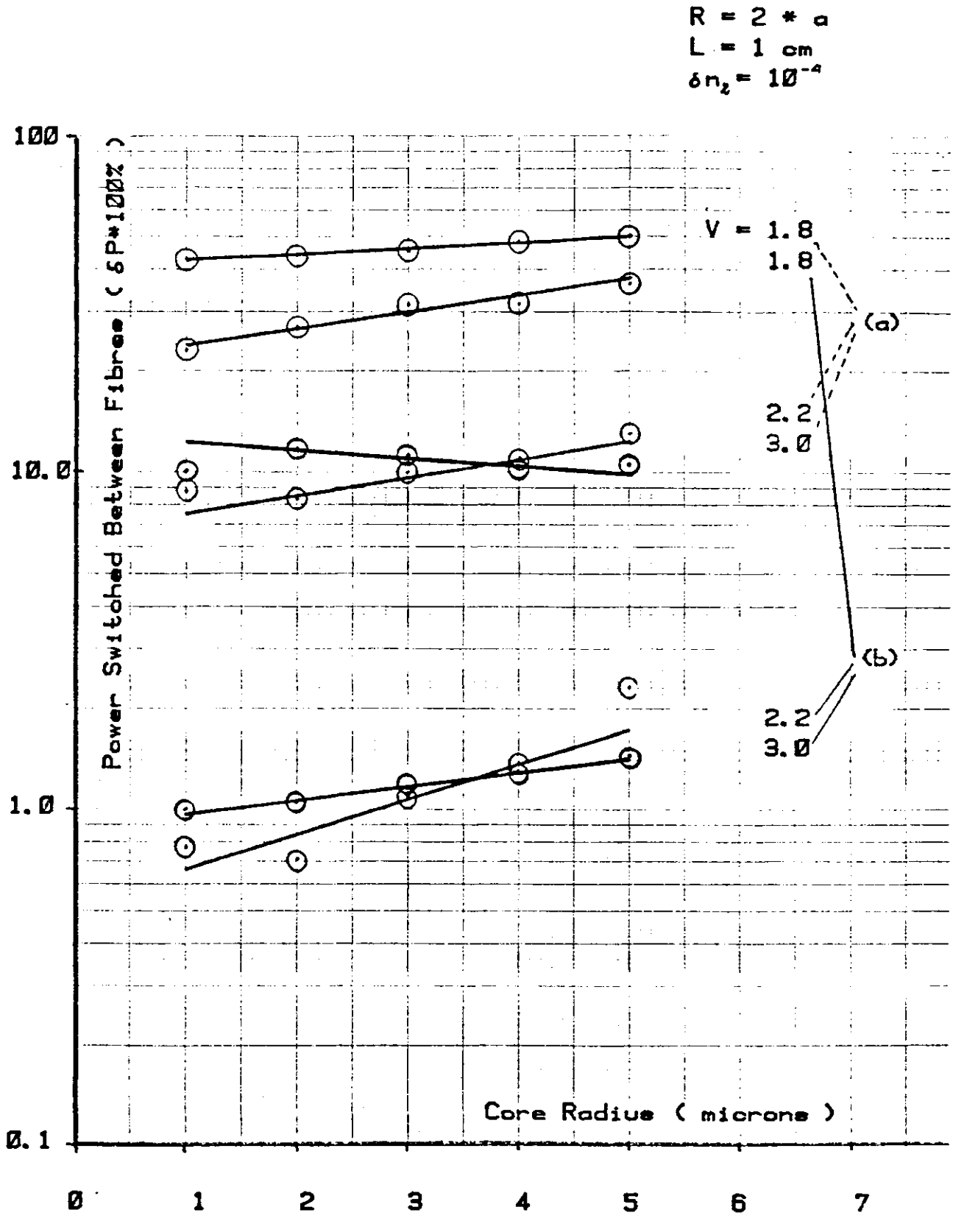

FIG[3.21] Percentage switched power as a function of core radius and normalized frequency for (a) $L=(2N+1)\pi/4c$ and (b) $L=N\pi/2c$.

CHAPTER 4 : ELECTRO-OPTIC CLADDING: PREPARATION AND PROPERTIES

4.1 Introduction

The performance of the coupler has so far been analysed theoretically and based on the assumption that the refractive index, n_2, of the cladding can be varied in step with the information signal. In fact, strictly speaking, it is $\Delta n = n_1 - n_2$ that should change with the modulating signal; ie varying either the core or the cladding index will be sufficient for the operation of the device. However, from a fabrication point of view it is very much simpler to change the refractive index of the cladding. The most commonly used physical effects for introducing a change of refractive index in a material are the electro-optic and the acousto-optic effects; the former is much more convenient to use at high frequencies and was selected for the coupler switch.

The material that we decided to use for the cladding was meta-nitroaniline (mNA), an organic crystal with a high electro-optic coefficient. Details of the properties of mNA, as well as a description of the methods that were used for growing it in single crystal form, are given later in this chapter. We start with a brief discussion of the electro-optic effect and the propagation of electromagnetic waves through anisotropic media.

4.2 Electro-Optic Effect

In their most general form Maxwell's equations for a non-magnetic dielectric material are (20)

$$\underset{\sim}{\nabla} \times \underset{\sim}{E} = -\mu \cdot \frac{\partial \underset{\sim}{H}}{\partial t} \tag{4.1}$$

$$\underset{\sim}{\nabla} \times \underset{\sim}{H} = \frac{\partial \underset{\sim}{D}}{\partial t} \tag{4.2}$$

where $\underset{\sim}{E}$, $\underset{\sim}{H}$ and $\underset{\sim}{D}$ are the time dependent vectors of the electric field, the magnetic field and the electric displacement respectively. The electric polarisation, $\underset{\sim}{P}$, of the propagation medium is related to the electric displacement by

$$\underset{\sim}{D} = \varepsilon_o \underset{\sim}{E} + \underset{\sim}{P} \tag{4.3}$$

For an isotropic medium the induced polarisation is parallel to the applied electric field and is related to it by a (scalar) factor that is independent of the direction in which the field is applied, ie

$$\underset{\sim}{P} = \varepsilon_o \chi_e \underset{\sim}{E} \tag{4.4}$$

where χ_e is the electric susceptibility of the material.

Combining (4.3) and (4.4) we obtain

$$\underset{\sim}{D} = \varepsilon_o(1 + \chi_e)\underset{\sim}{E} \tag{4.5}$$

$$\underset{\sim}{D} = \varepsilon\underset{\sim}{E} \tag{4.6}$$

where ε is the electric permeability of the material.

It can easily be shown (14) that the phase velocity, c, of a plane electromagnetic wave propagating in such a medium is given by

$$c = \frac{c_o}{\sqrt{\varepsilon/\varepsilon_o}} = \frac{c_o}{n} \tag{4.7}$$

where $c_o = \frac{1}{\sqrt{\mu_o\varepsilon_o}} = 3 \times 10^8$ m/s = the phase velocity in vacuum

and $n = \sqrt{\varepsilon/\varepsilon_o}$ = the refractive index of the material

A crystal, on the other hand, has an ordered structure, ie it is made up of a regular periodic array of atoms or ions (21). One would, therefore, expect that both the magnitude and the direction of the induced polarisation will depend on the direction of the applied electric field relative to the crystal axes. For an anisotropic material equation (4.4) must be replaced by

$$\left.\begin{aligned} P_x &= \varepsilon_o(\chi_{11}E_x + \chi_{12}E_y + \chi_{13}E_z) \\ P_y &= \varepsilon_o(\chi_{21}E_x + \chi_{22}E_y + \chi_{23}E_z) \\ P_z &= \varepsilon_o(\chi_{31}E_x + \chi_{32}E_y + \chi_{32}E_z) \end{aligned}\right\} \tag{4.8}$$

Here the capital letters represent the amplitudes of the various components of the electric field and electric polarisation vectors. The 3 x 3 array of χ_{ij} coefficients is called the electric susceptibility tensor. The magnitudes of the χ_{ij} coefficients must, of course, be dependant on the orientation of the x, y and z axes relative to the crystal structure. It is always possible to choose x, y and z in such a way that all the non-diagonal elements of the electric susceptibility tensor vanish, leaving

$$\left.\begin{aligned} P_x &= \varepsilon_o\chi_{11}E_x \\ P_y &= \varepsilon_o\chi_{22}E_y \\ P_z &= \varepsilon_o\chi_{33}E_z \end{aligned}\right\} \tag{4.9}$$

These directions are called the principal dielectric axes of the crystal.

The dielectric response of a crystal can alternatively be described using the electric permeability tensor ε_{ij}, defined by

$$\left.\begin{aligned} D_x &= \varepsilon_{11} E_x \\ D_y &= \varepsilon_{22} E_y \\ D_z &= \varepsilon_{33} E_z \end{aligned}\right\} \qquad (4.10)$$

From (4.5), (4.6) and (4.9) it follows that

$$\left.\begin{aligned} \varepsilon_{11} &= \varepsilon_o(1 + \chi_{11}) \\ \varepsilon_{22} &= \varepsilon_o(1 + \chi_{22}) \\ \varepsilon_{33} &= \varepsilon_o(1 + \chi_{33}) \end{aligned}\right\} \qquad (4.11)$$

Using (4.7) we can now define the principal refractive indices, n_x, n_y, n_z, of the crystal as follows

$$\left.\begin{aligned} n_x &= \sqrt{\varepsilon_{11}/\varepsilon_o} \\ n_y &= \sqrt{\varepsilon_{22}/\varepsilon_o} \\ n_z &= \sqrt{\varepsilon_{33}/\varepsilon_o} \end{aligned}\right\} \qquad (4.12)$$

A direct consequence of dielectric anisotropy is that the phase velocity of an electromagnetic wave propagating through a crystal depends on the direction of polarisation of its electric field, $\underset{\sim}{E}$; this phenomenon is called birefringence and is of great importance in optics (22, 23). In an isotropic material the magnitude of the induced polarisation is independent of the direction of the electric field vector so that $\chi_{11} = \chi_{22} = \chi_{33} = \chi$ and from (4.11) and (4.12) $n_x = n_y = n_z = n$. As a result, the phase velocity, $c = c_o/n$, is independant of the direction of polarisation. This argument clearly does not hold for a birefringent material. Consider an optical beam propagating along the z-axis of a crystal. If its $\underset{\sim}{E}$ vector is polarised in the x direction, according to (4.9) only Px is induced, the wave will effectively "see" n_x only (4.11) and will, therefore, propagate with a phase velocity given by $c_x = c_o/n_x$,(4.7). If on the otherhand the electric field is polarised along y, the beam will have a phase velocity $c_y = c_o/n_y$. If the optical beam is polarised such that the $\underset{\sim}{E}$ vector has non-zero components in both x and y directions, its propagation through the crystal will have to be analysed as a combination of two plane waves, one polarised along x and the other along y.

In fact the propagation of an electromagnetic wave in an arbitrary direction through a crystal can always be analysed in terms of two orthogonally polarised plane waves (22) and (23). The direction of polarisation of these plane waves as well as the magnitude of their phase velocities has to be determined. This can be done most conveniently with the aid of the index ellipsoid (indicatrix).

$$\frac{x^2}{n_x^2} + \frac{y^2}{n_y^2} + \frac{z^2}{n_z^2} = 1 \qquad (4.13)$$

This is the equation of a generalised ellipsoid with major axes parallel to x, y and z whose respective lengths are $2n_x$, $2n_y$ and $2n_z$. The procedure for finding the polarisation directions and the corresponding phase velocities for a given direction of propagation is as follows. Determine the ellipse formed by the intersection of a plane through the origin and normal to the direction of propagation and the index ellipsoid (4.13). The directions of the two allowed polarisations are those of the major and minor axes of this ellipse. The lengths of the two axes of this ellipse are $2n_1$ and $2n_2$ where n_1 and n_2 are the refractive indices for the two allowed solutions. The two waves thus propagate with phase velocities c_o/n_1 and c_o/n_2 where $c_o = (\mu_o \varepsilon_o)^{-\frac{1}{2}}$ is the phase velocity in vacuum. Since the two phase velocities are, in general, different, the state of polarisation of the wave changes periodically as it propagates through the crystal. If the wave is linearly polarised on entering the crystal it will, in general, gradually become elliptical, then circular, back to elliptical and then linear again (but 90^o rotated from the original direction) and so on. The polarisation of the wave as it leaves the crystal clearly depends on the difference between the two components of the phase velocity and the length of the crystal. A formal proof of the procedure for using the index ellipsoid as well as further examples of its use are given in references (22) and (23).

Electro-optic crystals have the property that the orientation and/or the dimensions of their index ellipsoid can be changed by the application of an external electric field. The refractive index 'seen' by a wave travelling through the crystal will therefore depend on the magnitude and the direction of the applied field. This forms the basis of operation of all electro-optic devices.

There are two basic types of electro-optic effects: linear and quadratic known as Pockels and Kerr effects respectively. The most convenient method of analysing the effect of applying a field to a material of refractive index n is to consider the change in $\frac{1}{n^2}$ rather than the direct change in n. The quantity $\frac{1}{n^2}$ can be written as

$$\frac{1}{n^2} = \frac{1}{n_o^2} + rE + RE^2 + \ldots\ldots\ldots \qquad (4.14)$$

where r and R are the linear and the quadratic electro-optic coefficients respectively, E is the applied electric field and n_o the refractive index of the material in the absence of the field. If the material has a centre of symmetry (21), reversing the direction of the field causes no change, that is to say, $\frac{1}{n^2}$ will be independant of the sign of E. From (4.14), however, we can see that the terms of odd power in E will change sign if E is replaced by -E. The coefficients of these terms must, therefore, be uniquely zero in centrosymmetric materials, and in particular r = 0. It follows that only non-centrosymmetric materials can exhibit the linear electro-optic effect. The classification of crystals as centrosymmetric or non-centrosymmetric is an elementary consideration in crystallography and this information is widely tabulated (21).

In the most general case when a field is applied to an electro-optic crystal the ellipsoid undergoes changes both in its dimensions and orientation. This means that the ellipsoid expands (or contracts) and also rotates. The general equation of the new ellipsoid can be written as

$$\left(\frac{1}{n^2}\right)_1 x^2 + \left(\frac{1}{n^2}\right)_2 y^2 + \left(\frac{1}{n^2}\right)_3 z^2 + 2\left(\frac{1}{n^2}\right)_4 yz + 2\left(\frac{1}{n^2}\right)_5 xz + 2\left(\frac{1}{n^2}\right)_6 xy = 1 \qquad (4.15)$$

Since x, y and z are parallel to the principal dielectric axes of the crystal, with zero field applied, (4.15) must reduce to (4.13); therefore,

$$\left.\begin{aligned} \left(\frac{1}{n^2}\right)_1 \Big|_{E=0} &= \frac{1}{n_x^2} \\ \left(\frac{1}{n^2}\right)_2 \Big|_{E.=0} &= \frac{1}{n_y^2} \end{aligned}\right\} \qquad (4.16)$$

$$\left(\frac{1}{n^2}\right)_3\Big|_{E=0} = \frac{1}{n_z^2}$$

and

$$\left(\frac{1}{n^2}\right)_4\Big|_{E=0} = \left(\frac{1}{n^2}\right)_5\Big|_{E=0} = \left(\frac{1}{n^2}\right)_6\Big|_{E=0} = 0 \qquad (4.16)$$

The linear change in the coefficients

$$\left(\frac{1}{n^2}\right)_i \ , \quad i = 1 \ , \ \ldots\ldots\ldots , \ 6$$

due to an arbitrary electric field $\underline{E}$ (E_x, E_y, E_z) is defined by

$$\Delta\left(\frac{1}{n^2}\right)_i = \sum_{j=i}^{3} r_{ij}E_j \qquad (4.17)$$

where in the summation over j we use the convention 1 = x, 2 = y, 3 = z.

Equation (4.17) can be expressed in matrix form as

$$\begin{vmatrix} \Delta\left(\frac{1}{n^2}\right)_1 \\ \Delta\left(\frac{1}{n^2}\right)_2 \\ \Delta\left(\frac{1}{n^2}\right)_3 \\ \Delta\left(\frac{1}{n^2}\right)_4 \\ \Delta\left(\frac{1}{n^2}\right)_5 \\ \Delta\left(\frac{1}{n^2}\right)_6 \end{vmatrix} = \begin{vmatrix} r_{11} & r_{12} & r_{13} \\ r_{21} & r_{22} & r_{23} \\ r_{31} & r_{32} & r_{33} \\ r_{41} & r_{42} & r_{43} \\ r_{51} & r_{52} & r_{53} \\ r_{61} & r_{62} & r_{63} \end{vmatrix} \begin{vmatrix} E_x \\ E_y \\ E_z \end{vmatrix} \qquad (4.18)$$

Using the rules of matrix multiplication, we have, for example

$$\Delta\left(\frac{1}{n^2}\right)_1 = r_{11}E_x + r_{12}E_y + r_{13}E_z$$

This 6 x 3 matrix with elements r_{ij} is called the electro-optic tensor. Symmetry considerations can be used to simplify the tensor; these dictate which of the 18 elements are zero, as well as the relationships that exist between the non-zero elements.

The crystallographic structure of meta-nitroaniline is of the mm2 symmetry group. Details of such crystallographic classifications and the properties of each symmetry group can be found in reference (21). For the purposes of this work it is sufficient to understand that the electro-optic tensor for the mm2 symmetry group has five non-zero elements, (22), ie

$$r_{ij} = \begin{vmatrix} 0 & 0 & r_{13} \\ 0 & 0 & r_{23} \\ 0 & 0 & r_{33} \\ 0 & r_{42} & 0 \\ r_{51} & 0 & 0 \\ 0 & 0 & 0 \end{vmatrix} \qquad (4.19)$$

The coefficients r_{51} and r_{42} are skew terms and describe rotations of the indicatrix for applied fields along the x and y principal axes respectively. Therefore, if only E_z is applied to the crystal the ellipsoid does not rotate but only undergoes a change in size, ie it either expands or contracts. The magnitudes of the index changes clearly depend not only on the strength and direction of the electric field but also on the values of the electro-optic coefficients and the refractive indices.

4.3 Meta-Nitroaniline (mNA)

This is a yellow, biaxial, organic crystal of the mm2 symmetry group (21). Some of the main features of mNA that made it a suitable choice for this work are as follows:

(i) relatively easy to grow in single-crystal form (see section 4.5),

(ii) very large electro-optic coefficients, and

(iii) low melting point.

The electro-optic as well as the physical and chemical properties of mNA have been studied and reported extensively (24). Here the discussion will be limited to outlining those properties of mNA which are essential for a complete understanding of the operation of the directional coupler modulator.

The three principal refractive indices of mNA at room temperature for $\lambda = 0.633$ μm are

$n_x = 1.805$

$n_y = 1.715$

$n_z = 1.675$

where, x, y and z are the directions of the principal axes of the crystal. Equation (4.18) and (4.19) show that in order to induce a change in these indices an electric field must be applied along the crystallographic z direction. The standard methods of identifying the directions of the principal axes of a crystal are based on X-ray diffraction techniques (21). However, for mNA the task is much simpler; the crystal grows along the z-axis and cleaves easily in the xz plane (24). The principal axes can, therefore, be identified very easily without the use of X-rays - see section 4.5. The three principal electro-optic coefficients of mNA at $\lambda = 0.633$ μm are, (24),

$$\left.\begin{aligned} r_{13} &= 7.4 \pm 0.7 \\ r_{23} &= 0.1 \pm 0.6 \\ r_{33} &= 16.7 \pm 0.2 \end{aligned}\right\} \times 10^{-12}\ \mathrm{mV}^{-1}$$

Since r_{33} has by far the largest magnitude, the design of the directional coupler switch must be such that the refractive index change is achieved via r_{33}. It can be seen from equations (4.18) and (4.19) that the only refractive index affected by r_{33} is n_z. In fact the change, Δn_z, in n_z as a result of applying an electric field E_z to the crystal is given by*

$$\Delta n_z = \tfrac{1}{2} n_z^3\, r_{33}\, E_z \qquad (4.20)$$

Using this equation a graph of Δn_z v E_z was plotted, Fig (4.1). It illustrates clearly that very large electric fields are required for index changes of greater than about 10^{-5}, see section 3.5.

---

* From (4.18) and (4.19)

$$\frac{1}{(n_z + \Delta n_z)^2} = \frac{1}{n_z^2} + r_{33} E_z$$

Expanding the l.h.s. and neglecting Δn_z^2, Δn_z^3 etc leads to equation (4.20).

4.4 Structure Of The Directional Coupler

Clearly the orientation of the fibres relative to the principal axes of the crystal are of utmost importance. It was shown in the previous section that the electric field must be applied along the crystal z-axis. It is also clear that the most convenient direction for applying a voltage to the device is at right angle to the fibres, Fig (2.3). It, therefore, follows that the fibres must be positioned in the xy plane of the crystal. In fact, it will be shown later that for best performance the fibres must be orientated parallel to the y-axis of the crystal. It has already been shown that n_z undergoes the largest change for a given applied field, E_z. The radius, a, and refractive index, n, of the core glass must, therefore, be chosen such that the composite crystal-cladded fibres will be single-moded with $n_z = 1.675$ as the cladding index, ie

$$\frac{2\pi a}{\lambda} \sqrt{n^2 - n_z^2} \leqslant 2.405$$

where, λ is the operating wavelength - see section 1.3.
For realistic values of a, n will always be smaller than both n_x and n_y; typical values are

$$\left.\begin{aligned} n &= 1.67564 \\ n_z &= 1.67500 \\ a &= 5.0\ \mu m \\ \lambda &= 0.633\ \mu m \\ V &= 2.3 \end{aligned}\right\} \qquad (4.21)$$

In contrast to an ordinary optical fibre the cladding here is strongly anisotropic Fig (4.2); clearly the implications of this must be considered. The HE_{11} mode has very small axial field components and behaves very nearly like a linearly polarised transverse mode, (5) (6). The light launched into the core of the fibre in Fig (4.2b) can be represented by two HE_{11} modes that are orthogonally polarised along the x and z axes. With the aid of the index ellipsoid it becomes clear that the corresponding electric fields 'see' n_x and n_z respectively. The field component along x will not be bound to the core because it sees a cladding with a higher refractive index, $n_x = 1.805$, than the core, $n = 1.6756$. The component along z encounters n_z ($<n$) and is guided by the structure. Since only the field components in the z direction are guided, the crystal-cladded fibre is not only single-moded but also single-polarisation.

The effect of the anisotropy in the axial direction - ie the fact that the axial fields 'see' $n_y = 1.715$ while the transverse components 'see' a different index, $n_z = 1.675$ - is much more complicated to determine. However, as a first approximation it can be argued that since the axial field components are much smaller than the transverse fields, it is unlikely that the anisotropy would have a significant effect on the propagation characteristics of the fibre. The "effective" refractive index of the cladding will probably be slightly higher than $n_z = 1.675$ as a result of the anisotropy. If this increase in the cladding index is comparable to the core-cladding index difference, it might cause a leakage of optical energy into the cladding as the light propagates along the fibre. In other words the axial anisotropy might increase the attenuation of the fibre slightly. Since only a very short length ($\simeq$ 1 cm) of fibre is involved the extra loss is unlikely to be significant. Clearly this axial anisotropy is smallest when the fibres are positioned along the y-axis of the crystal.

4.5 mNA Crystal Growth

Relatively large single-crystals of mNA were grown, fairly easily, using vapour phase epitaxy (VPE). A schematic representation of the apparatus used for the VPE growth is shown in Fig (4.3). The meta-nitroaniline, as supplied (British Drug Houses, GPR), was first loaded into pyrex tubes (length $\simeq$ 30 cm, i.d. $\simeq$ 0.5 cm) and purified by zone refining (21). A significant improvement in the purity of the material - as indicated by colour change - was achieved after about ten passes through the zone refiner. The purified mNA was loaded into the glass capsule, Fig (4.4), via the loading arm which was then sealed. The capsule was connected to a vacuum pump via the other arm and when the pressure inside the capsule had dropped to about 10^{-4} cmHg the arm was sealed. The capsule was then suspended from a geared motorised puller and allowed to completely immerse in a thermostatically controlled oil-bath (Townson and Mercer, E270, Series III). The oil was heated to just over the melting temperature (113°C) of mNA, in order to clear any material remaining in the capsule taper. The motorised puller was used to lift the capsule out of the oil at a very slow rate (0.1 - 1 mm/h). The mNA vapour which now existed in the capsule recrystallised in the vertex of the taper soon after this had been lifted out of the oil. The crystal

thus formed acted as a seed for further crystallisation which occurred as the capsule was pulled slowly (0.1 - 1 mm/h) out of the oil.

The oil bath had double glass windows which allowed continuous observation of the capsule. By monitoring the growth of the crystal it was possible, in case of polycrystallisation occurring, to stop the process, melt the unwanted part of the crystal - by lowering the capsule back into the oil bath - and restart the growth. It was necessary to adjust the puller speed occasionally in order to ensure single-crystal growth. It took, on average, about a week to produce a good quality single-crystal about 2 cm long.

The identification of the crystal axes was very much simplified by the fact that mNA has perfect cleavage in the xz plane. Furthermore, during the growth, the crystal z-axis lines up almost exactly with the axis of the capsule (24). A complete identification of the crystal axes could, therefore, be carried out very simply and without X-ray analysis.

A wet-string saw, with ethanol as the solvent, was used to cut discs of mNA from the boule; the cleavage plane was used as reference, Fig (4.5). In order to achieve a good optical finish, the cut surfaces were polished using graded diamond paste (Marcon Kristalap) on a cloth lap. The discs were examined under a microscope between crossed polarisers to ensure single crystallisation. The discs thus prepared were later used as substrates in the fabrication of the coupler switch. However, it was first necessary to grow a single-crystal of mNA around a glass fibre; the techniques used for this purpose are described in the next section.

4.6 Fabrication Of A Crystal-Cladded Fibre

It was necessary to fabricate the structure shown in Fig (4.6) as a first step towards the construction of the coupler switch. Since vapour phase epitaxy had proved very successful for the growth of the bulk mNA, it was decided to employ the same technique again. The intention was to use the mNA substrates already prepared as seeds for further crystallisation using VPE. For this purpose the capsule shown in Fig (4.4) was modified as illustrated in Fig (4.7). The tapered section of the original capsule was replaced by a plunger-like

arrangement consisting of a glass tube and three tightly fitting O-rings; this design allowed the same capsule to be used several times.

The source material was loaded into the capsule from the top. The plunger, carrying the seed crystal, was then positioned inside the capsule such that the seed crystal was about 15 cm from the source material. The capsule was evacuated to about 10^{-4} Torr - via the side arm which was then sealed - and placed in the oil bath such that the seed crystal was just above the oil level. The rest of the growth procedure was exactly as described in section 4.5 .

The new layer of crystal that was formed was completely polycrystalline and contained numerous needle growths. This was attributed largely to a fast growth process but also to bad finish and contamination of the surface of the seed crystal. The experiment was repeated several times paying much more attention to the surface quality of the seed crystal. This eliminated the needle growths but polycrystallisation persisted. Several steps were taken to reduce the rate of crystallisation, including:

(i) reducing the speed of the puller;
(ii) increasing the distance between the seed crystal and the source material;
(iii) elimination of the heatsink rod, thus reducing the temperature difference between the source and the seed;
(iv) using a higher capsule pressure ($\simeq 10^{-2}$ Torr).

Only minor improvements were observed in the new crystal layer which remained polycrystalline.

It was decided that the temperature gradient between the source and the seed had to be reduced even further. The oil bath method of heating the capsule was abandoned in favour of an electrical technique. Figure (4.8) gives a schematic representation of the resistance heating method that was used. The number of turns of resistance wire per unit length of the capsule was adjusted such that only a very small temperature gradient was established between the source and the seed. The current through the wire was adjusted to give the correct temperature inside the capsule. The same form of polycrystalline growth was obtained again; altering the distribution of the

resistance wire per unit length did not improve the quality of the crystal. It was, therefore, decided not to pursue the VPE approach any further and instead a growth technique based on liquid phase epitaxy (LPE) was developed.

Fig (4.9) shows the various stages of the new method of growth. The substrate was placed about 1 cm below a resistance heater, Fig (4.9a), that consisted of a syringe tube (length ≃ 5 cm, o.d. ≃ 2 mm) connected via a transformer and a variac to the mains. The variac was adjusted until a thin layer of the substrate melted Fig (4.9b). By gradually reducing the current in the heater to zero the mNA melt was allowed to recrystallise. By adjusting the heating and the cooling of the crystal it was possible to melt a thin (≃ 300 μm) layer of the substrate and then recrystallise it with the same initial orientation. Only minor surface degredations were observed; the substrate retained its single-crystal orientation. This was confirmed by examining the processed substrates under a microscope between crossed polarisers.

The next stage of the work, ie embedding a fibre in the crystal, was completed quite easily. A piece of glass fibre about 20 cm in length and 10 μm in diameter was placed on the substrate prior to heating. Very small pieces of Blu-Tack were attached to the ends of the fibre to ensure that it stayed firmly in contact with the crystal, Fig (4.10a). When the substrate was heated the fibre, under the weight of the Blu-Tack, sank in the melt, Fig (4.10b). Slow, controlled cooling allowed the melt to recrystallise around the fibre and assume the same orientation as the substrate, Fig (4.10c). Examination of the crystal under a microscope and through crossed polarisers showed no deterioration of the orientation.

The glass core was chosen quite arbitrarily just to demonstrate the growth technique. In the construction of the coupler switch, however, one requires two glass cores with a precisely pre-determined refractive index. The next chapter is mainly devoted to describing the techniques used and the difficulties encountered in the construction of the coupler switch.

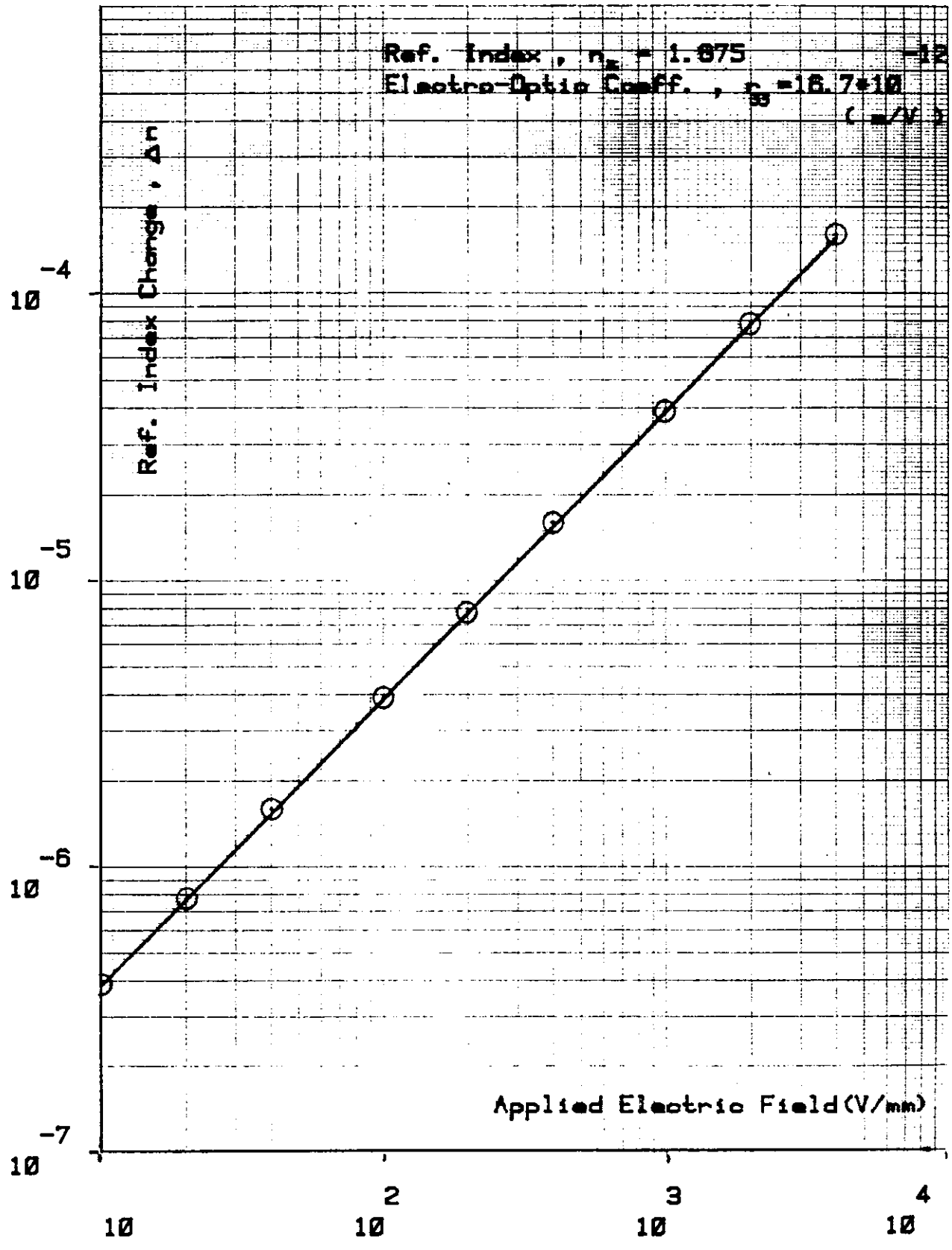

FIG[4.1] Change in the refractive index of mNA as a function of the applied electric field.

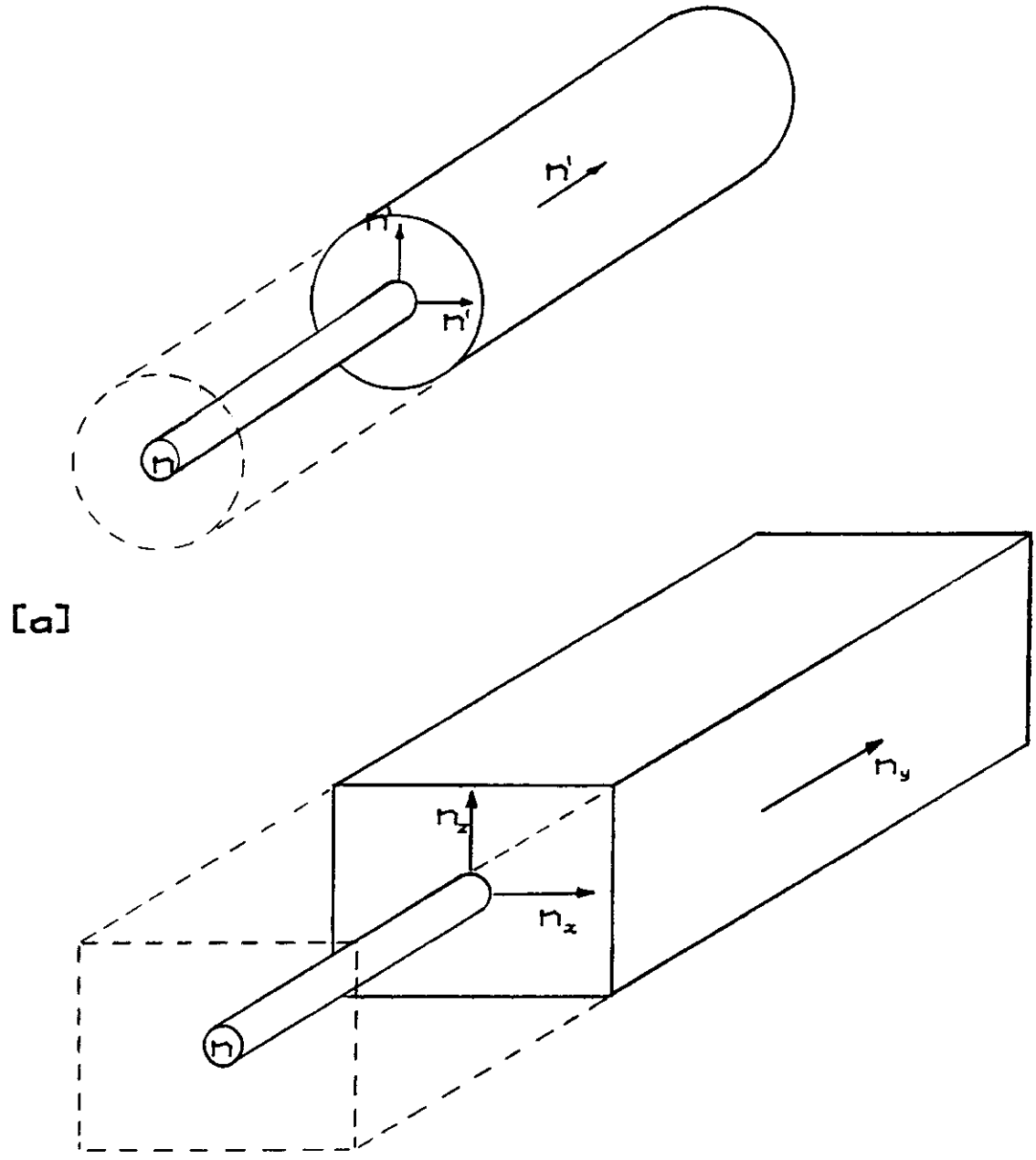

FIG[4.2] Comparison of fibres with [a] isotropic and [b] anisotropic claddings.

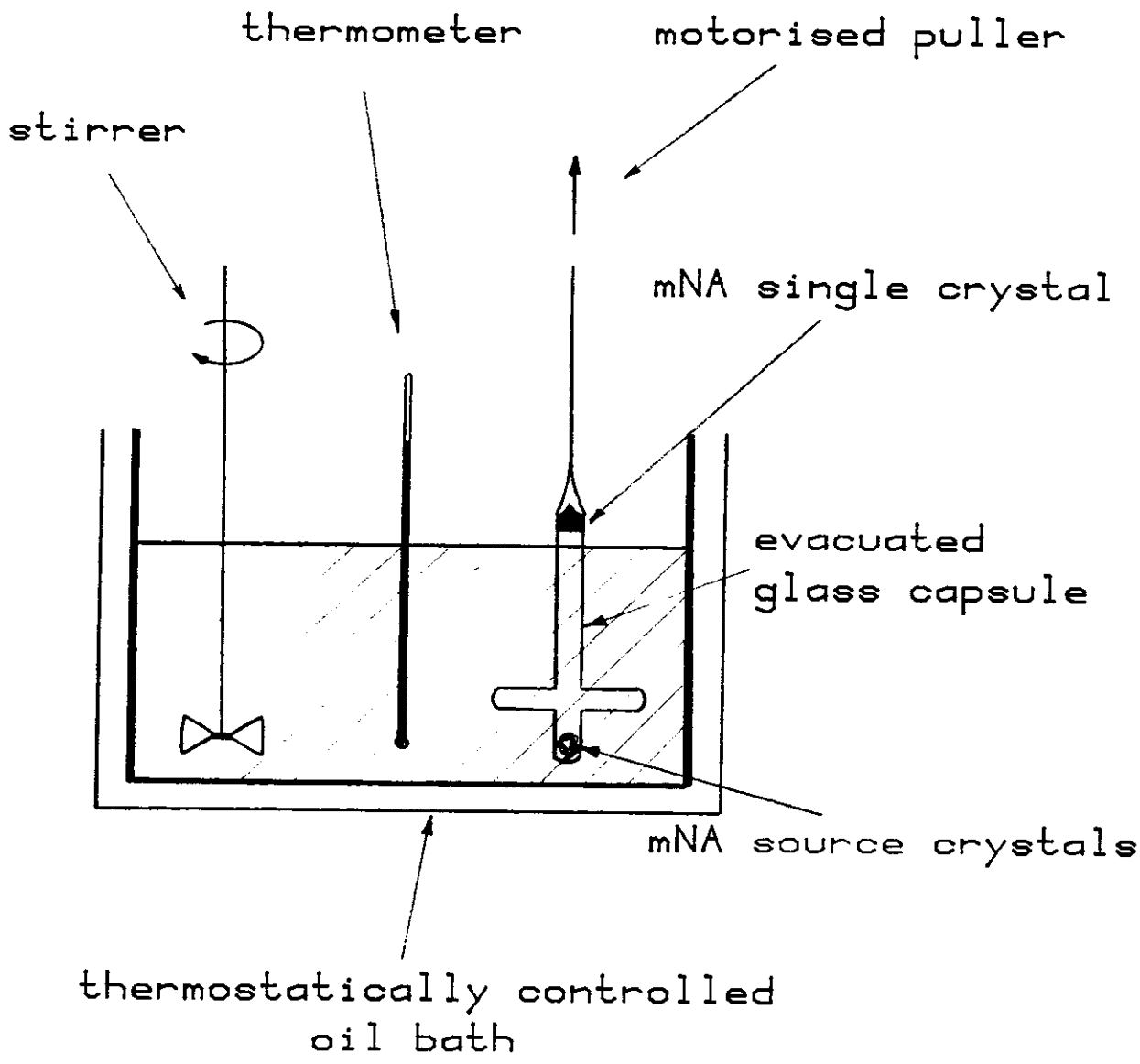

FIG[4.3] Apparatus used for VPE growth of meta nitroaniline.

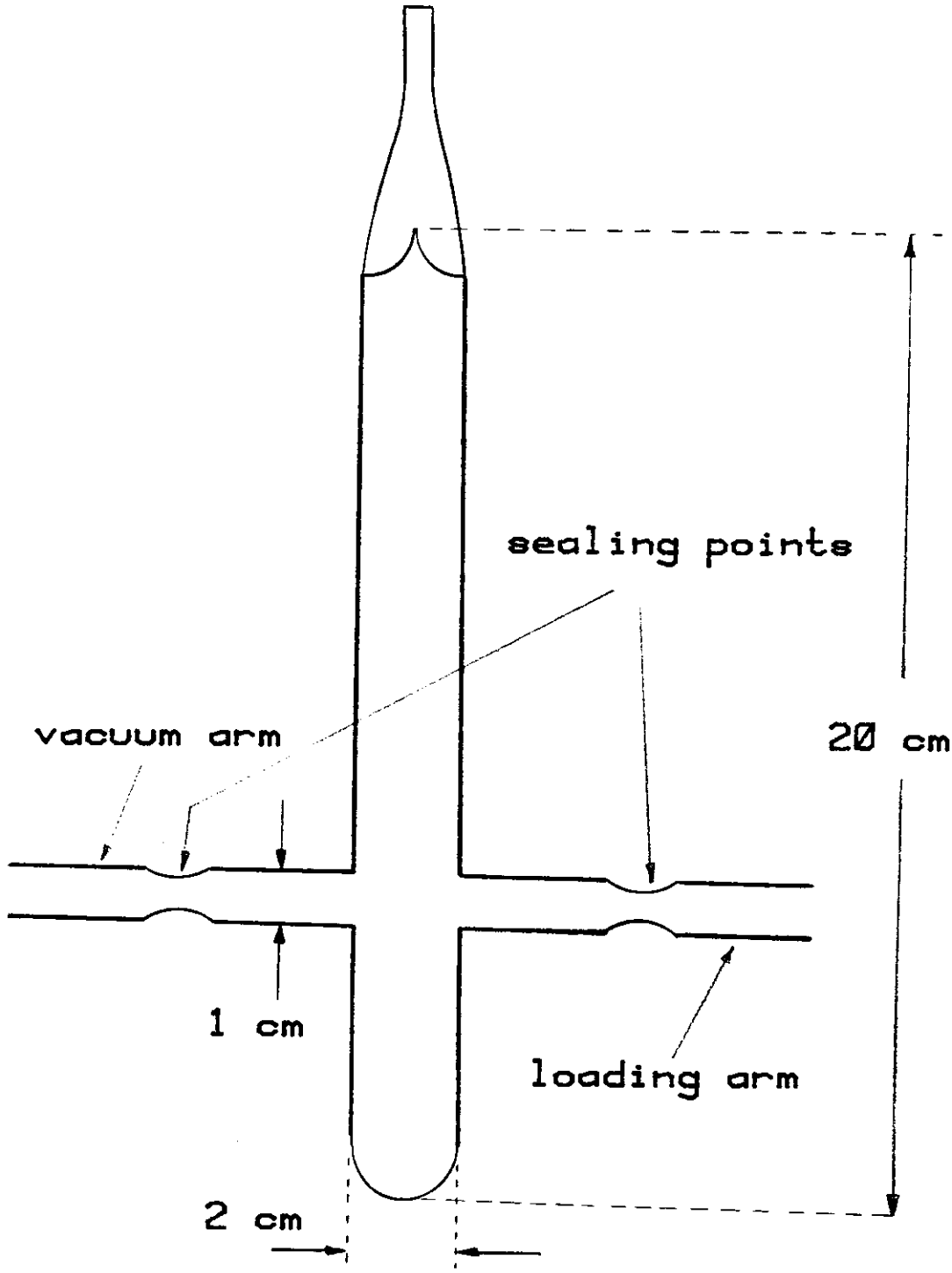

FIG[4.4] Glass capsule used in the VPE growth of mNA.

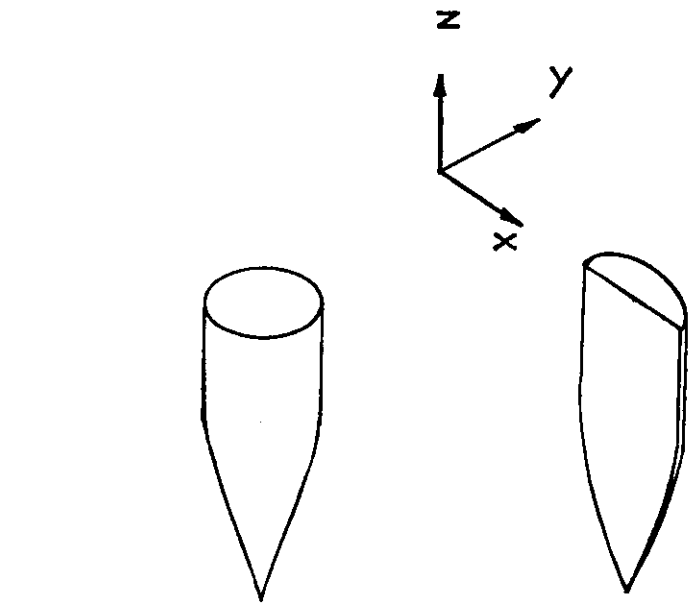

[a] as grown boule [b] cleaved boule

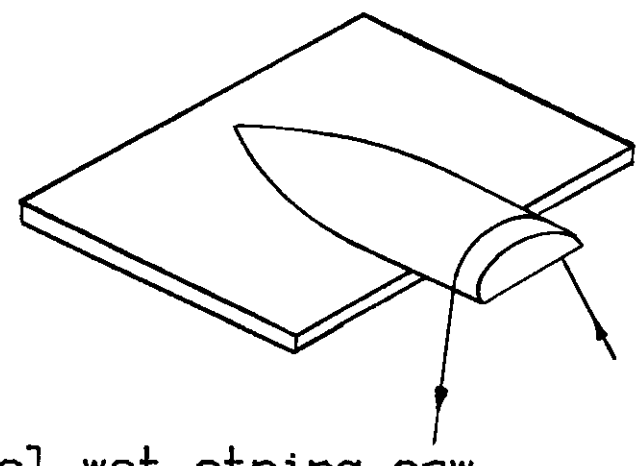

[c] wet string saw [d] z cut disc

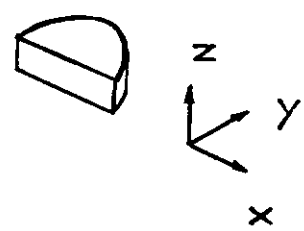

FIG[4.5] Preparation of mNA discs with the required orientation.

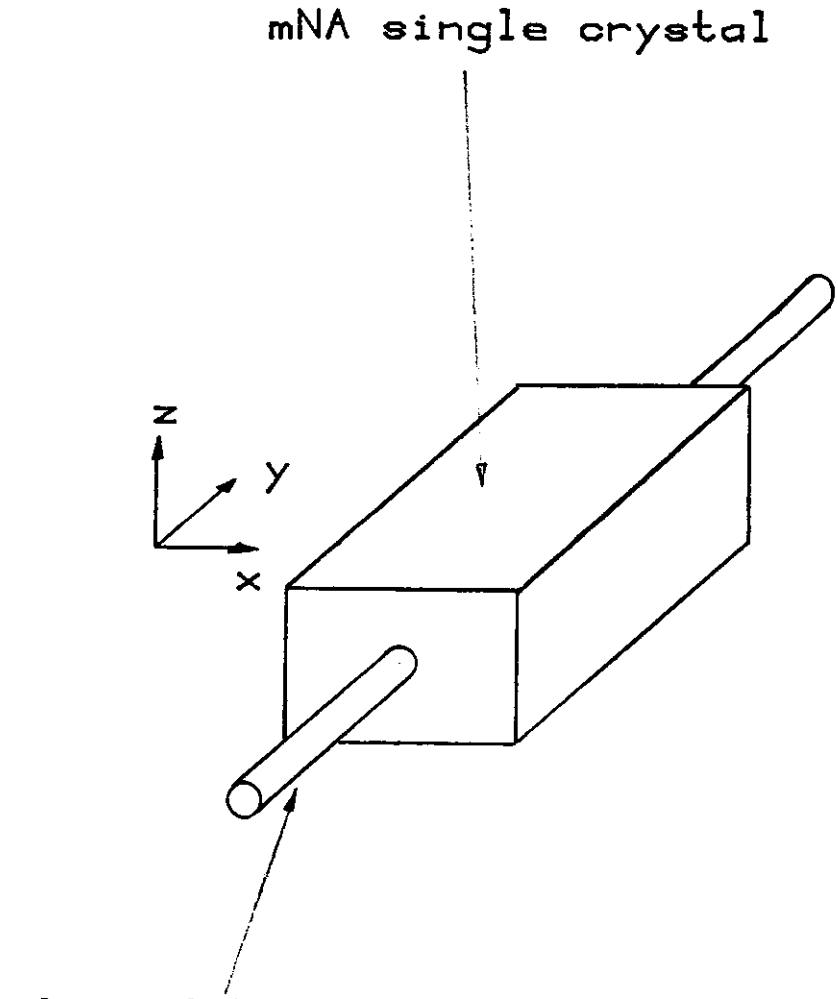

FIG[4.6] Glass fibre embedded in a single crystal of mNA

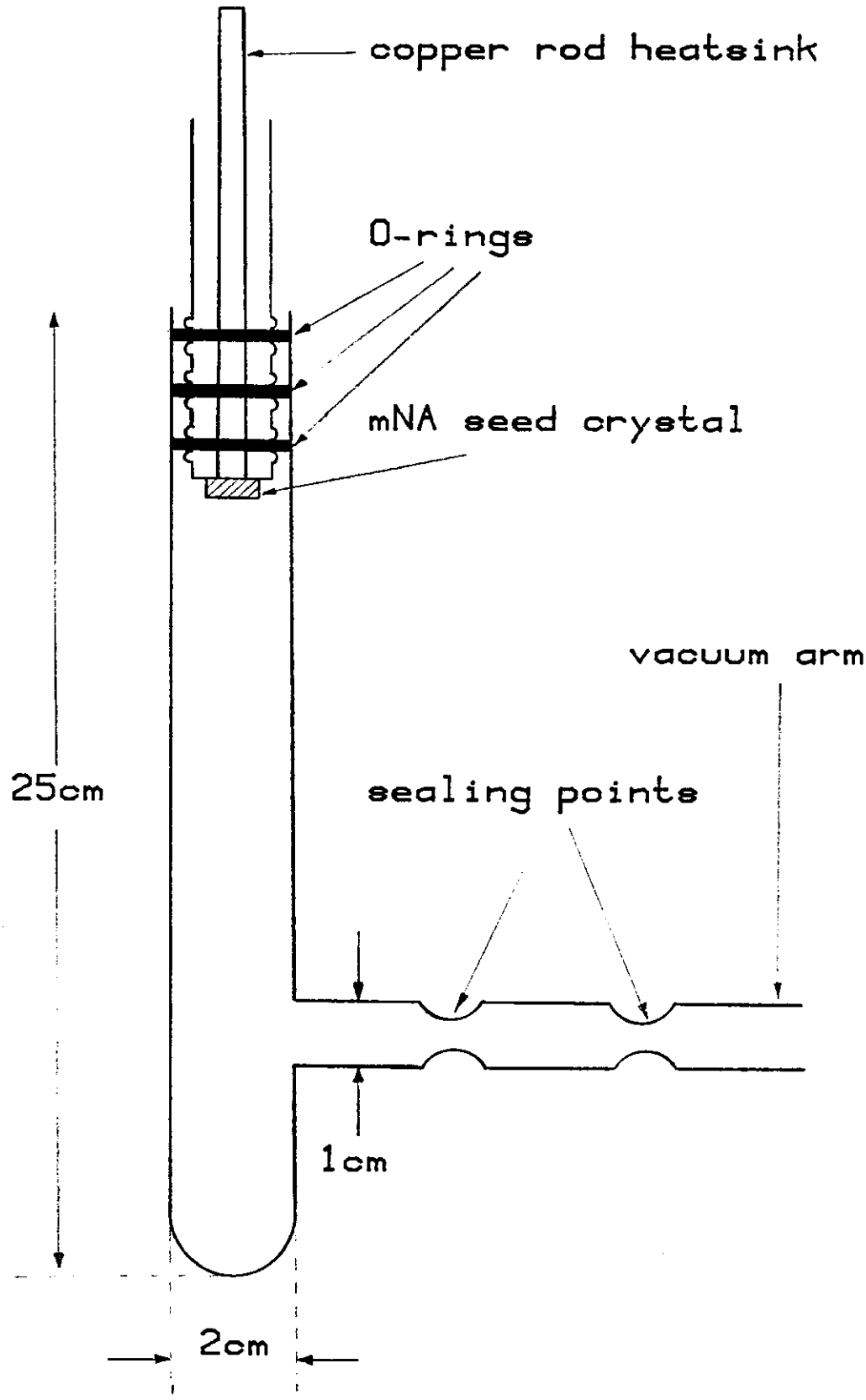

FIG[4.7] Glass capsule for VPE growth of mNA from a seed crystal.

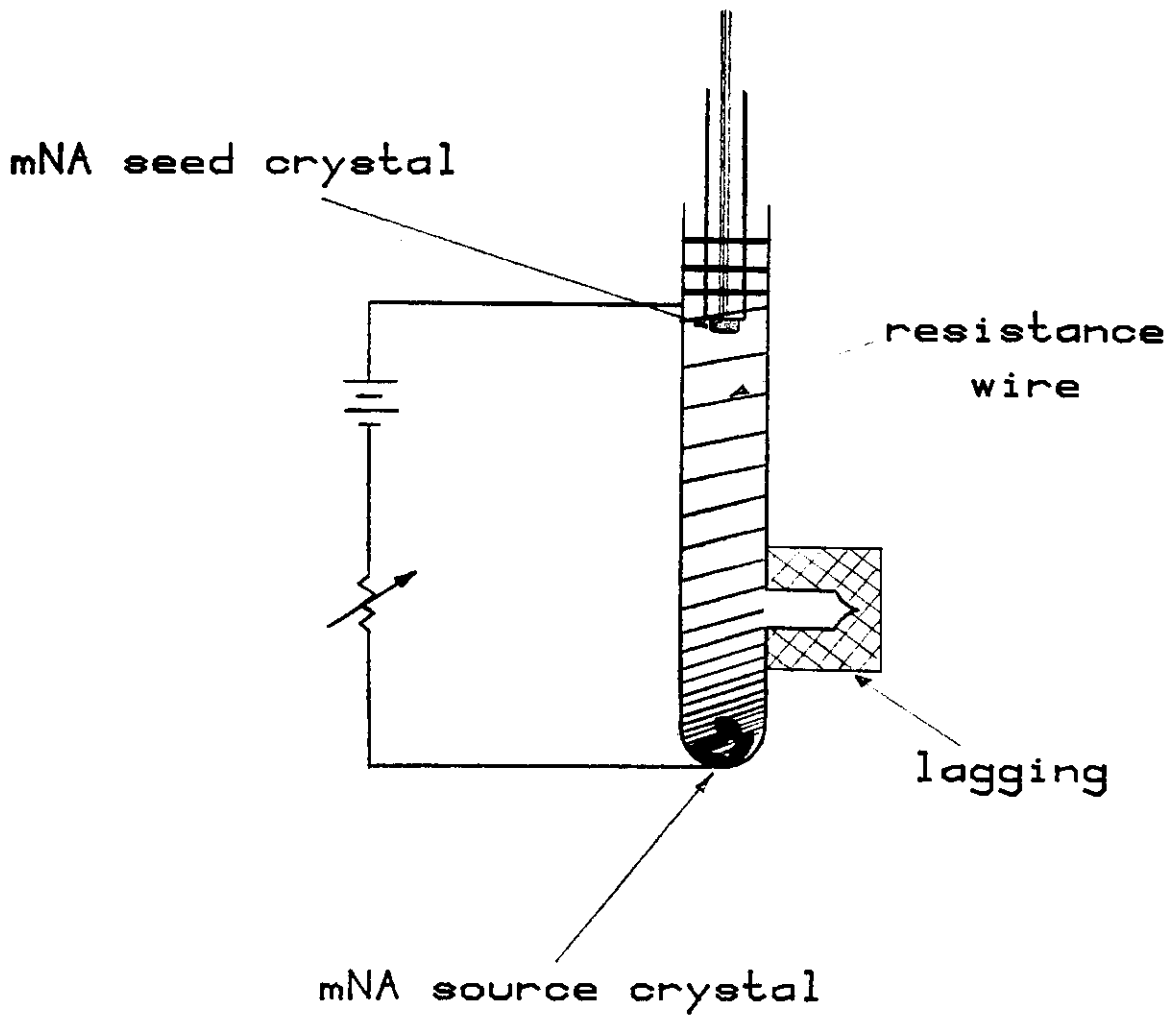

FIG[4.8] Electrical heating technique for VPE growth of mNA.

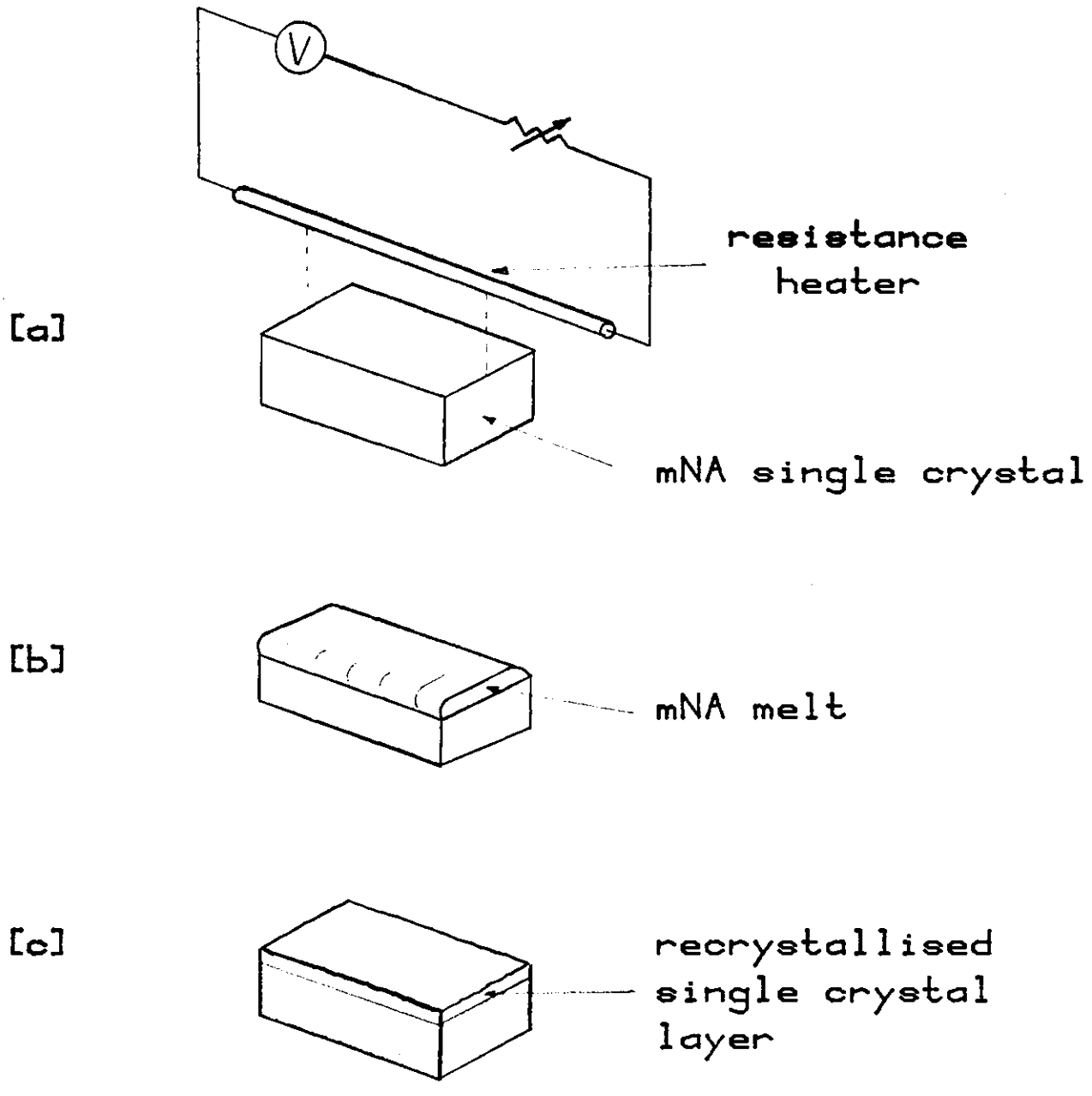

FIG[4.9] Modified LPE technique for growing a thin single crystal layer of mNA.

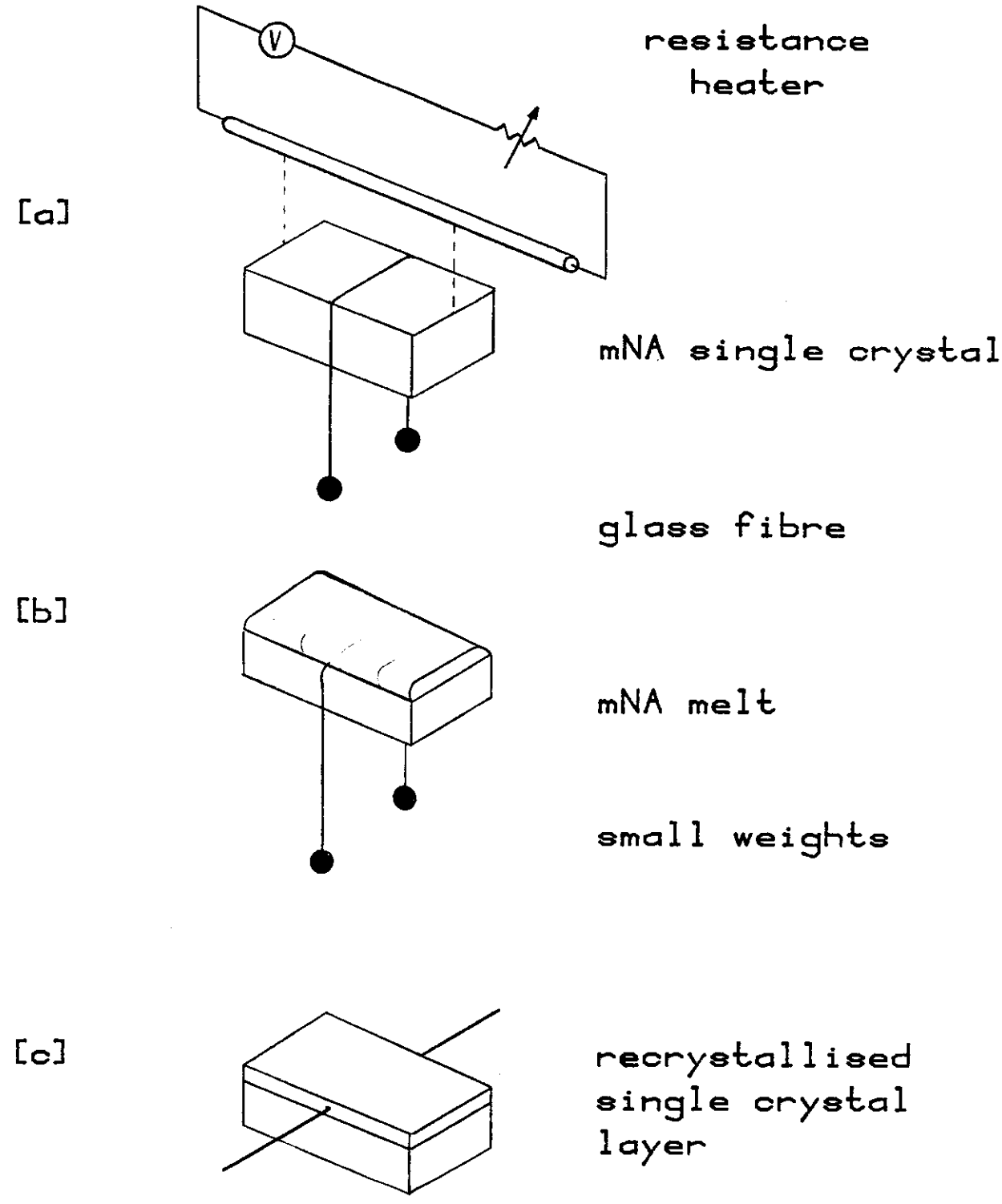

FIG[4.10] Embedding a glass fibre into a single crystal of mNA.

CHAPTER 5 : FABRICATION OF THE COUPLER SWITCH

5.1 Fabrication Problems

The essential practical problem in designing and fabricating the coupler switch is that a single-mode guide is required in which the core and cladding materials are totally dissimilar. This is in complete contrast to the manufacture of single-mode fibres where virtually the same material is used for the core and the cladding. None of the standard fibre manufacturing techniques can, therefore, be used and it becomes necessary to fabricate the core and the cladding separately and then assemble them. This results in the requirement that the core radius, a, should be large enough (eg ≥ 5 μm) to allow manipulation of the fibre. Since for single-mode operation one requires (5, 6)

$$V = \frac{2\pi a}{\lambda} \sqrt{n_c^2 - n_{cl}^2} \quad < 2.405$$

large values of a place severe restrictions on the required core-cladding index difference, Δn. This is illustrated in Table (5.1) for three values of V at $\lambda = 633$ nm.

TABLE (5.1)

n_{cl}=1.675	Δn		
a(μm)	V = 1.8	V = 2.2	V = 2.4
1	9.8×10^{-3}	1.5×10^{-2}	1.7×10^{-2}
2	2.5×10^{-3}	3.7×10^{-3}	4.4×10^{-3}
3	1.1×10^{-3}	1.6×10^{-3}	1.9×10^{-3}
4	6.1×10^{-4}	9.2×10^{-4}	1.1×10^{-3}
5	3.9×10^{-4}	5.9×10^{-4}	7.0×10^{-4}
6	2.7×10^{-4}	4.1×10^{-4}	4.8×10^{-4}
7	2.0×10^{-4}	3.0×10^{-4}	3.6×10^{-4}
8	1.5×10^{-4}	2.3×10^{-4}	2.7×10^{-4}
9	1.2×10^{-4}	1.8×10^{-4}	2.2×10^{-4}
10	9.8×10^{-5}	1.5×10^{-4}	1.7×10^{-4}

The difficulty of achieving such small index differences between two totally dissimilar materials is further complicated by the fact that the indices of commercially available optical glasses are rarely guaranteed to better than $\pm 2 \times 10^{-4}$; even this tolerance can be worsened during the drawing process. Furthermore, the core radius can not be measured to better than about ± 1 μm accuracy with an optical microscope. It was, therefore, impossible to design and fabricate the coupler according to strict specifications and allowances had to be made for possible variations in the core radius and refractive index. The graph in Fig (5.1) combines the results of Table (5.1) with the possible errors in a and n_c; several Schott glasses (26) that were considered for the core material and their corresponding "operating points" are also shown.

Since values of a smaller than 5 μm would have made the handling of the fibres extremely difficult, it was decided to use LaKN12 (bulk index = 1.67539 at $\lambda = 0.633$ μm) as the core glass. Clearly, this left very little room for index variations during the drawing stage. It was anticipated that the main cause for any index variations was likely to be stress induced birefringence which could be eliminated by proper annealing. The annealing time becomes shorter for smaller objects and for a glass fibre of about 10 μm diameter it is of the order of a few minutes (27). For a slow drawing speed (eg ≈mm/min) it was expected that the fibre would be automatically annealed as it was drawn, thus maintaining its original index.

The fabrication of the core fibres was carried out in two stages. Initially short lengths of glass fibre (length ≈25 cm, diameter ≈ 0.5 mm) were drawn from molten LaNK12 glass, Fig (5.2). These were then used as preforms for drawing the 5 μm radius fibres. The second stage of fibre drawing was carried out using a small electrically heated furnace with a digital temperature control unit (28), Fig (5.3). The desired temperature (~ 800°C) could be reached in a few minutes and maintained to better than ±2°C. The pulling speed was adjusted by attaching weights to the preform, Fig (5.3). Since there was no feeder mechanism the fibres were always drawn with some taper. However, by adjusting the temperature and the weights it was possible to draw short lengths (~30 cm) of fibre with the required radius and no measurable taper.

Pairs of touching fibres were embedded in mNA using the technique described in the previous chapter. Conducting paint (Radio Spares, RS 555 - 156) was then used to form electrodes on the two faces of the crystals. Figure (5.4) shows some of the devices made. It was later discovered that the solvent in the paint dissolved the top layer of the crystal, thus exposing the fibres and causing severe attenuation. The electrodes were modified so that conducting paint was used only on the lower face of the crystal; on the top face the electrode consisted of a metal plate lightly pressed against the surface. Despite the new electrode arrangement it was still not possible to obtain any appreciable throughput of light. We checked and confirmed that there were no breaks in the fibres within the crystal. It was necessary to measure the refractive index of the core glass in order to establish if the coupler was guiding at all.

The oil immersion method, (33), was used for this purpose, the two liquids being Di-Iodomethane (n_D = 1.743) and 1-Bromonaphthalene (n_D = 1.658) both supplied by BDH Chemicals Ltd. It was found that the refractive index, n, of the LaKN12 fibre was in the range $1.666 \leqslant n < 1.671$. This, of course, confirmed that the coupler was not guiding since $n_c < n_{cl}$.

It was thought that it should be possible to restore the initial value of the refractive index by annealing. In order to investigate this, a 30 cm long piece of LaKN12 was cut into two equal lengths; one half was heated at 650°C* for 4 hours and then allowed to cool slowly ($\simeq$ 1°C/min). The other half was left untreated. The indices of the two were then measured using the immersion method. The results were as follows

$1.665 \leqslant n < 1.668$ (untreated)
and $1.668 \leqslant n < 1.672$ (annealed)

Annealing, therefore, caused very little, if any, improvement in the refractive index.

Fibres were made from several other glasses using the same technique; the refractive indices of these were measured and are shown in

---

* The transformation temperature of LaKN12 is 621°C (26).

TABLE (5.2)

Glass	Bulk Index	Fibre Index	% Change
SF1	1.7126	$1.7059 \leqslant n < 1.7076$	$\simeq -0.4$
LaKN12	1.6754	$1.6660 \leqslant n < 1.6710$	$\simeq -0.6$
BaF50	1.6796	$1.6554 \leqslant n < 1.6665$	$\simeq -1.4$

Table (5.2) and Fig (5.6). The dotted line in Fig (5.6) corresponds to no change in the refractive index. The indices of all the glasses that were tested dropped by about 1% during the drawing process. None of the indices were suitable for the coupler. They were either smaller than the index of the crystal, thus resulting in no guiding, or they were so much larger that it was impossible to construct a practical single-mode fibre with them.

The melting of the glass was considered the most likely cause of the index variation. It was, therefore, eliminated from the drawing process. Instead the preforms were made by cutting rectangular blocks ($\simeq$ 40 x 5 x 5 mm) of glass and grinding them to an approximately cylindrical shape (radius $\simeq$ 4 mm). The cylindrical preforms of BaF50 were drawn in the furnace, Fig (5.3), to produce 0.3 mm diameter rods which could be pulled again to make fibres of smaller radii. The refractive index, n, of the 0.3 mm BaF50 rods was measured to be $1.6679 \leqslant n < 1.6705$, ie despite the improvement (cf Table (5.2)), the index was still too low. Changing the pulling speed had virtually no effect on the refractive index, Table (5.3), and therefore could not be used to control the index variation.

TABLE (5.3)

BaF50, Bulk Index = 1.6796 at λ = 0.633μm		
Pulling Speed (Temp = 690°C)	Fibre Index	% Change In Index
500 m / hour	$1.6679 \leqslant n < 1.6709$	$\simeq$ - 0.69%
0.2 m / hour	$1.6692 \leqslant n < 1.6694$	$\simeq$ - 0.61%

In all the tests the refractive indices of all the glasses dropped, by varying amounts, during pulling. It was, therefore, conceivable that by starting with high index glass, one might be able to draw a fibre with the correct refractive index. This work could only have been carried out on a trial and error basis. It was decided that this uncertainty coupled with the 2-3 months delivery time for new glasses made the experiment impractical. Instead it was decided to demonstrate the principle of operation of the coupler using a much simpler structure in which an index matching oil was used in place of the electro-optic crystal, section 5.2.

It was, however, necessary to gain some insight into the possible causes of the occurrence of the index changes. For this purpose, small rectangular blocks (≈ 10 x 4 x 2 mm) of BaF50 were cut and polished. Each sample was maintained at some particular temperature, T_o, for 25 minutes. The furnace was then switched off, and the sample cooled to room temperature in about 30 minutes. The refractive index was then measured* using an Abbé refractometer. The change in the refractive index as a function of T_o is plotted in Fig (5.7). For temperatures below 550°C (ie the transformation temperature of BaF50) no change in index was observed. As a first step towards establishing the cause of the index variation we verified that this was not a surface effect.

Examination of the test samples under crossed polarisers showed that there had been some degree of birefringence induced in the blocks of glass during heat treatment. This was more pronounced in those samples that were heated to higher temperatures. Clearly, it was important to eliminate the birefringence before any conclusions could be drawn about possible causes of the index variation. The heat treatment procedure that was used for this purpose was as follows. Each sample was heated to the same temperature that it was subjected to in the earlier part of the experiment. It was kept at that temperature for 10 minutes and was then allowed to cool at the rate of 1°C/minute. The refractive index was measured again at room temperature; the dotted curve in Fig (5.7) was thus obtained.

---

* The heating caused surface deformations in some cases and the blocks had to be repolished before any index measurements could be made.

The heat treated samples showed much less - but not zero - birefringence when viewed through crossed polarisers. The fact that the birefringence was not completely eliminated must have been due to incorrect or incomplete annealing.*

Had we been able to completely remove the stress induced birefringence, it would have been possible to attribute the remaining index variation to chemical changes. Incomplete annealing, however, prevents us from drawing this conclusion. Nevertheless, the heat treatment of the samples led to a substantial reduction in the stess-induced birefringence and yet gained very little improvement in the index variation. Chemical changes, therefore, cannot be discounted as a possible cause of the index variations.

5.2 Thermally Induced Switching

The design of the directional coupler considered so far involves a crystalline cladding, whose index has a fixed, well-defined, value. For single-mode operation, the necessary small index difference between core and cladding imposes very strict limits on the index of the glass cores. As we have seen, the indices of these glasses are prone to variation, to an extent that overwhelms the very tight specification.

For the purposes of testing the basic ideas in the coupler, and indeed, as a potentially useful passive device, we decided to treat the glass core indices as the fixed parameter, and adjust the cladding index appropriately. Clearly, crystalline materials cannot be used for this purpose. We chose to use an oil whose index varied quite rapidly with temperature, so that the required tuning could be readily achieved thermally.

A thermally switchable directional coupler was constructed using the arrangement shown schematically in Fig (5.8). The principle of operation of this coupler is exactly the same as the electro-optic device shown in Fig (2.3). The structure, however, is made much

---

* For most glasses there is an annealing temperature, T, that the sample must be kept at for t minutes; they must then be cooled at a rate which is dependant on the dimensions of the sample (27). The parameters T and t are both material properties of the glass and were not available for the Schott glasses.

simpler by using an index-matching oil for the cladding. Heating the oil changes its refractive index and results in the switching of light between the two fibres.

The fibre cores used were made of pyrex ($n = 1.4723$ at $\lambda = 633$ nm) and had 10 μm radii. The index matching oil was Palma Rose (Bush Boake Allen, London) and its index variation with temperature is shown in Fig (5.9). Figure (5.10) illustrates the variation of the normalised frequency, V, of the fibre with temperature. The graph in Fig (5.9) can be represented by the following straight line*

$$n = 1.48176 - 4.24 \times 10^{-4} \times T \qquad (5.1)$$

where n is the refractive index at $T^{\circ}C$. On cooling the refractive index returned to its initial value along the same straight line. Note that for $T < 22.6^{\circ}C$ there can be no guiding since $n > 1.4723$. Furthermore, it can be seen from Fig (5.10) that for $T > 23^{\circ}C$, V is greater than 2.405 and the fibres are no longer single-moded. It was found, however, that by careful adjustment of the launching conditions, it was possible to excite predominantly the HE_{11} mode in the fibres even for values of V as high as 15.

The variation of n with temperature as given by (5.1) is valid only if the oil is not exposed to air while being heated. Exposure to air during heating caused chemical changes in the oil that resulted in erratic and irreversible variations of the refractive index - the index generally increased with increasing temperature. In order to overcome this problem, the structure shown in Fig (5.11) was used for housing the fibres and the oil. The amount of oil exposed to air was, therefore, negligibly small and did not affect the index variation.

The blocks A and B, Fig (5.11) were both made of silica ($n \simeq 1.45$) so that their effects on the propagation properties of the fibres were minimised. It was very important that the oil should be heated uniformly over the interaction length of the fibres. For this purpose the assembly shown in Fig (5.11) was placed under a semi-cylindrical aluminium cover and heated, from above, by an infra-red lamp, Fig (5.12). Using a fine thermocouple it was verified that the oil temperature was constant over the entire length of the device.

---

* The curve fitting routine of an HP67 calculator was used for this purpose. The correlation coefficient was 0.9992.

Figure (5.13) illustrates the variation in temperature as the oil was heated and then allowed to cool. It was quite impractical to position the thermocouple in the oil during the actual coupling experiment. Once it was confirmed that the graph of Fig (5.13) was exactly repeatable, we were able to determine the oil temperature by measuring the cooling time and referring to Fig (5.13) - the heating was kept constant at 2 minutes for all the experiments.

The coupling experiment consisted of the following stages:

(i) Two lengths of identical, clean, uniform fibres approximately 15 and 30 cm long, with properly cut ends, were placed in contact over a length of about 7 cm. The fibres usually remained in contact quite firmly, but in some cases a Zerostat gun had to be used to increase the electrostatic forces between the fibres. The two-fibre structure was examined under a microscope to ensure that there were no twists or gaps between the fibres.

(ii) The twin-fibre was placed in B, Fig (5.11), with no oil present, and light was launched into the longer fibre. The uniformity of the twin-fibre structure over the interaction length was checked by observing the scattered light from this region. The examination of the far field patterns of the two fibres enabled us to determine if the fibre ends had been cut properly.

(iii) The index matching oil was then added. A and the aluminium cover were placed in position, Fig (5.11) and Fig (5.12), and the infra-red lamp was switched on for 2 minutes.

(iv) Two large area (radius $\simeq$ 1 cm) PIN photodiodes were used to monitor the variations in the light outputs of the fibres as the oil cooled. The detected signals were amplified and then plotted using a chart recorder. Figure (5.14) shows the simple amplifier circuit that was used.

Typically, a temperature variation of about 10°C, corresponding to an index change of about 3.5×10^{-3}, resulted in two complete switching cycles between the fibres, Fig (5.15) and Fig (5.16). In addition to showing the switching action, Fig (5.15) also illustrates the fact that HE_{11} is the predominant mode in both fibres. The extinction ratio was typically about 10 dB, Fig (5.16), but values as low as 5 dB and as much as 20 dB were also obtained. Considering, that the

fibres were not single-moded and that some light must have been launched into higher order modes, which in general have different switching requirements to the HE_{11}, one must conclude that an extinction ratio of 10 dB is in fact an encouraging result.

The other interesting point illustrated in Fig (5.16) is the gradual reduction of the light intensity in the fibres as the temperature, and hence the normalised frequency, V, is reduced. As the V value of a fibre is reduced a progressively larger fraction of the total power in each guided mode propagates in the cladding material (5, 6). Many factors now combine to increase the total loss suffered by the guided modes. For example, the attenuation of the oil is higher than the glass. Also the interfaces between the oil and blocks A and B contribute to the scattering loss. Furthermore, the higher order modes can couple to radiation modes as the fibre becomes more weakly guiding. Clearly these effects become more pronounced as larger fractions of the fields extend outside the fibre cores, ie as V becomes smaller.

In order to make a comparison between the results of the experiment and the theoretical analysis of the previous chapters, we calculated the variation of the coupling coefficient for the coupler of Fig (5.11) as a function of the normalised frequency, V, Fig (5.17). The interaction length between the fibres was 7 ± 0.2 cm. Using equation (3.64) we find that for two complete switching cycles, we require c_h to change by 89.7 rad/m. Assuming that the starting value of V is 4 (ie temperature $\simeq 24^{\circ}C$, Fig (5.10)), Fig (5.17) can be used to find the required change in V, $\delta V = 7.3$. This is in good agreement with the experimental results, Fig (5.16), that showed two switching cycles for $\delta V \simeq 8$.

We thus demonstrated the principle of operation of the proposed coupler switch and obtained experimental data supporting our numerical analysis. It was decided that more detailed and precise experiments with these fibres were not warranted since the results would be obscured by the effects of the rather ill-defined structure of the cladding and the uncertainty of the number of modes being excited.

5.3 Summary And Discussion

The aim of this work was to design and fabricate a single-mode switch operating on directional coupler principles. The structure that was considered consisted of two thin parallel glass fibres placed in contact with one another and embedded in a single crystal of meta-nitroaniline. Initially a numerical investigation was carried out to determine the performance of such a device. It was further established how the performance of the coupler varied with such parameters as the V value, core radius, device length and the change in the refractive index of the electro-optic cladding. It was shown that for efficient operation the coupler should be designed with a V value of less than 2.2. It was determined that the operation of the switch depended very strongly on the separation between the fibre cores and that touching cores did not necessarily provide the most efficient switching condition. The analysis also demonstrated that the device would be virtually insensitive to polarisation.

Single crystals of meta-nitroaniline were grown, by vapour phase epitaxy, and subsequently cut into discs with the required crystallographic orientation, Chapter 4. Glass fibres of 5 μm radius were drawn from several (bulk) Schott glasses. A variation of the liquid phase epitaxy technique was used for embedding these fibres into the mNA discs. It was found that the glass fibres underwent a change of refractive index as a result of the drawing process, section 5.1. Although this variation was small in magnitude - about 1% - it, nevertheless, exceeded the allowed tolerances and thus prevented us from making a single-mode coupler. We briefly investigated the possible causes of the index change but were unable to come to any firm conclusions.

Finally, we constructed a thermally switchable directional coupler and successfully demonstrated its operation. The data obtained from this experiment were in good agreement with the results of our numerical analysis. A more detailed comparison between the experimental and the theoretical results was not warranted since the coupler was in fact multimoded, whereas our numerical analysis only applied to a single-mode device. By using fibres with very much smaller core radii,

one can ensure that the coupler remains single-moded throughout a large temperature range.* This will allow a detained comparison to be carried out between the experimental data and the numerical results, albeit with much increased fibre handling difficulties.

When this project started it was intended that the proposed device would be a switch/modulator in much the same way as the directional couplers made in integrated optics. Clearly our device would be superior to the integrated optics switches over such important parameters as attenuation, polarisation sensitivity and compatibility with optical fibres. Our work, however, has shown that the proposed device suffers from two major weaknesses. The first and the most important is the difficulty of matching the refractive indices of the glass cores and the crystalline cladding. The correct glass-crystal combination will almost certainly have to be found on a trial and error basis making this a potentially expensive and time-consuming problem to solve. The strict tolerances on the core-cladding index difference can, however, be relaxed if the core radius is made small; this, of course, will mean increased handling difficulties.

The other main weakness of the device is that it requires rather large voltages for switching, sections 3.5 and 4.3. It must be emphasised, however, that the electric field required is of the order of 4V/μm which is about the same as for integrated optical switches. It is, therefore, possible to reduce the driving voltage substantially by reducing the spacing between the electrodes. However, in order to accommodate the evanescent fields in the crystal, the minimum spacing between the electrodes must not be less than about 12a, where a is the core radius, Fig (5.18). It is, therefore, clear that the driving voltage can be reduced by using fibres with small core radii. It is important to note that even for a core radius of only 2 μm, the required voltage is unlikely to be much less than about 100 V. One can reduce the driving voltage further by placing the electrodes closer than 12a; this, however, increases the attenuation of the switch.

---

*eg: for $a = 2\ \mu m$
$n_1 = 1.4723$
$n_2 = 1.4700$ to 1.4674 (ie temperature = 28° to $34^\circ C$)
we get from equation (1.34)
$V = 1.63$ to 2.38
Therefore, fibre remains single-mode over the range 28° - $34^\circ C$.

But since the coupler is potentially a very low loss device, it may be possible to reach a compromise that will allow a low driving voltage and an acceptable level of attenuation.

These are very serious problems and not until they have been solved can one even begin to take advantage of the full potentials of the coupler as a switch/modulator. Our work, however, has shown that the basic design of the coupler is such that it offers great flexibility and allows its use for many applications. It can, for example, be used as a variable fibre tap, allowing one to monitor the flow of power and information through the main fibre. By an appropriate choice of cladding (eg liquid, gas, amorphous solid, crystal, etc) one can use the same basic structure to act as a sensor to detect for example, variations in temperature and pressure. The use of twin-cored single-mode fibres (34) should make the fabrication of such devices much simpler and should at the same time, increase their sensitivity by allowing much longer interaction lengths to be used.

It is hoped that with its versatile design and potentially simple structure, the coupler may find many more applications as a sensor. Furthermore, given the necessary research effort, the two problems mentioned earlier can be solved and the device can become a very competitive electro-optic switch/modulator.

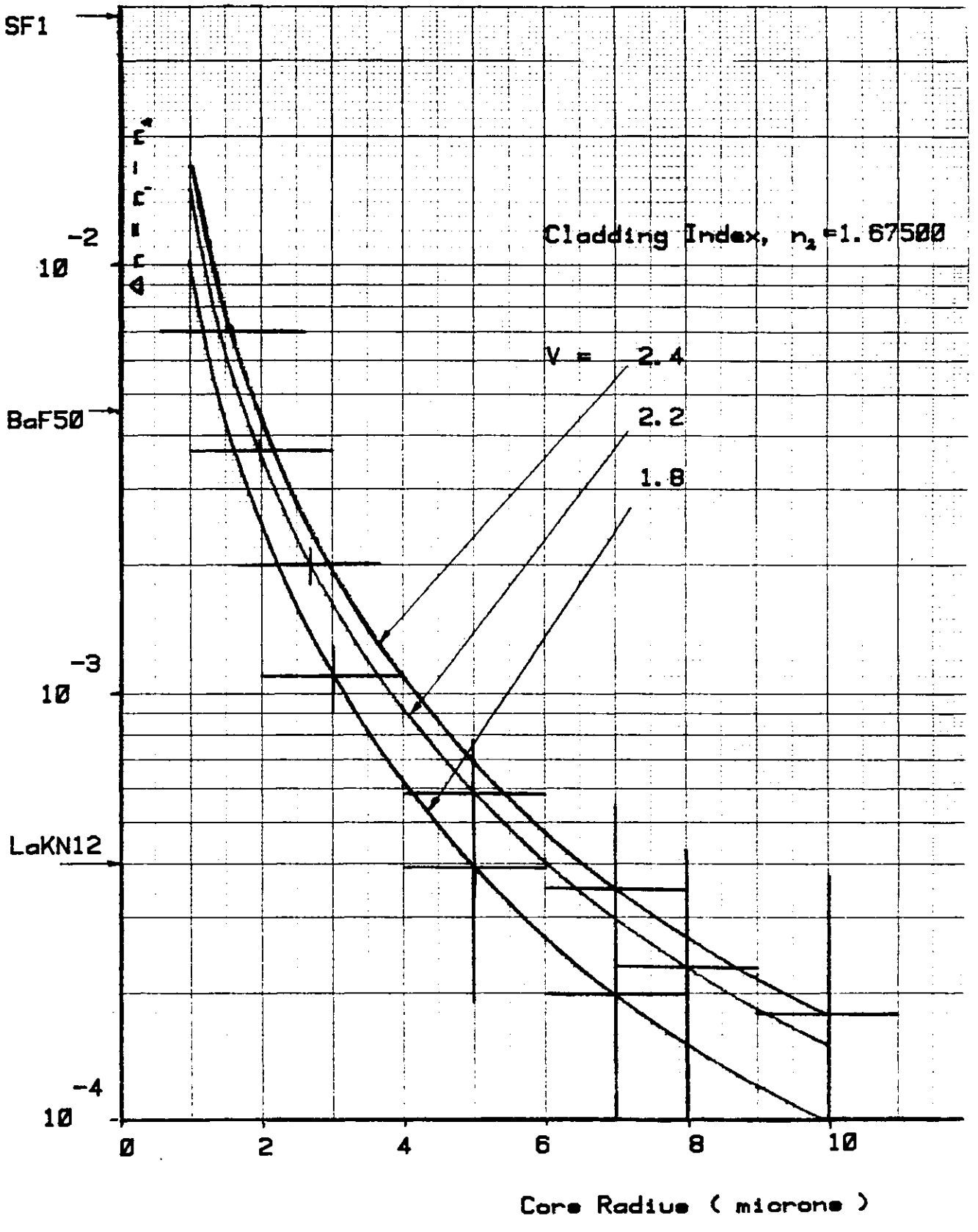

FIG[5.1] Core-cladding index difference as a function of normalized frequency and core radius.

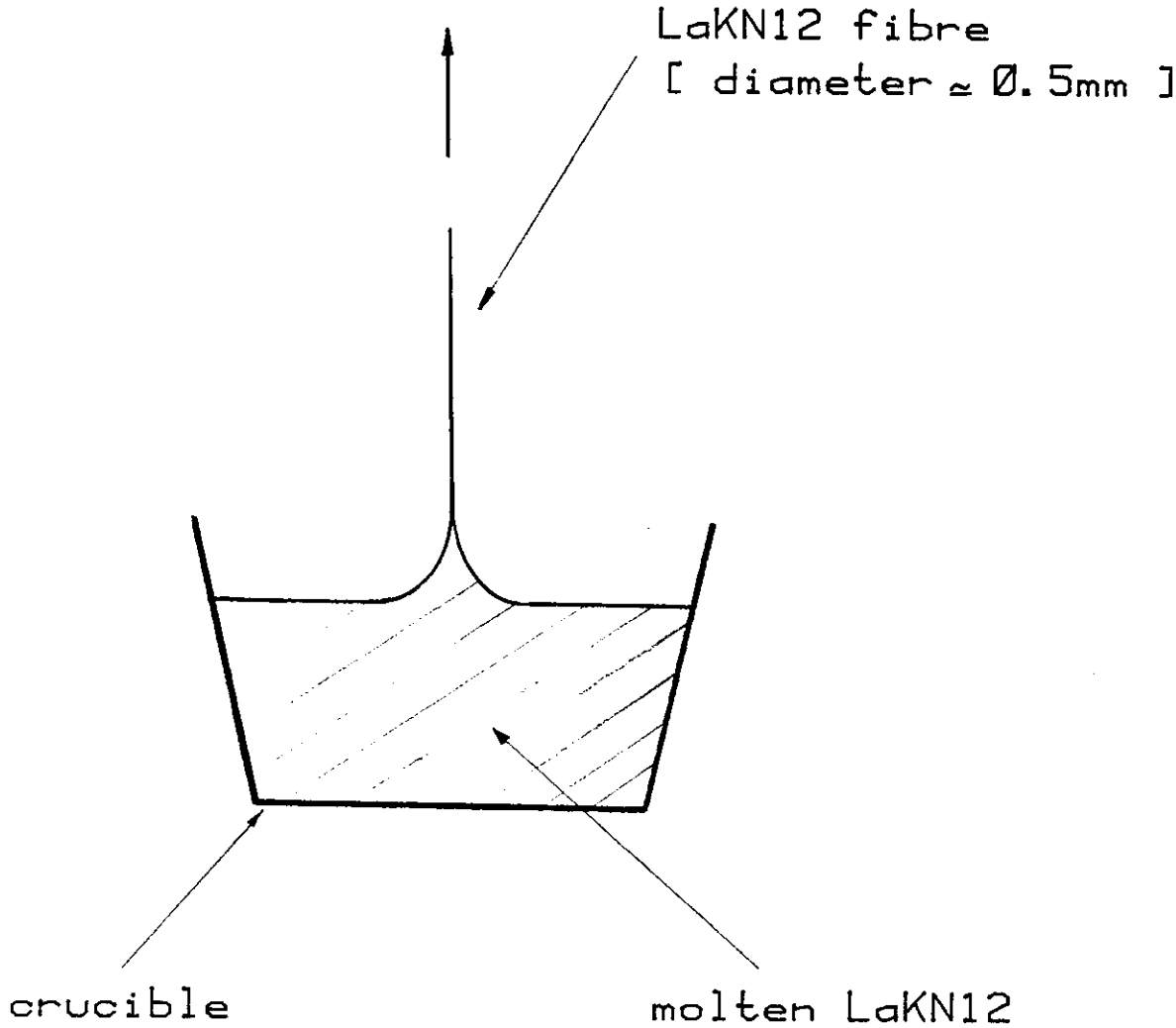

FIG[5.2] Drawing fibre from molten glass.

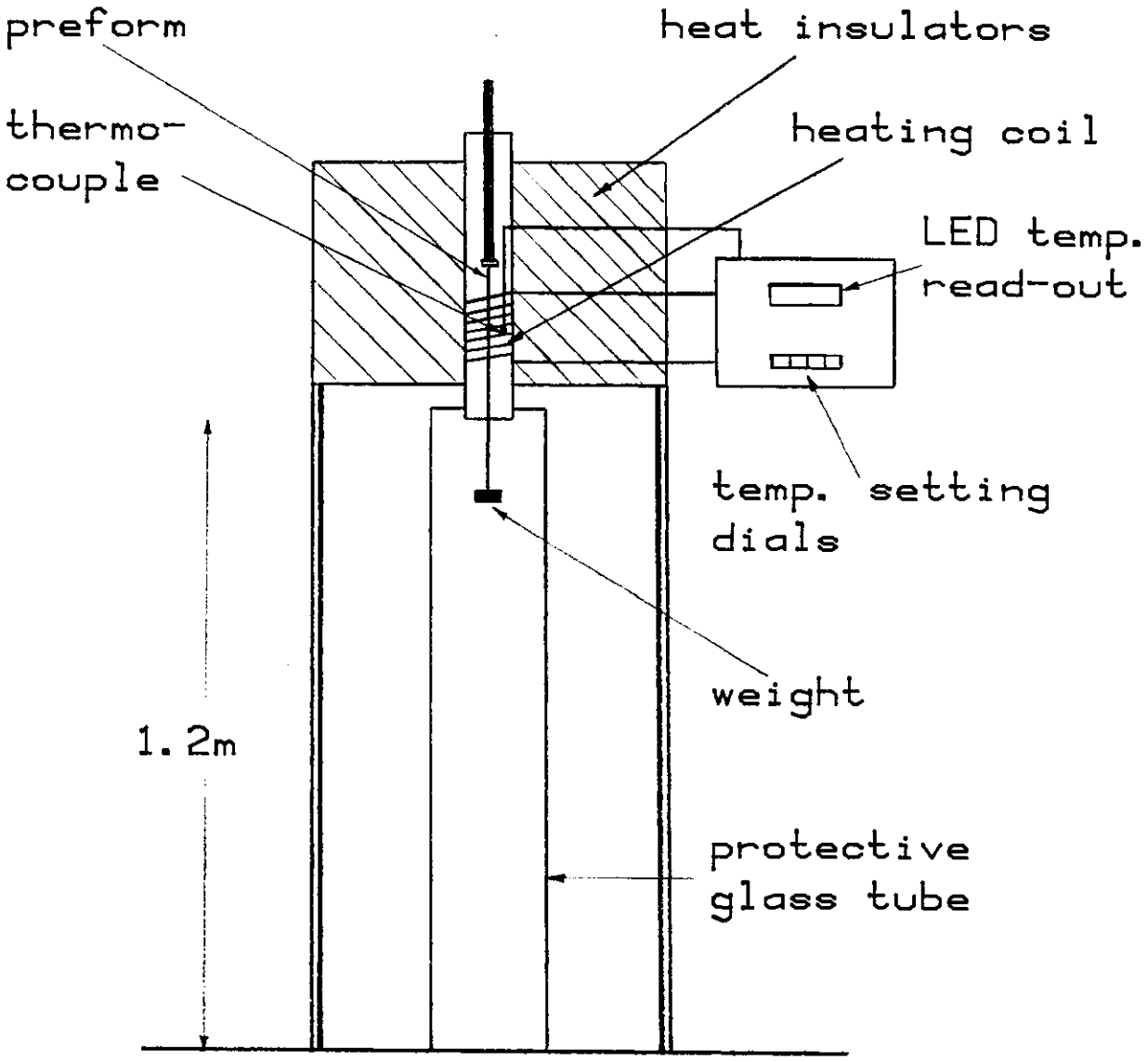

FIG[5.3] Furnace for pulling fibres.

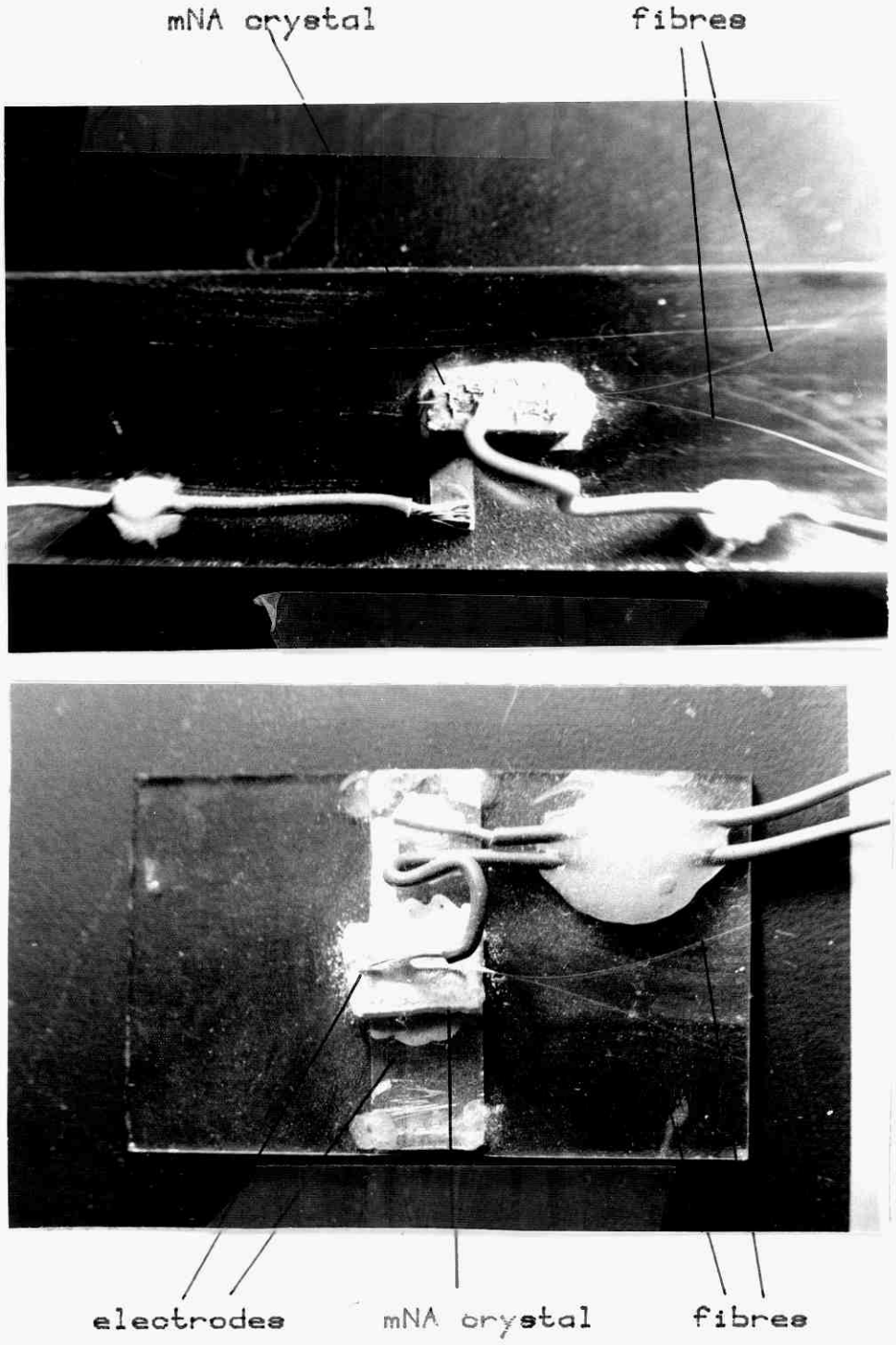

FIG[5.4] Two prototypes of the switch / modulator .

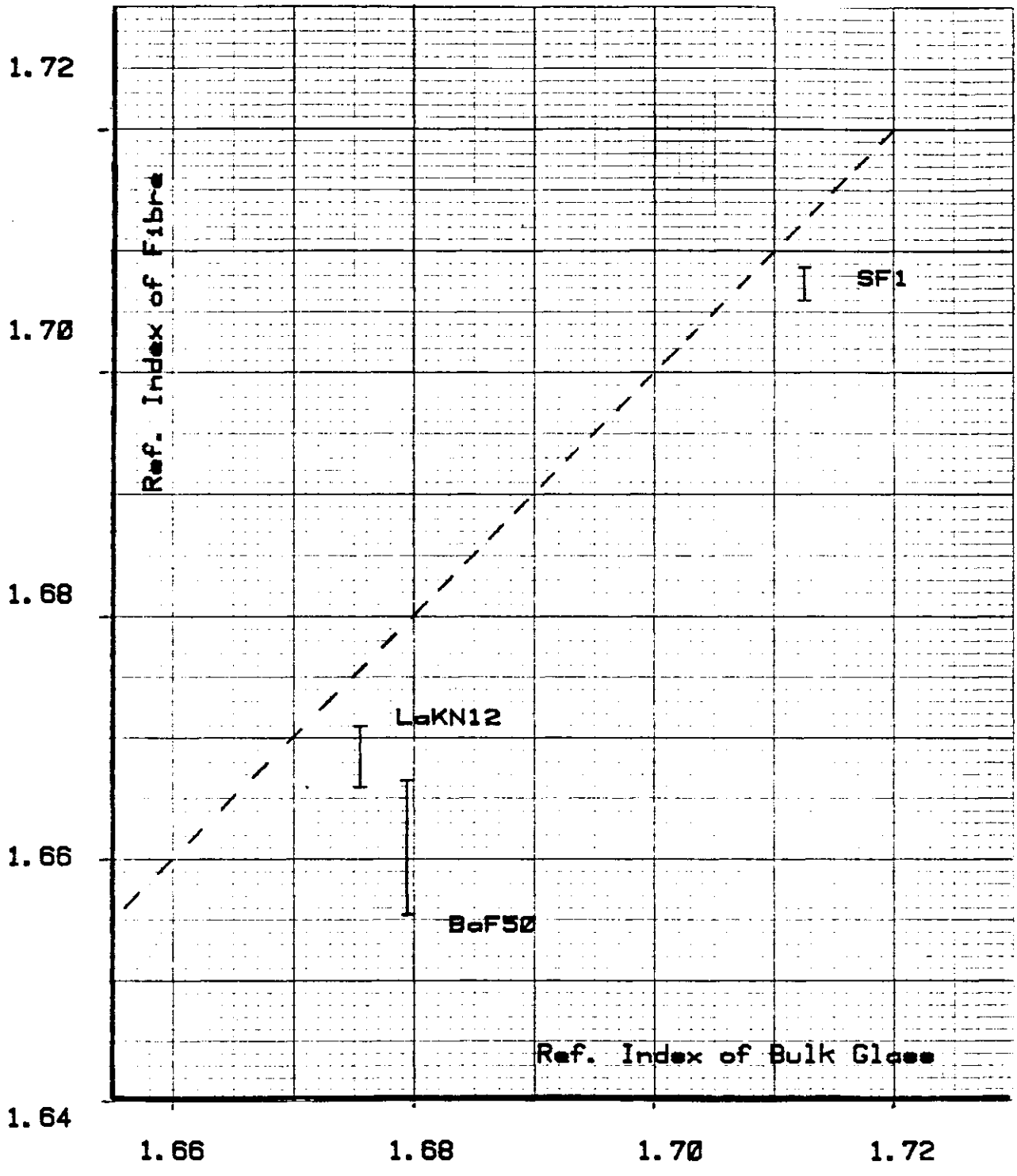

FIG[5.6] Refractive indices of several glasses before and after being drawn into fibres.

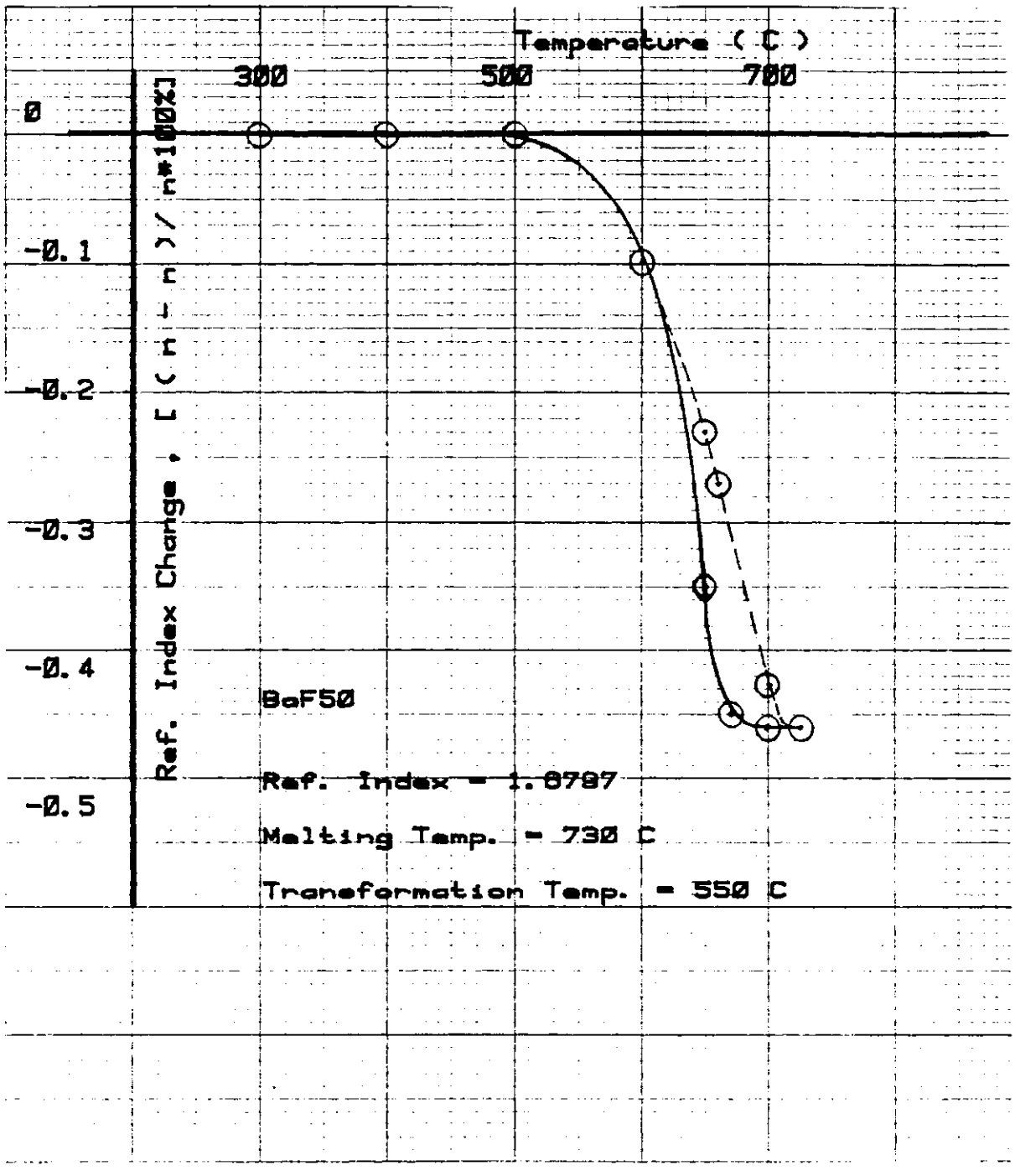

FIG[5.7] Percentage change in the refractive index of BaF50 glass as function of temperature.

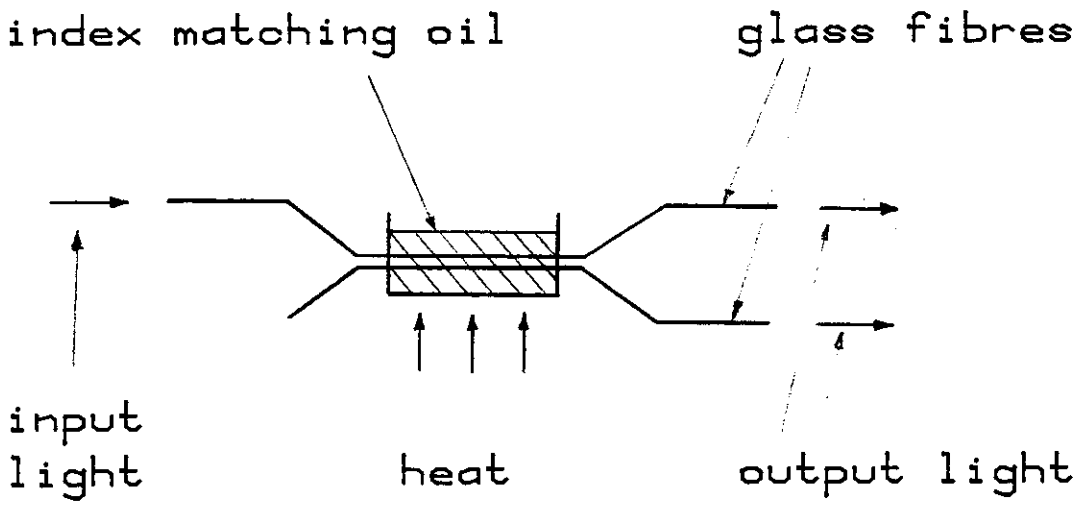

FIG[5.8] Schematic arrangement for a thermally switchable fibre coupler.

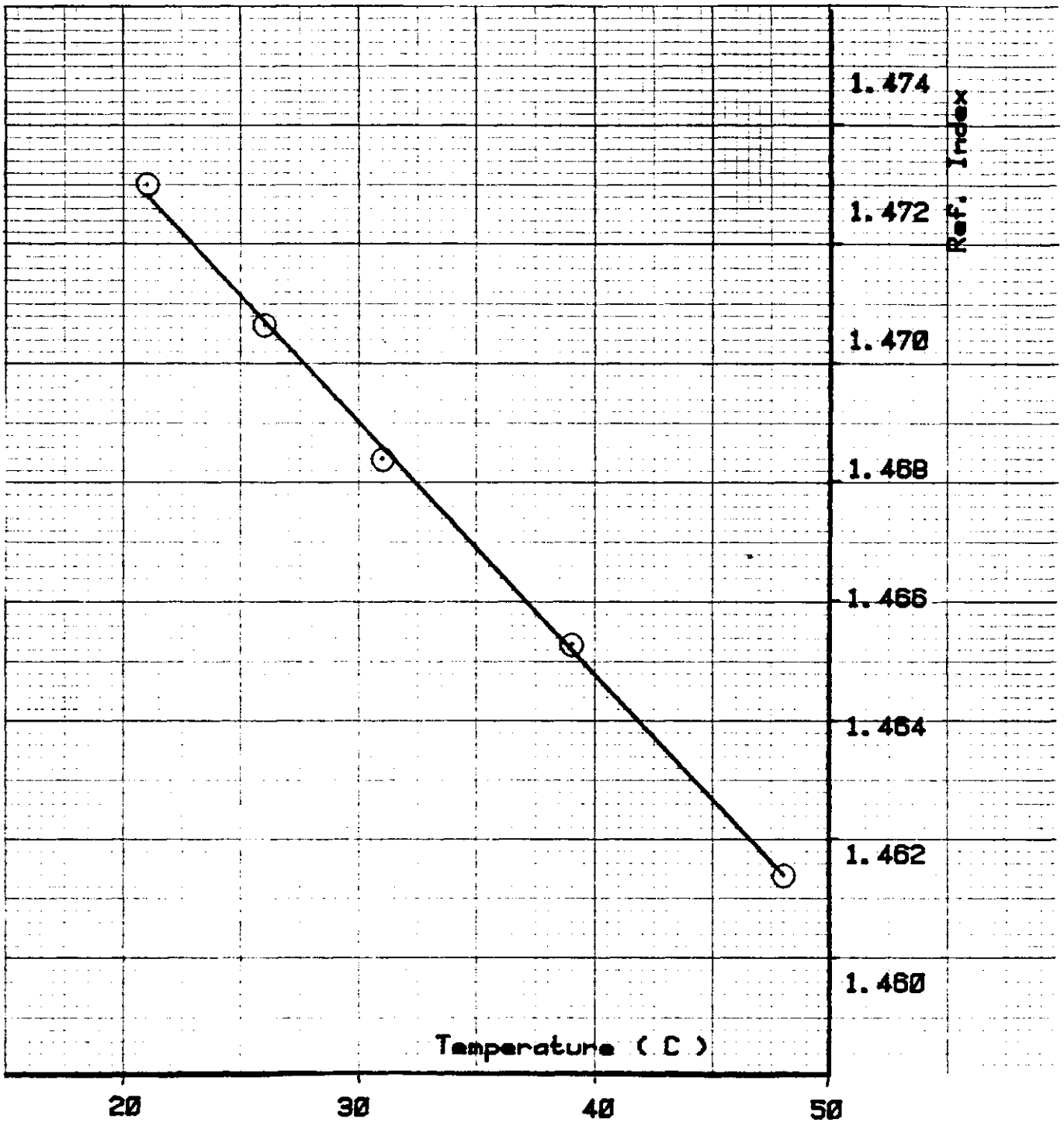

FIG[5.9] Refractive index of Palma Rose oil as a function of temperature.

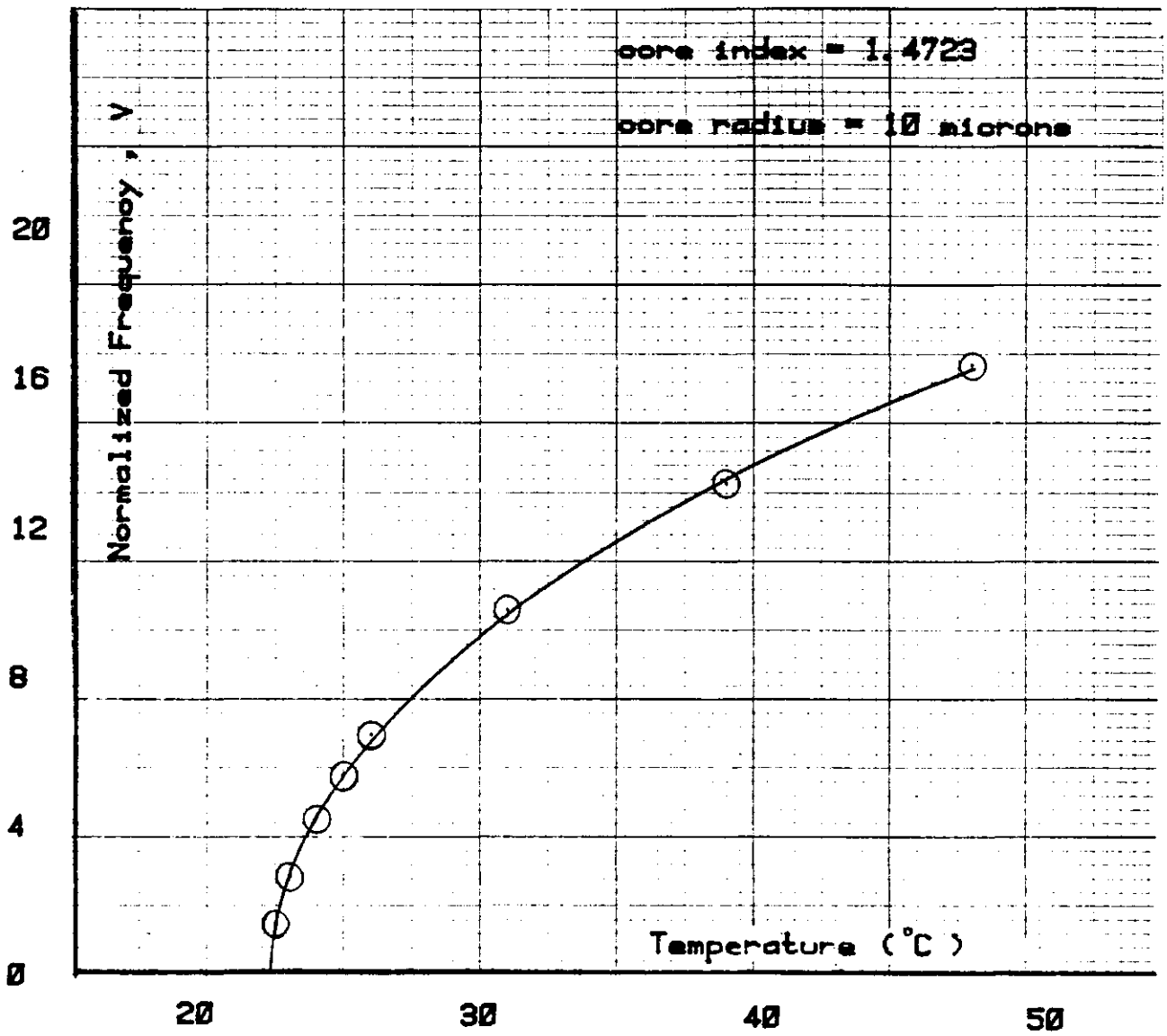

FIG[5.10] Normalized frequency of the oil cladded fibre as a function of temperature.

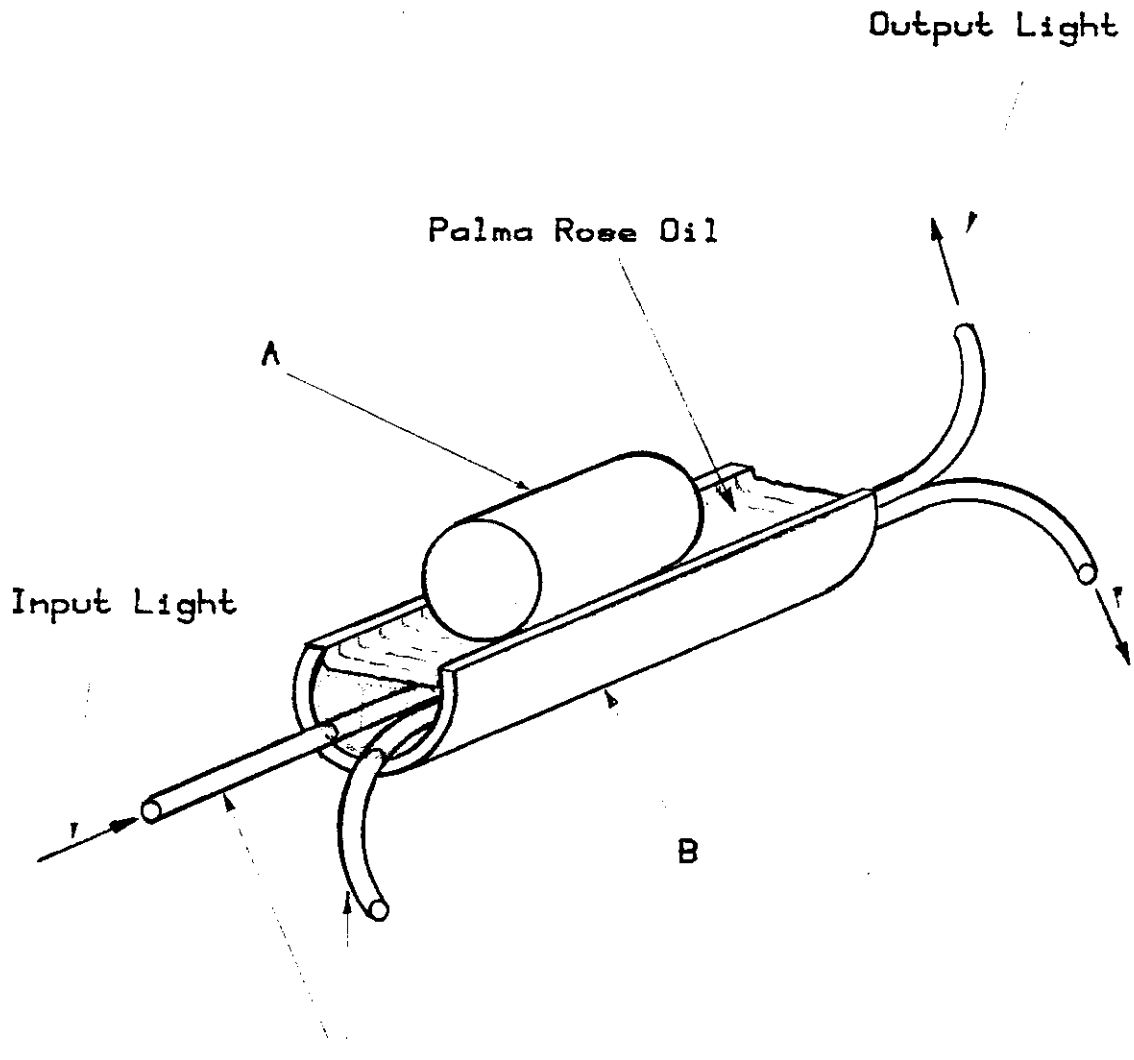

FIG[5.11] Thermally switchable directional coupler .

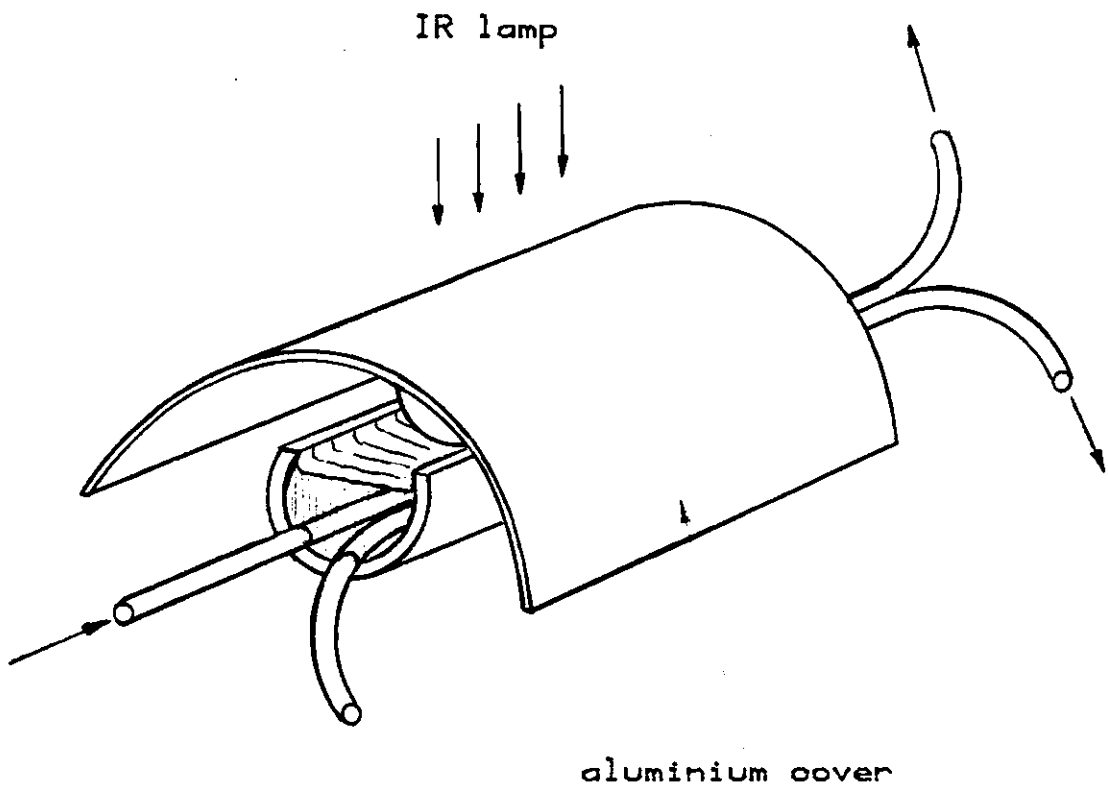

FIG[5.12] Schematic arrangement for ensuring uniform heating of the coupler .

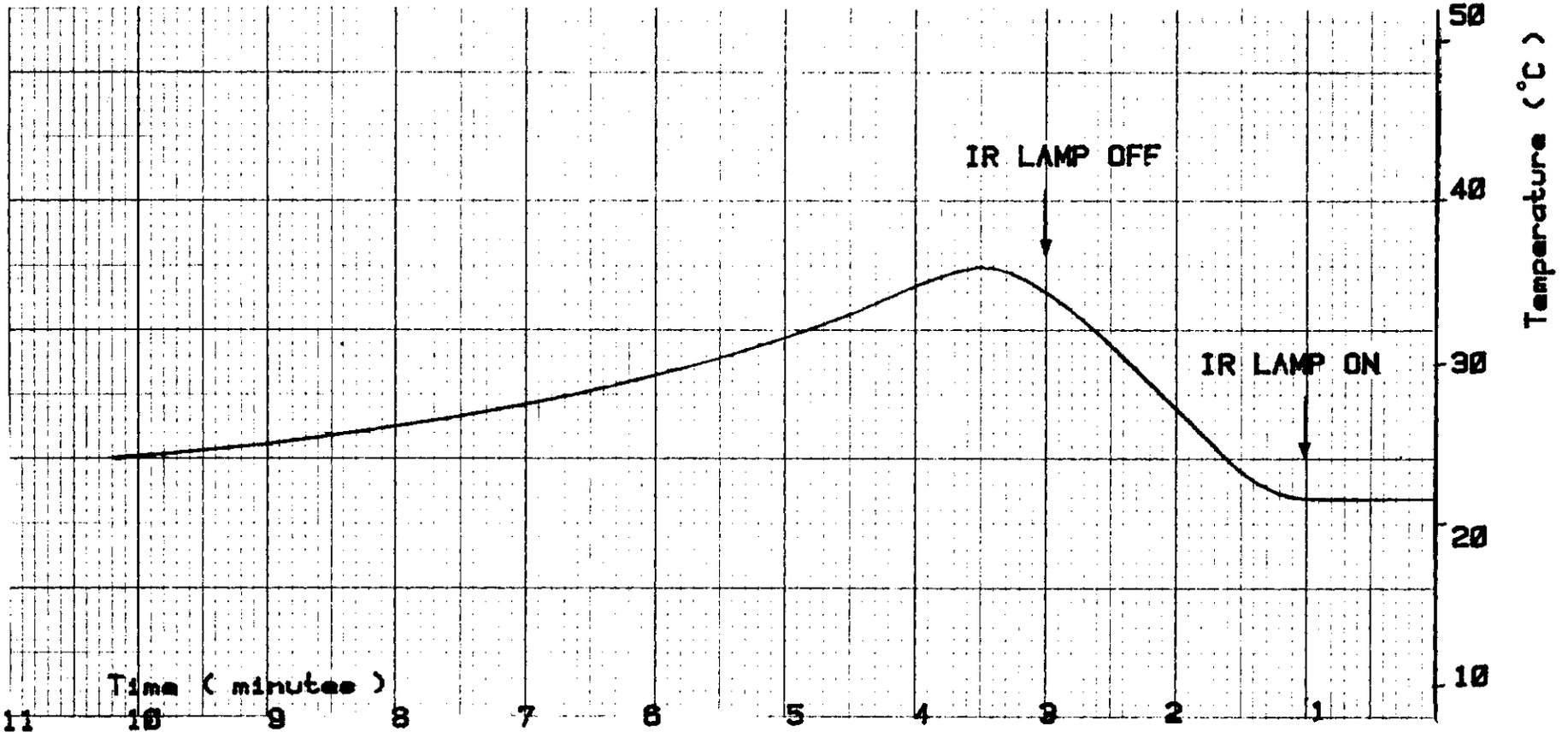

FIG[5.13] Temperature of the thermally switchable coupler as a function of time.

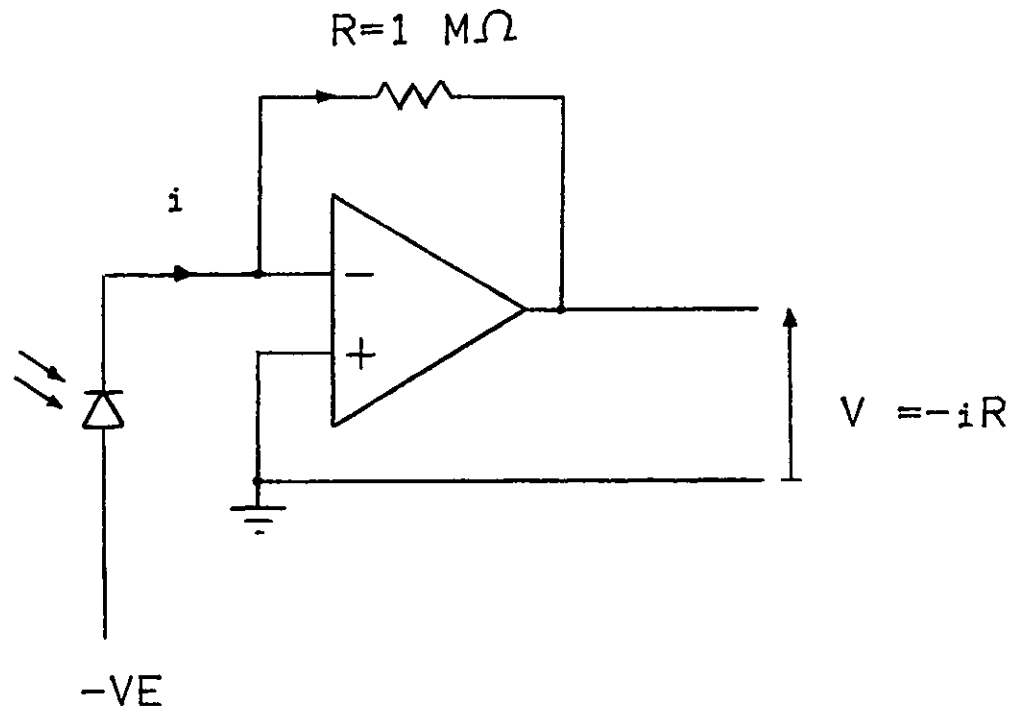

FIG[5.14] Schematic amplifier circuit.

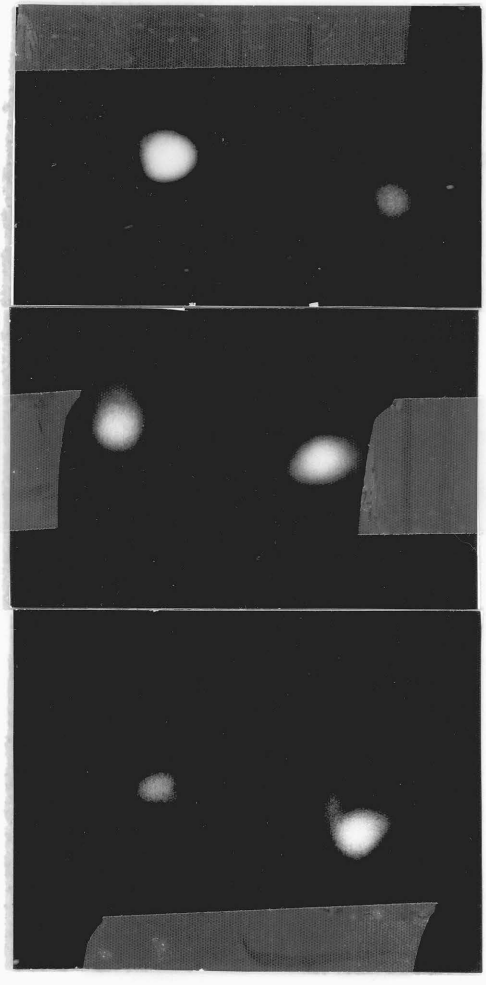

FIG[5.15] Power switching between the fibres in the thermally switchable coupler.

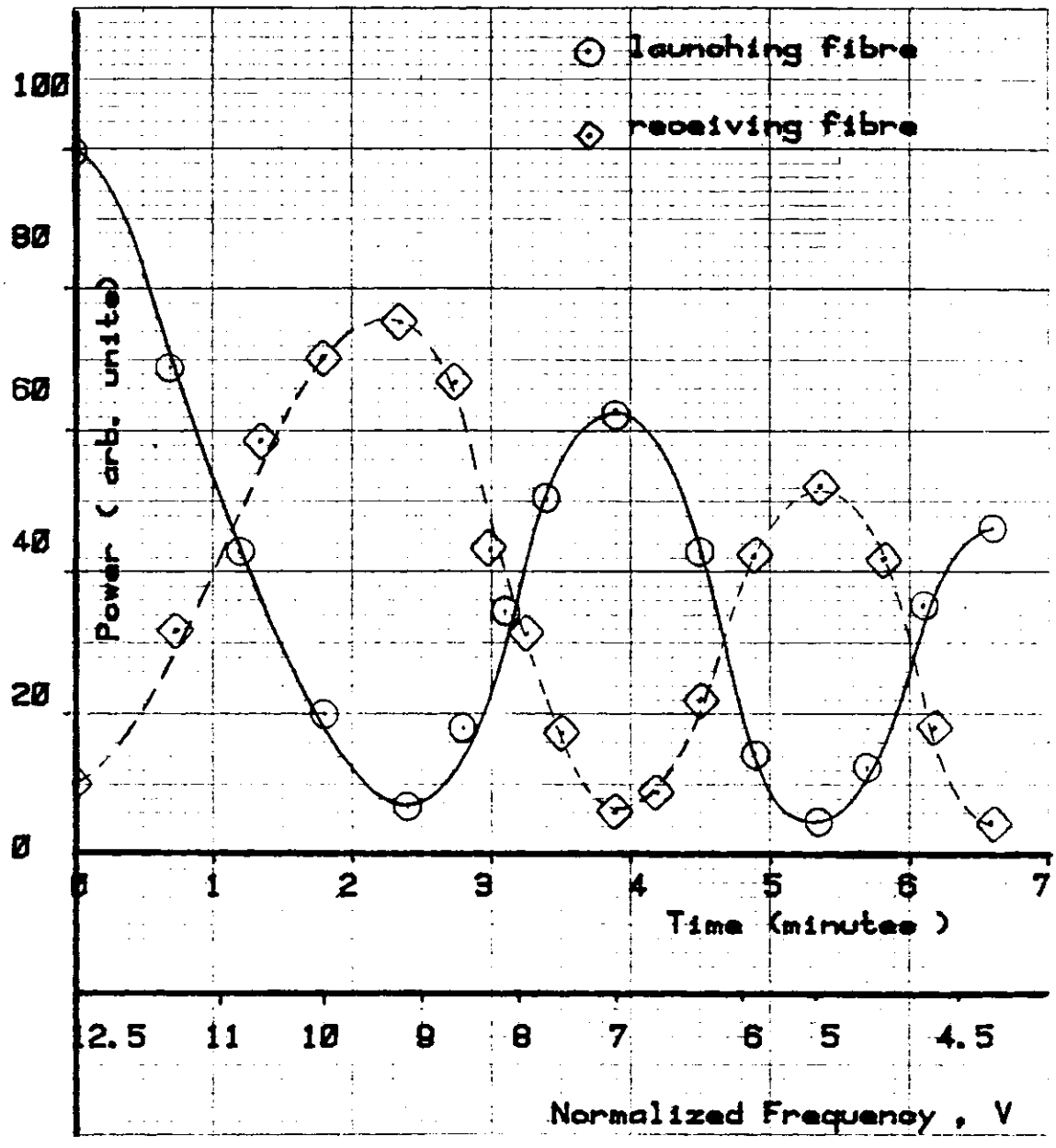

FIG[5.16] Power switching between the two fibres as a function of time and normalized frequency, V.

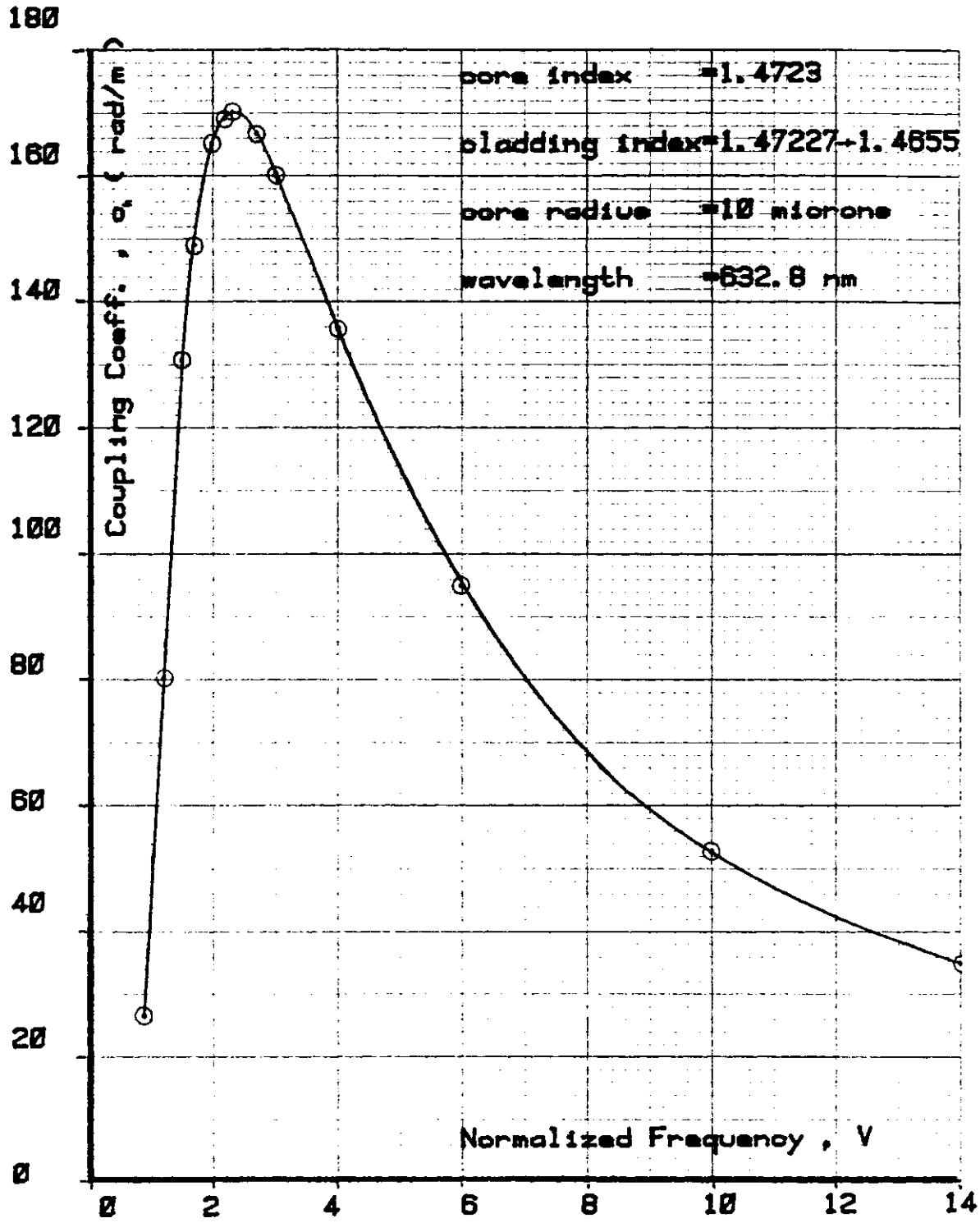

FIG[5.17] Coupling coefficient , c_h , as a function of normalized frequency , V.

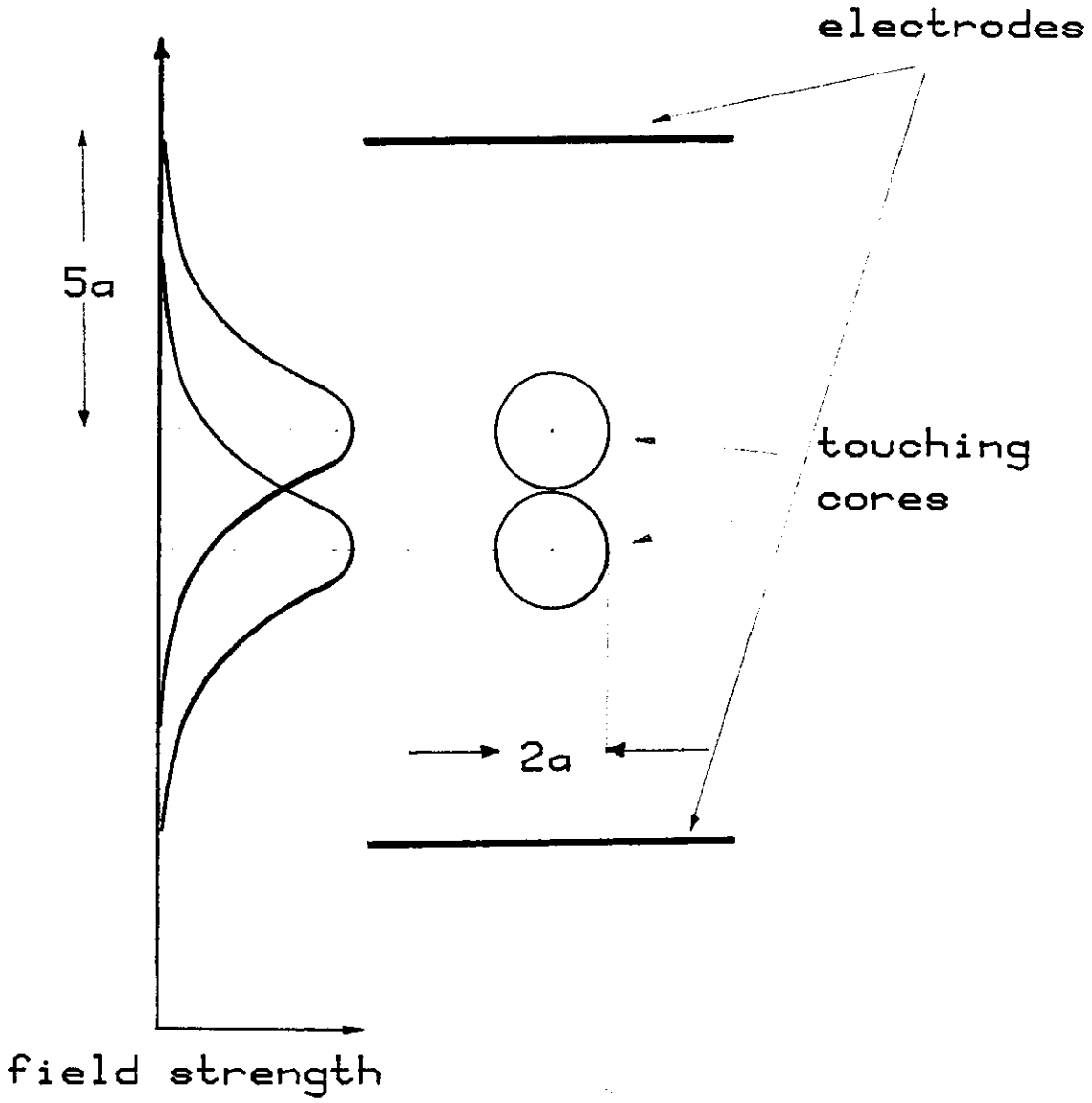

FIG[5.18] Minimum electrode spacing determined by the field in the crystal.

REFERENCES

(1) T H Maiman, "Stimulated optical radion in ruby", Nature (London), 6, 106, 1960.

(2) K C Kao, G A Hockham, "Dielectric-fibre surface waveguides for optical frequencies", Proc. IEEE, 133, p.1151, 1966.

(3) T Miya, Y Terunuma, T Hosaka, T Miyashita, "Ultimate low-loss single-mode fibre at 1.55 μm", Elec. Lett., Vol.15, pp.106-108, Feb 15, 1979.

(4) J D Love, A W Snyder, "Optical fibre eigenvalue equation: plane wave derivation", App. Opt., Vol.15, No.9, pp.2121-2125, September 1976.

(5) D Marcuse, "Light transmission optics", Van Nostrand Reinhold, 1972.

(6) J E Midwinter, "Optical fibres for transmission", John Wiley and Sons, 1979.

(7) For example, Ref (5) page 304, or any standard text on guided electromagnetic waves, eg S Ramo, J R Whinnery, T Van Duzer "Fields and waves in communication electronics", 2nd Edn, Wiley, New York, 1965.

(8) S E Miller, A G Chynoweth, "Optical fibre telecommunications", Academic Press Inc, 1979, p.8.

(9) For example, E Jahnke, P Emde, "Tables of functions with formulas and curves", 4th Edn, Dover Publications, New York 1945, or I S Gradshteyn, I M Ryzhik, "Tables of integrals, series and products", 4th Edn, Academic Press, New York, 1965.

(10) D N Payne, W A Gambling, "Zero material dispersion in optical fibres", Elec. Lett., Vol.11, pp.176-178, April 1975.

(11) T Okoshi, "Heterodyne and coherent optical fibre communications: recent progress", IEEE Trans MTT, Vol. MTT-30, No.8, p.1138, August 1982.

(12) L Figueroa, C W Slayman, H W Yen, "High frequency characteristics of GaAlAs injection lasers", IEEE Trans MTT, Vol. MTT-30, No.10, p.1706, October 1982.

(13) J E Geusic, W B Bridges, J I Pankove, "Coherent optical sources for communications", Proc. IEEE 58, p.1419, 1970.

(14) See for example, I P Kaminow, "Polarisation in optical fibres", IEEE J.Q.E., Vol. QE-17, No.1, p.15, January 1981.

(15) G G Windus, "Fibre optic systems for analogue transmission", The Marconi Review, Vol. XLIV, No.221, p.77, Second Quarter 1981.

(16) R V Schmidt, R C Alferness, "Directional coupler switches, modulators and filters using alternating Δβ techniques", IEEE Trans CAS, Vol. CAS-26, No.12, p.1099, December 1979.

(17) B K Nayar, "Crystal-cored optical fibres", PhD Thesis, Elec. Eng. Dept., Imperial College, London, 1983.

(18) V J Tekippe, "Evanescent wave coupling of optical fibres", Conf. on the Physics of Fibre Optics, 82nd Annual Meeting of the American Ceramic Society, Chicago, Illinois, April 27-30, 1980.

(19) P D McIntyre, A W Snyder, "Power transfer between optical fibres", J. Opt. Soc. of Am, Vol.63, No.12, p.1518, December 1973.

(20) S Ramo, J R Whinnery, T Van Duzer, "Fields and waves in communication electronics", 2nd Edn, Wiley, New York, 1965.

(21) J F Nye, "Physical properties of crystals", Oxford University Press, 1979.

(22) A Yariv, "Quantum Electronics", John Wiley and Sons, 1967.

(23) M Born, E Wolf, "Principles of Optics", 5th Edn, Pergamon Press, 1975.

(24) J L Stevenson, "The electro-optic properties and crystallography of meta-nitroaniline", PhD Thesis, Elec. Eng. Dept., Imperial College, London, March 1973.

(25) D Marcuse, "Theory of dielectric optical waveguides", Academic Press, 1974.

(26) Schott Optical Glass Catalogue, Glaswerk Schott & Gen, Mainz, W Germany.

(27) H R Lillie, H N Ritland, "Fine annealing of optical glass" J. Am. Ceram. Soc., Vol. 34, p.466, 1954.
A Q Tool, "Relation between inelastic deformability and thermal expansion of glass in its annealing range", 48th Annual Meeting, The American Ceramic Society, Buffalo, NY, May 1, 1946.

(28) V A Handerek, "Polarised light in circular and elliptical optical fibres", PhD Thesis, Elec. Eng. Dept., Imperical College, London, 1982.

(29) T Sueta, M Izutsu, "High speed guided-wave optical modulators", Journal of Optical Communications, p.52, 3, 2, 1982.

(30) R C Alferness, "Waveguide electro-optic modulators", IEEE Trans MTT, Vol. MTT-30, No.8, p.1121, August 1982.

(31) G H B Thompson, "Physics of semiconductor laser devices", John Wiley and Sons, 1980.

(32) R Lang, "Injection locking properties of a semiconductor laser", IEEE J.Q.E., Vol.QE-18, No.6, p.976, June 1982.
D W Smith, D J Malyon, "Experimental 1.51 μm monomode fibre link containing an injection locked repeater", Elec. Lett., Vol.18, No.1, p.43, 7th January 1981.

(33) W C McCrone, L B McCrone, J G Delly, "Polarised light microscopy", Ann Arbor Science, pp.125-133, USA, 1978.

(34) G Schiffner, H Schneider, G Schoner, "Double-core single-mode optical fibre as directional coupler", Applied Physics (by Springer-Verlag) 22, 1-5, 1980.
Y Murakami, S Sudo, "Coupling characteristics measurements between waveguides using a two-core fibre coupler", App. Opt., Vol.20, No.3, p.417, 1 February 1981.